ROLE OF INSULIN SIGNALING IN PANCREATIC BETA CELLS AND MEASUREMENT OF INSULIN RELEASE FROM ISLETS OF LANGERHANS USING A MICROFLUIDIC CHIP

By

MICHAEL GABRIEL ROPER

A DISSERTATION PRESENTED TO THE GRADUATE SCHOOL
OF THE UNIVERSITY OF FLORIDA IN PARTIAL FULFILLMENT
OF THE REQUIREMENTS FOR THE DEGREE OF
DOCTOR OF PHILOSOPHY

UNIVERSITY OF FLORIDA

2003

To my family for their love and support.

ACKNOWLEDGMENTS

I would like to thank my advisor, Professor Robert Kennedy, for his support during my graduate career. I thank my committee members, Professor James Winefordner, Professor Richard Yost, Professor Jon Stewart, and Professor Susan Frost, for their guidance through my tenure at the University of Florida. Also, thanks go to Dr. Benjamin Smith and Dr. Kathryn Williams for substituting on my committee. Past and present members of the Kennedy group have always challenged me to become a better chemist. I thank Dr. Weijun Qian for help in obtaining data for Chapter 3 and Mr. Jonathan Shackman for help with Chapter 4. This dissertation would not be possible without the help of Tiffany L. Correll.

I thank Dr. Rohit N. Kulkarni and Dr. C. R. Kahn from the Joslin Diabetes Center at Harvard Medical School for IRS-1 wildtype and knockout mice, and Dr. Bei Zhang from Merck Research Laboratories for supplying L-783,281. I would like to thank Eastman Chemical Company, American Chemical Society, and the University of Florida for fellowships during my course as a graduate student.

TABLE OF CONTENTS

Page

ACKNOWLEDGMENTS iii

ABSTRACT vi

CHAPTER

1 INTRODUCTION 1

Background 1
Insulin Signaling Pathway 2
Islets of Langerhans 13
Outline of Dissertation 21

2 ROLE OF IRS-1 IN GLUCOSE-, GLYCERALDEHYDE-, AND ARGININE-STIMULATED CALCIUM CHANGES AND SECRETION IN PANCREATIC BETA CELLS 23

Introduction 23
Experimental 27
Results and Discussion 30
Conclusions 47

3 EFFECT OF THE INSULIN MIMETIC L-783,281 ON INTRACELLULAR CALCIUM CONCENTRATION AND SECRETION FROM PANCREATIC BETA CELLS 49

Introduction 49
Experimental 51
Results and Discussion 56
Conclusions 67

4 MICROFLUIDIC CHIP FOR ONLINE MONITORING OF INSULIN SECRETION FROM AN ISLET OF LANGERHANS 68

Introduction 68
Experimental 71
Results and Discussion 78
Conclusion 87

5 PERFUSION OF ISLETS 89

Top Down Perfusion 89
Pressure From Perfusion Channel 93
Perfusion Via Electroosmotic Flow 95
Conclusion 99

6 SUMMARY AND FUTURE STUDIES 100

Insulin Signaling Pathway 100
Microfluidic Chips 101

APPENDIX

A FABRICATION OF MICROFLUIDIC CHIPS 110

Material Specifications 110
Photolithography 111
Wet Etching of Glass 113
Bonding Chips 116

B EVERYDAY USE AND PROBLEMS OF MICROFLUIDIC CHIPS 118

Experiments with Microfluidic Chips 118
Clogging 119

LIST OF REFERENCES 123

BIOGRAPHICAL SKETCH 131

Abstract of Dissertation Presented to the Graduate School
of the University of Florida in Partial Fulfillment of the
Requirements for the Degree of Doctor of Philosophy

ROLE OF INSULIN SIGNALING IN PANCREATIC BETA CELLS AND MEASUREMENT OF INSULIN RELEASE FROM ISLETS OF LANGERHANS USING A MICROFLUIDIC CHIP

By

Michael Gabriel Roper

August 2003

Chair: Robert T. Kennedy
Major Department: Chemistry

Insulin resistance in peripheral tissues and defective insulin secretion from pancreatic β-cells leads to non-insulin dependent diabetes mellitus, more commonly known as type 2 diabetes. It has been proposed that a defect in the insulin signal transduction pathway could lead to both hallmarks of type 2 diabetes. To determine how a defect in the insulin signal transduction pathway would affect normal β-cell function, intracellular Ca^{2+} changes and secretion were measured from genetically-modified pancreatic β-cells upon stimulation with various secretagogues.

Application of glucose, glyceraldehyde and arginine initiates secretion from insulin receptor substrate-1 (IRS-1) wildtype (WT) and knockout (KO) pancreatic β-cells as measured by amperometry with microelectrodes; however, the amount of secretory events from IRS-1 KO β-cells is significantly less. Additionally, IRS-1 deletion disrupts intracellular Ca^{2+} handling as KO β-cells have an increase in latency to Ca^{2+} changes and

a decrease in duration of stimulated Ca^{2+} levels compared to WT control cells. Islets of Langerhans, microorgans composed of 2000-5000 cells of which the majority are β-cells, display irregular Ca^{2+} oscillations in the presence of stimulatory glucose levels. An insulin mimetic, which stimulates glucose uptake in peripheral tissues by activating the insulin signaling pathway, also initiates secretion from β-cells through an IRS-1 dependent process. Thus, the insulin signaling pathway appears to contribute to Ca^{2+} homeostasis in pancreatic β-cells and disruption of this pathway can lead to defective insulin secretion. These results provide evidence for the insulin signal transduction pathway as a link between insulin resistance and defective insulin secretion.

To monitor insulin secretion from islets of Langerhans, a microfluidic chip is used to house an islet and perform a capillary electrophoresis competitive immunosassay. Insulin is electrokinetically sampled through a 4 cm heated reaction channel where it mixes with fluorescein isothiocyanate-labeled insulin (FITC-insulin) and anti-insulin immunoglobulin (Ab). The resulting mixture is injected every 15 s onto a 1.5 cm separation channel and separation of FITC-insulin:Ab complex and free FITC-insulin occurs in 5 s. The method allows the kinetics of first and second phase insulin release to be measured from single islets with high temporal resolution.

CHAPTER 1
INTRODUCTION

Background

Insulin is secreted from pancreatic β-cells primarily due to chemical signals produced during glucose metabolism. The conventional view of glucose-stimulated insulin secretion [Henquin, 2000] begins with glucose transport into beta cells through glucose transporters. Upon entering the cell, glucose is metabolized via glycolysis and the citric acid cycle increasing the amount of adenosine triphosphate (ATP). An increase in the ratio of ATP to adenosine diphosphate closes ATP-sensitive potassium channels, thereby depolarizing the cell membrane. Consequently, voltage-gated Ca^{2+} channels open allowing extracellular Ca^{2+} to enter the cell. An increase in intracellular Ca^{2+} concentration ($[Ca^{2+}]_i$) induces release of insulin in a process known as exocytosis.

Beta cells are found in groups of 2000-5000 cells known as islets of Langerhans. Several cell types are present in islets, including α-, δ-, and pp-cells, which secrete glucagon, somatostatin, and pancreatic poly(peptide), respectively. The combination of these peptides and other receptor-mediated signals helps to tightly regulate insulin release. The released insulin then signals peripheral tissues to take up glucose from the blood, thereby maintaining normal glucose levels. In some individuals, these processes of insulin secretion and glucose uptake are disrupted, leading to non-insulin dependent diabetes mellitus, also known as type 2 diabetes [Kahn, 1994].

Prior to development of type 2 diabetes, both increased insulin secretion and insulin resistance in peripheral tissues are observed. Insulin resistance is defined as increased

amounts of insulin, compared to normal levels, which are needed to initiate glucose uptake [Kahn, 1994]. Throughout insulin resistance, β-cells increase secretion of insulin to maintain glucose uptake and to decrease glucose production by the liver. It is unclear if β-cells increase insulin secretion to compensate for insulin resistance, or if the large amounts of insulin released by β-cells cause insulin resistance. Nevertheless, over time, beta cells cannot compensate for insulin resistance and the subject becomes diabetic [Taylor, 1999; Porte, Jr. and Kahn, 2001].

Diabetes and its complications account for approximately 19% of deaths in individuals over the age of 25, while direct and indirect costs associated with diabetes accounted for $132 billion in 2000 [Centers for Disease Control and Prevention, 2002]. Although the prevalence of type 2 diabetes has increased the last several decades [Kenny *et al.*, 1995], the cause of insulin resistance and defective insulin secretion has not been fully elucidated. The signal transduction pathways that regulate insulin secretion from beta cells and islets of Langerhans are under investigation in the hope of gaining further insight into the regulatory mechanisms that may be awry in diabetics.

Insulin Signaling Pathway

A hypothesis has been proposed that links defective insulin secretion from beta cells to insulin resistance in peripheral tissues and involves the insulin signaling pathway [Taylor, 1999; Rutter, 1999; Hussain, 1999; Withers and White, 2000]. β-cells are known to have components of the insulin signaling pathway, including insulin receptors [Verspohl and Ammon, 1980; Patel *et al.*, 1982], insulin receptor substrates [Rothenberg *et al.*, 1995; Velloso *et al.*, 1995], and phosphatidylinositol 3-kinase [Rothenberg *et al.*,

1995; Velloso *et al.*, 1995], similar to proteins involved in regulating glucose uptake in peripheral tissues [Holman and Kasuga, 1997].

Insulin Receptors

Insulin receptors are 350 kDa proteins composed of two α and two β subunits [Gupta, 1997]. The α-subunits reside exclusively outside the cell and are the target for insulin binding. β-subunits are composed of an extracellular domain, transmembrane domain, and an intracellular domain. Disulphide bonds link the α subunits together and link α-subunits to extracellular domains of β-subunits. Insulin binding to α-subunits commences a conformational change in the β-subunit activating intrinsic tyrosine kinase activity [Krook and O'Rahilly, 1996]. The β-subunit kinase initiates autophosphorylation of at least six tyrosine residues, necessary for phosphorylation of other substrates that amplify the insulin binding event [Kahn, 1994].

Insulin Receptor Substrates

Upon activation of insulin receptor kinase, several substrates of the insulin receptor are phosphorylated. Insulin receptor substrate-1 (IRS-1) was the first protein found that "docked" to the insulin receptor and was phosphorylated [White *et al.* 1985]. IRS-1 serves as a prototype for a family of substrates including IRS-2, IRS-3, and IRS-4 (Figure 1-1) [White, 1998]. The use of substrates such as IRS-1 enables amplification of the binding event as docking proteins typically do not interact stoichiometrically with receptors. Also, multiple receptors can signal the same docking protein to integrate signaling pathways [White, 1998].

IRS-1 is a 132 kDa protein that is expressed in many tissues at low numbers [Kahn, 1994]. IRS-1 becomes phosphorylated on at least eight different tyrosine residues

[Saltiel, 1996], although it has the potential to be phosphorylated on 22 residues [Kahn, 1994]. Tyrosine phosphorylation of IRS-1 binds non-covalently to src homology 2 (SH2) domain-containing proteins initiating downstream signaling.

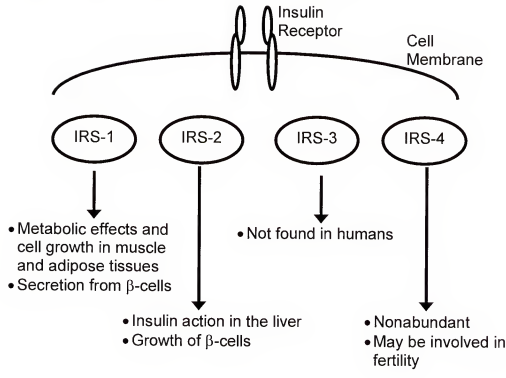

Figure 1-1. Function of insulin receptor substrates. Autophosphorylation of the insulin receptor β-subunit signals insulin receptor substrates to bind. All insulin receptor substrates contain a pleckstrin homology domain capable of binding membrane phospholipids and a phosphotyrosine binding domain involved in the association of the substrate to the receptor. The substrate involved in the signaling depends on several variables including the subcellular location of substrates and the amount of substrate present. Adapted from [Sesti *et al.*, 2001; Withers *et al.*, 1999].

Phosphatidylinositol 3-Kinase

Tyrosine phosphorylated compounds with an YXXM amino acid motif bind SH2 domain-containing proteins, for example, the regulatory subunit of phosphatidylinositol 3-kinase (PI3-K) [Kahn, 1994; Saltiel, 1996]. IRS-1 has nine YXXM motifs [White, 1998] and is known to activate PI3-K upon insulin stimulation [Holman and Kasuga,

1997]. PI3-K is composed of an 85 kDa regulatory subunit that contains the SH2 binding domain and a 110 kDa catalytic subunit. Binding to the regulatory subunit causes the catalytic unit to become active through an unknown mechanism [Kahn, 1994].

The catalytic site of PI3-K phosphorylates membrane-bound lipids known as phosphatidylinositols (PIs). Phosphorylated PIs are implicated in a wide variety of pathways, from movement of glucose transporters [Okada *et al.*, 1994] to themselves being substrates of various enzymes, thereby continuing the insulin signaling pathway [White, 1998]. Thus, a single binding event of insulin can stimulate multiple pathways, for example, glucose uptake, lipid synthesis, and cell growth [Kahn, 1994].

The roles of these proteins in insulin-stimulated glucose uptake in peripheral tissues are well known and have been the discussion of multiple reviews [Pessin *et al.*, 1999; Gupta, 1997; Holman and Kasuga, 1997]. However, the role of the signaling proteins in β-cells has only recently been discovered and indicates that this pathway may be necessary for normal β-cell function.

Insulin Pathway in Pancreatic β-Cells

A quantitative assessment found that 60% of β-cells in rat islets had detectable levels of insulin receptors on their cell surface [Patel *et al.*, 1982]. Stimulation with glucose or insulin induces autophosphorylation of insulin receptor β-subunits and phosphorylation of IRS-1 [Rothenberg *et al.*, 1995; Velloso *et al.*, 1995]. These same stimuli also induce an association of phosphorylated IRS-1 with the regulatory subunit of PI3-K [Rothenberg *et al.*, 1995; Velloso *et al.*, 1995]. Thus, stimulation of β-cells with glucose appears to activate the insulin signaling pathway by secreted insulin binding to insulin receptors on the cell and activating the intrinsic tyrosine kinase.

The products of PI3-K are also known to be involved in intracellular signaling in pancreatic β-cells. For example, maximum production of phosphatidyl-(3,4,5)-trisphosphate (PIP_3), a product of PI3-K, corresponds to maximum insulin secretion implying that PI3-K is active [Alter and Wolf, 1995]. PIP_3 can stimulate several pathways in the cell responsible for maintaining Ca^{2+} homeostasis and growth [Gupta, 1997; Avruch, 1998]. A role for the insulin signal transduction pathway is apparent when the effect of insulin is examined at the single cell level or using genetically engineered cells [Kulkarni *et al.*, 1999b; Porzio *et al.*, 1999].

Function of Insulin Signaling Pathways in β-Cells

Upon stimulation of single β-cells with insulin, intracellular Ca^{2+} increases and insulin is released (Figure 1-2), effects mediated by insulin receptors [Aspinwall *et al.*, 1999b]. The insulin receptor substrate used for this process is believed to be IRS-1 as β-cell tumor lines with IRS-1 genetically deleted do not release insulin or increase $[Ca^{2+}]_i$ upon insulin stimulation [Aspinwall *et al.*, 2000]. Blockade of PI3-K with wortmannin, an irreversible inhibitor of PI3-K [Powis *et al.*, 1994], also inhibits Ca^{2+} increases and insulin secretion. Protein kinase C (PKC) is necessary for insulin-stimulated secretion as use of bisindolylmaleimide I, an antagonist of PKC, inhibits release but does not affect changes in $[Ca^{2+}]_i$ [Aspinwall *et al.*, 2000]. PKC can be activated by products of PI3-K (for example, PIP_3 [Good *et al.*, 1998]) and is believed to phosphorylate exocytotic proteins making them more sensitive to Ca^{2+} [Metz, 1988]. Several of these proteins are also implicated in maintaining insulin production; for example, transcription of insulin is dependent on insulin binding to insulin receptors and activating PI3-K [Leibiger *et al.*, 1998]. In addition to transcription, the translation of insulin increases upon a glucose

stimulation, partly due to metabolism of glucose and partly to secreted insulin binding to insulin receptors [Leibiger *et al.*, 2000]. Therefore, a defect in one of these proteins can negatively influence insulin production and/or secretion.

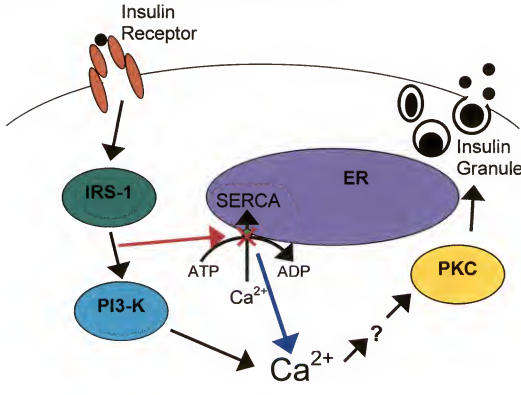

Figure 1-2. Proposed pathway of insulin-stimulated secretion in pancreatic β-cells. Released insulin binds to insulin receptors initiating the intrinsic tyrosine kinase activity. IRS-1 is phosphorylated and binds to the SH2 domain of PI3-K. Activation of IRS-1 and PI3-K are necessary for increases in $[Ca^{2+}]_i$, possibly by inhibiting sarco/endoplasmic reticulum Ca^{2+}-ATPase (SERCA) pumps on the endoplasmic reticulum (ER). Passive diffusion of Ca^{2+} out of the ER then increases $[Ca^{2+}]_i$. PI3-K or its products can then activate protein kinase C (PKC) through an undetermined mechanism. An increase in $[Ca^{2+}]_i$ and activation of PKC are needed to stimulate release of insulin granules.

Defects in Insulin Signaling Observed in Pancreatic β-Cells

Examples of defects in the insulin signaling pathway having negative effects on $[Ca^{2+}]_i$, insulin secretion, and insulin production in β-cells come from genetically engineered cells. In RIN 1046-38 cells, a pancreatic β-cell tumor line, incorporation of a

mutant IRS-1 (Gly972→Arg) decreases its association with the regulatory subunit of PI3-K and decreases glucose and sulfonylurea-stimulated insulin secretion as compared to wildtype cells [Porzio *et al.*, 1999]. In IRS-1 knockout islets of Langerhans, glucose- and arginine-induced insulin secretion is reduced compared to wild type controls [Kulkarni *et al.*, 1999b]. The effect of the insulin signaling pathway on insulin production is observed in IRS-1 null β-cell tumor lines which have a loss of insulin content; however, insulin production is partially restored by re-expression of IRS-1 [Kulkarni *et al.*, 1999b]. Another example of the importance of the insulin pathway in maintaining homeostasis is by overexpression of insulin receptor and IRS-1 in a pancreatic β-cell tumor line. These tumor cells have increased basal $[Ca^{2+}]_i$ and fractional insulin secretion, defined as insulin secreted/total insulin content [Xu *et al.*, 1999]. *In vivo*, mice lacking β-cell insulin receptors have reduced insulin secretion upon glucose stimulation, similar to type 2 diabetics [Kulkarni *et al.*, 1999a].

Defective Insulin Signaling in Peripheral Tissues

Defects in the same proteins involved in regulating insulin production and secretion in β-cells are found in peripheral tissues of type 2 diabetics. In adipocytes from type 2 diabetics, expression of IRS-1 and subsequent activation of PI3-K are reduced in comparison to adipocytes from healthy individuals [Rondinone *et al.*, 1997]. In skeletal muscle from type 2 diabetics, a loss in glucose transport upon insulin stimulation occurs. This loss in glucose transport is not due to a decrease in IRS-1 expression, but rather a decrease in IRS-1 phosphorylation and activation of PI3-K [Krook *et al.*, 2000]. The same Gly972→Arg variant that disrupts secretion from β-cell tumor lines is twice as likely to be found in diabetics as in healthy individuals [Sesti *et al.*, 2001]. Human islets

with the same mutation in IRS-1 have an increased number of apoptotic β-cells compared to islets without the IRS-1 mutation [Federici *et al.*, 2001].

Thus, a common signaling pathway appears to exist in pancreatic β-cells and peripheral tissues. In both cell types, insulin binding to insulin receptors activates the inherent tyrosine kinase activity of the receptors, which then phosphorylates IRS-1. Binding of phosphorylated IRS-1 to the regulatory subunit of PI3-K initiates translocation of glucose transporters to the cell surface and the eventual uptake of glucose from blood in peripheral tissues [Holman and Kasuga, 1997], while in pancreatic β-cells, PI3-K activation can initiate insulin secretion. This convergence of pathways in β-cells and peripheral tissues has led to the hypothesis that a defect in one of the signal transduction proteins would lead to defective insulin secretion and reduced glucose uptake, linking two hallmarks of type 2 diabetes [Taylor, 1999; Hussain, 1999; Rutter, 1999; Withers and White, 2000].

Although the roles of the insulin signaling pathway have been explored in tumor cell lines, primary islets, and *in vivo*, it is important to determine the role of insulin signaling from single primary β-cells. Tumor cell lines do not always share the same characteristics as primary cells [Poitout *et al.*, 1996] and islets and *in vivo* measurements can be complicated by paracrine interactions and other factors that may regulate secretion. In fact, earlier work stimulating islets of Langerhans with insulin gave conflicting reports on the effect of insulin on islet function [reviewed in Leibiger *et al.*, 2002]. Therefore, to gain an uncomplicated view of how a defect in the insulin signaling pathway would affect glucose-stimulated insulin secretion, single primary β-cells need to be tested.

L-783,281: An Insulin Mimetic

L-783,281 (Figure 1-3), a non-peptidyl fungal metabolite, induces insulin receptor tyrosine kinase activity in Chinese hamster ovary cells which overexpress insulin receptors [Zhang *et al.*, 1999]. Activation of insulin receptor tyrosine kinase by L-783,281 increases phosphorylation of IRS-1 and consequent activation of PI3-K.

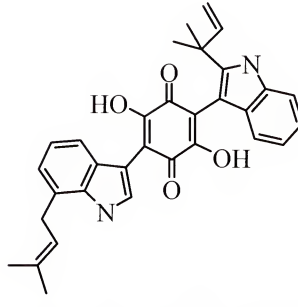

Figure 1-3. Structure of L-783,281. L-783,281 binds to the β-subunit of the insulin receptor thereby activating the tyrosine kinase activity. Administration of the insulin mimetic initiates glucose uptake in peripheral tissues of diabetic rodent models [Zhang *et al.*, 1999].

Administration of the insulin mimetic to hyperglycemic mice lowers blood glucose levels by increasing glucose transport in peripheral tissues. Although L-783,281 activates the insulin signaling pathway in peripheral tissues, its effect on insulin secretion is questionable. Recent reports indicate L-783,281 increases insulin secretion from islets of Langerhans at high glucose concentrations [Westerlund *et al.*, 2002], while others report an inhibitory effect of L-783,281 on insulin secretion at basal and stimulatory glucose levels [Persaud *et al.*, 2002]. The nature of the interaction of L-783,281 with isolated

pancreatic β-cells has not been determined. Agents capable of decreasing blood glucose by simultaneously increasing insulin secretion from pancreatic beta cells and glucose uptake in peripheral tissues represent significant pharmaceutical candidates for the treatment of diabetes.

Methods to Monitor Secretion and $[Ca^{2+}]_i$ From Single Cells

The measurement of insulin from single cells is hindered by the low mass of insulin released and the time in which exocytosis occurs. Insulin is stored in vesicles as a solid granule with six insulin molecules bound to two Zn^{2+} ions [Foster *et al.*, 1993]. Upon an increase in $[Ca^{2+}]_i$, these vesicles fuse with the plasma membrane and open to the extracellular space where the solid insulin granule dissociates, dissolves, and diffuses away from the cell. Figure 1-4 is an electron micrograph of a β-cell undergoing exocytosis. One vesicle in the figure has fused with the plasma membrane, whereas the other vesicle has fused with the membrane and the granule is in the process of dissolution. In human β-cells, each insulin vesicle has an average diameter of

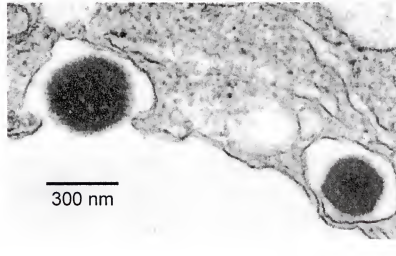

Figure 1-4. Electron micrograph of a β-cell undergoing exocytosis. The two dark circles are solid insulin granules in vesicles of a β-cell [Orci *et al.*, 1988]. Each vesicle contains approximately 2 amol of insulin, necessitating a highly sensitive technique to measure single release events.

approximately 300 nm and contains approximately 1.7 amol of insulin per vesicle [Huang *et al.*, 1995]. The dissociation and diffusion of a single insulin granule occur on the order of 100 ms [Aspinwall *et al.*, 1997]. In order to determine the effect of various substrates on isolated pancreatic β-cells, the techniques used to determine insulin secretion must be able to measure attomole quantities of insulin with millisecond temporal resolution. To meet the analytical demands of monitoring secretion from single cells, amperometry with microelectrodes has been employed.

To measure release, a microelectrode is placed above a cell and a potential sufficient to oxidize or reduce the vesicular contents is applied. As exocytosis occurs, the contents diffuse to the electrode surface where they are oxidized or reduced rendering a change in current. By plotting the current of the microelectrode as a function of time, a current trace is obtained where individual spikes in current are associated with single exocytotic events [Wightman *et al.*, 1991].

Single insulin release events from isolated beta cells can be measured with a ruthenium oxide/cyanoruthenate (RuOx/CN-Ru) modified microelectrode, where insulin is detected by oxidation of the disulfide bonds [Kennedy *et al.*, 1993; Huang *et al.*, 1995; Gorski *et al.*, 1997]. The use of RuOx/CN-Ru microelectrodes enables detection of single exocytotic events; however, the modified microelectrode is unstable over long periods of time unless the potential is lowered [Kennedy *et al.*, 1993]. Also, the sensitivity of measurements is dependent on the species of the β-cell [Aspinwall *et al.*, 1999a]. To ameliorate problems of detecting secretory events with RuOx/CN-Ru electrodes, unmodified carbon fiber microelectrodes can be used to detect 5-hydroxytryptamine (5-HT) release as a marker of insulin secretion. Beta cells are

incubated in media that contains 5-HT allowing the accumulation of the amine into secretory vesicles [Falck and Hellman, 1963; Gylfe, 1978; Hutton *et al.*, 1983]. Upon exocytosis of insulin, 5-HT is co-released and its detection can serve as an indicator of the number of exocytotic events induced by a stimulus [Aspinwall *et al.*, 1999a].

Intracellular Ca^{2+} levels are typically measured with a ratiometric fluorescent dye, such as Fura-2 [Grynkiewicz *et al.*, 1985]. Fura-2 binds Ca^{2+} with a dissociation constant of 130 nM, and is excited at 340 nm and 380 nm for Fura-2 bound to Ca^{2+} and free Fura-2, respectively. Fluorescence emission is collected at 520 nm and the ratio of the fluorescence intensity generated from 340 nm and 380 nm excitation provides quantitative values of $[Ca^{2+}]_i$. Measurement of $[Ca^{2+}]_i$ is important as this secondary messenger is involved in regulating glucose- and insulin-stimulated insulin secretion [Henquin, 2000; Aspinwall *et al.*, 2000].

Amperometry with microelectrodes and Fura-2 have been used to discern the effect of exogenous insulin on pancreatic β-cells [Aspinwall *et al.*, 1999b] and the insulin signal transduction pathway in β-cells [Aspinwall *et al.*, 2000]. These techniques should also allow the effect of the insulin pathway in mediating glucose-stimulated insulin secretion and the effects of L-783,281 from primary β-cells to be investigated.

Islets of Langerhans

Perfusion of islets of Langerhans (Figure 1-5) with glucose induces both oscillations in $[Ca^{2+}]_i$ and insulin secretion with periods of approximately 5 min [Gilon and Henquin, 1995]. In addition to slow oscillations of Ca^{2+}, fast oscillations are observed superimposed on the slow oscillations, with typical periods of 10-30 s. One hypothesis is that slow intracellular Ca^{2+} oscillations induce insulin secretory oscillations

[Jonas *et al.*, 1998], although fast oscillations of insulin release have not been observed. The importance of monitoring secretory oscillations is due to altered insulin oscillations being an early indicator of type 2 diabetes [Pørksen, 2002].

To monitor insulin release from islets of Langerhans, single secretory events from cells do not need to be measured; however, due to other hormone-releasing cell types present in islets, highly specific measurements of insulin are required. In addition, islets secrete insulin in complex patterns, dictating a measurement technique with a large linear dynamic range and high temporal resolution. To achieve these criteria, insulin secretion from single islets of Langerhans is typically monitored by an immunoassay.

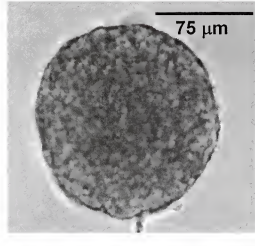

Figure 1-5. Brightfield image of an islet of Langerhans. Islets are composed of 2000-5000 cells, the majority being pancreatic β-cells. Other cell types present in the islet help regulate insulin secretion, maintaining euglycemia.

Methods to Monitor Secretion from Islets of Langerhans

Immunoassays provide a sensitive measurement for trace levels of a variety of molecules. In addition to high sensitivity, immunoassays rely on antigen-antibody interactions yielding a highly selective measurement. The most common method for measuring insulin release is by radioimmunoassay.

In a typical competitive radioimmunoassay (RIA) for insulin, an islet or several islets are perfused with a stimulatory solution and fractions of the perfusate are collected and mixed with radiolabeled insulin (insulin*). This mixture is then incubated with an insulin antibody (Ab) immobilized on a solid support. Determination of insulin* bound to Ab provides a quantitative value of insulin released from the islet [Yalow, 1978; Mathews and Van Holde, 1996; Bao, 1997]. Simultaneous measurements of insulin secretion by RIAs and intracellular Ca^{2+} are also possible and have been used to determine the temporal relationship of changes in $[Ca^{2+}]_i$ with insulin release [Gilon and Henquin, 1995; Ravier *et al.*, 1999]. The ability to perform simultaneous measurements is an advantage; however, several disadvantages are inherent using RIAs. Although low detection limits can be attained with RIAs (femtomole), the technique is labor intensive and time consuming. In addition, because RIAs are mass sensitive, a volume of perfusate must be collected that contains a sufficient amount of insulin to be detected. The temporal resolution of the system is therefore limited, leading to typical sampling rates of one insulin determination per minute. Faster sampling rates have been reported (for example, once every 20 s [Lin *et al.*, 1999; Lin *et al.*, 2001a]), although the time involved in collecting and analyzing each fraction has not made these faster methods common. Thus, if the temporal resolution of insulin secretory measurements is increased while still allowing for a high level of automation, the ability to routinely observe fast oscillations of release may be possible. Also, if these fast oscillations are found altered in diabetics (similar to slow oscillations), an earlier diagnosis of the disease may be possible.

Capillary electrophoresis (CE) immunoassays are used to increase temporal resolution and automation of measurements [Bao, 1997]. In CE immunoassays for

insulin, both incubation of reagents and separation of B and F occur in solution phase [Schultz and Kennedy, 1993; Schultz *et al.*, 1995]. To further increase the automation and precision of measurements, reagents are mixed online prior to injection onto a separation capillary [Tao and Kennedy, 1996]. In order to determine rapid changes in insulin release from islets of Langerhans, fast separations are performed.

Online measurements of insulin release from single islets of Langerhans have been performed using a CE immunoassay [Tao *et al.*, 1998]. As seen in Figure 1-6, an islet was held in a piece of Teflon tubing and perfused with a buffer containing 3 mM glucose or 20 mM glucose. Output of the Teflon tubing was connected to a reaction capillary where insulin released from the islet mixed with insulin* and Ab. After traversing the

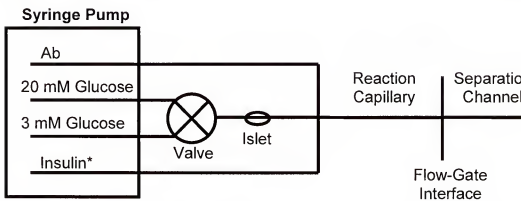

Figure 1-6. Capillary electrophoresis setup to monitor insulin secretion. An islet was placed in a piece of Teflon tubing and perfused via a syringe pump with either a basal or stimulatory glucose solution. Insulin released from the islet mixed with Ab and insulin* in a 35 cm reaction capillary prior to injection onto a 5 cm separation capillary. Adapted from Tao *et al.*, 1998.

reaction capillary, injections were made onto a separation capillary via a flow-gate interface. High electrical fields (2000-4000 V/cm) were used and separation of insulin*:Ab and insulin* was accomplished in less than one second. Unfortunately, several disadvantages of this system limited its applicability. The islet was difficult to load into the Teflon tube and was held in place with cotton screens. Housing the islet in a

Teflon holder precluded measurements of secondary messengers, such as Fura-2 measurements for $[Ca^{2+}]_i$. Finally, the setup for the online CE immunoassay was bulky, encompassing a syringe pump, multiple capillaries, valves, unions, high voltage supply, and detection optics, not allowing the system to be easily transferred, as to a clinical setting for diagnostic purposes.

To circumvent several of these problems in the CE immunoassay for measuring insulin secretion, microfabricated "lab-on-a-chip" devices, or microfluidic chips, can be used. These chips integrate multiple components onto a single substrate, such as reaction channels, valves, and separation channels, reducing dead volume and footprint of the system (Figure 1-7). By placing a living islet in a microfluidic chip and performing a CE immunoassay for insulin release, it may be possible to maintain high temporal resolution measurements of insulin. Also, if an optically transparent substrate is used to house the islet, assays for intracellular messengers could be performed simultaneously as insulin measurements enabling temporal relationships of signaling pathways to be determined.

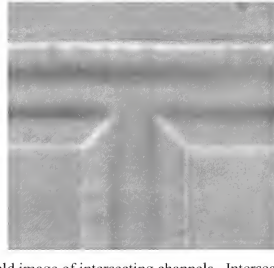

Figure 1-7. Brightfield image of intersecting channels. Intersections of channels have low dead volume due to the fabrication of all components in one substrate. Electroosmotic flow is often used to manipulate and valve fluids in channels such as these.

Microfluidic Chips

Prior to a description of microfluidic immunoassays, a background on the fabrication and use of microfluidic chips is given to demonstrate the advantages and disadvantages of these systems. Production of glass microfluidic chips (Figure 1-8) begins with aligning a photomask with the intended channel design to a glass wafer with a layer of photoresist on top. The glass wafer is exposed to ultraviolet (UV) light through the photomask and the exposed regions are removed with an aqueous solvent. The underlying glass is etched with hydrofluoric acid resulting in a mixture of products, including hexafluorosilicate ions [Kern and Deckert, 1978].

HF etches glass isotropically, rendering trapezoidal channels with the width at the top of channels equal to twice the depth plus the linewidth of the photomask. Remaining photoresist is removed and the etched chip and a top plate are bonded together by direct bonding [Haisma and Spierings, 2002], adhesive bonding [Huang *et al.*, 2001], or more commonly, thermal bonding [Roulet *et al.*, 2001].

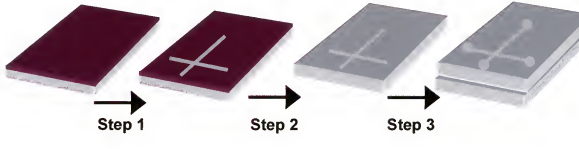

Figure 1-8. Fabrication of a glass microchip. In step 1, a glass plate (gray) with positive photoresist (purple) is exposed to UV light through a photomask. The exposed photoresist is then developed leaving a pattern of the photomask. In step 2, the glass is etched with HF producing trapezoidal channels. The remaining photoresist is then removed rendering a glass plate with etched channels. Step 3 consists of drilling reservoirs at the end of each channel and vigorously cleaning the glass. After cleaning, the etched glass plate is bonded to another piece of glass, forming a complete chip.

The production process results in hollow channels in the glass substrate (Figure 1-9) where the channels can be used, for instance, as polymerase chain reaction platforms [Lagally *et al.*, 2001], electrophoresis channels [Harrison *et al.*, 1993], or pumps [Unger *et al.*, 2000].

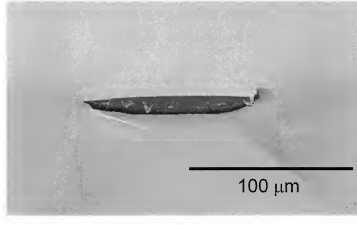

Figure 1-9. Microfabricated channel. The electron micrograph is a vertical cross-section of a channel that is approximately 100 μm wide by 10 μm deep. Notice the characteristic shaped channels produced by isotropic etching of glass. Also, no boundary is observed between the two pieces of glass after thermal bonding.

Both pressure-induced flow and electroosmotic flow (EOF) can be used to drive fluids through these channels, although EOF is the most common method for transporting reagents. Application of voltages to electrodes situated at the end of each channel allows facile control of flow rates in the channels. Since the bulk component of glass is SiO_2, at pH > 4 there is a large coverage of deprotonated silanol groups on channels allowing for high EOF and fast separations. The heat dissipation properties of glass and high surface area to volume ratios of channels allow the use of high voltages for separations. Furthermore, glass is optically transparent allowing conventional low-background optical detection schemes and fluorophores. However, when using electrokinetic transport, solutions must be amenable to EOF. In this way, there must be charge on the walls to

generate EOF, low salt buffers to ensure no Joule heating, and the surface of channels cannot change over time, that is, no adsorption of analytes onto channel walls or the channels cannot degrade over time.

Microfluidic Immunoassays

Several groups have used microfluidic chips to perform non-competitive and competitive immunoassays in both heterogeneous and homogeneous formats. Heterogeneous assays are defined here as immunoassays with one component, for example Ab, immobilized on a solid support such as beads or channel walls. This format of immunoassay has enabled detection of several biologically relevant molecules, including IgM [Eteshola and Leckband, 2001], anti-dinitrophenyl antibodies [Yang *et al.*, 2001], and C-reactive protein [Christodoulides *et al.*, 2002]. However, immobilization on surfaces can affect the natural binding of proteins, possibly decreasing the sensitivity and reproducibility of the assays. In addition to the problems of protein immobilization, incubation, washing, elution, and detection steps are needed in heterogeneous formats. These additional steps can increase the time needed for analysis, undesirable when attempting to monitor fast changes in analyte levels.

Homogeneous immunoassays, where mixing and separation of reagents are performed in solution phase, allows for more automated and rapid determination of analyte. Successful detection of cortisol [Koutny *et al.*, 1996], thyroxine [Schmalzing *et al.*, 1997], estradiol [Taylor *et al.*, 2001], anti-bovine serum albumin [Chiem and Harrison, 1997; Chiem and Harrison, 1998a], anti-theophylline [Chiem and Harrison, 1997], and theophylline [Chiem and Harrison, 1997] have been detected by mixing reagents offline and separation performed on a microfluidic chip. To increase reproducibility and make the system more automated, online mixing of reagents has also

been demonstrated for theophylline [Chiem and Harrison, 1998b], ovalbumin [Cheng *et al.*, 2001], anti-bovine serum albumin [Qiu and Harrison, 2001] and anti-estradiol [Cheng *et al.*, 2001]. For example, in the online assay for theophylline [Chiem and Harrison, 1998b], unlabeled and labeled theophylline were mixed in a 2.7 cm channel prior to mixing with anti-theophylline in an 8.2 cm channel. Separations were performed in approximately 30 s using an effective separation length of 5.6 cm.

This example indicates that performing immunoassays with online mixing is possible in chips; however, to apply this technique for measuring insulin release from an islet on a chip, several factors must be addressed. First, islets need to be housed in a physiological buffer to maintain viability. These types of buffers are not amenable to sampling by EOF due to high salt content. Second, continuous sampling of the physiological buffer should be performed to maintain high temporal resolution, unattainable with most separation schemes used with microfluidic chips. Finally, fast separations must be performed to maintain insulin*:Ab complex and to measure fast changes in insulin levels.

The ability to measure insulin release directly from an islet of Langerhans by a CE immunoassay on a microfluidic chip should allow for high temporal resolution monitoring. In addition, simultaneous assays of intracellular signals, such as $[Ca^{2+}]_i$ should be possible with an optically transparent substrate.

Outline of Dissertation

Chapter 2 examines the role of the insulin signaling pathway in glucose-, glyceraldehyde-, and arginine-stimulated secretion. The effect of the pathway was determined by comparing the number of exocytotic events from IRS-1 WT and KO β-

cells. In addition, differences in intracellular Ca^{2+} handling of IRS-1 WT and KO cells and islets were monitored using the ratiometric fluorescent dye, Fura-2.

Chapter 3 explores the effect of L-783,281, previously shown to increase glucose uptake in peripheral tissues and diabetic rodent models, on 5-HT secretion from pancreatic β-cells. The pathway by which the insulin mimetic induces an increase in $[Ca^{2+}]_i$ and secretion was examined using Fura-2 and amperometry with microelectrodes.

Chapter 4 investigates production and use of a microfabricated chip to monitor insulin secretion from an islet of Langerhans using a microchip immunoassay. To increase reproducibility, online mixing of Ab, insulin*, and insulin was performed by electrophoretically sampling solutions through a 4 cm heated reaction channel. Samples were injected onto a 1.5 cm separation channel and insulin*:Ab and insulin* was determined every 15 s.

Chapter 5 explains several methods used to perfuse islets on the chip. No method attempted was completely successful; however, explanations of why the methods failed are given.

Chapter 6 provides a summary of the work and presents ideas for future studies on both insulin signaling and microfluidic chips.

CHAPTER 2
ROLE OF IRS-1 IN GLUCOSE-, GLYCERALDEHYDE-, AND ARGININE-STIMULATED CALCIUM CHANGES AND SECRETION IN PANCREATIC BETA CELLS

Introduction

Insulin secreted from pancreatic β-cells is the primary regulator of euglycemia in mammals. Anaerobic respiration of glucose initiates an increase in intracellular Ca^{2+} concentration ($[Ca^{2+}]_i$), which precedes the release of insulin [Ravier *et al.*, 1999]. Application of glucose to beta cells also stimulates insulin signal transduction pathways as secreted insulin binds to insulin receptors [Rothenberg *et al.*, 1995; Velloso *et al.*, 1995]. Activation of insulin receptor tyrosine kinase phosphorylates insulin receptor substrates (IRS), which then bind Src Homology 2 domain-containing proteins, such as phosphatidylinositol 3-kinase (PI3-K) [Rothenberg *et al.*, 1995, Velloso *et al.*, 1995]. Although the insulin signaling pathway is intact in β-cells and becomes activated upon insulin secretion, the effect of the pathway on β-cell function is questionable. Recent evidence indicates that the autocrine action of insulin may provide positive feedback for insuliln production and secretion.

Stimulation of mouse β-cells with glucose or insulin increases the transcription of glucokinase, monitored by an increase in green-fluorescent protein expression [Leibiger *et al.*, 2001]. This increase in transcription is mediated by insulin receptors and involves PI3-K and protein kinase B. Transcription of pre(pro)insulin (PPI), the precursor to insulin, is initiated by insulin binding to insulin receptors and activating PI3-K [Leibiger *et al.*, 1998]. The increase in expression is not dependent on glucose metabolism, as

transcription of PPI increases independent of ATP production [da Silva Xavier *et al.*, 2000]. However, translation of PPI requires both metabolism of glucose and the autocrine action of insulin [Leibiger *et al.*, 2000]. It appears that initiation of the insulin receptor tyrosine kinase is needed for expression of insulin as a natural product insulin receptor activator, L-783,281, increases insulin gene transcription [Xu *et al.*, 2000].

Through genetic manipulation of islets of Langerhans and β-cell tumor lines, evidence is provided of a pivotal role in insulin signaling, in particular IRS-1, in regulating secretion and $[Ca^{2+}]_i$. Long term exposure (72 hours) of insulin to βTC6-F7 cells increases glucose-stimulated insulin secretion and increases basal $[Ca^{2+}]_i$ [Xu *et al.*, 2000]. Overexpression of IRS-1 in βTC6-F7 cells, termed βIRS1-A cells, increases basal $[Ca^{2+}]_i$ due to inhibition of sarco/endoplasmic reticulum Ca^{2+} ATPase (SERCA) pumps [Xu *et al.*, 1999]. Although glucose-stimulated Ca^{2+} levels are not significantly different in βIRS-1A cells compared to βTC6-F7 cells, glucose-stimulated fractional insulin secretion (amount of insulin released/amount of total insulin content) is increased from βIRS-1A cells in comparison to control cells [Xu *et al.*, 1999]. βIRS-1A cells also have decreased SERCA3 gene expression and an increase in fractional insulin secretion upon application of K^+ or leucine when compared to βTC6-F7 cells [Xu *et al.*, 2000]. Mutation of IRS-1 (Gly972→Arg) in a rodent insulinemia β-cell line does not effect phosphorylation of IRS-1 upon glucose or insulin stimulation; however, a decrease in binding of IRS-1 to PI3-K occurs with a concomitant decrease in insulin secretion compared to wild type control cells [Porzio *et al.*, 1999]. Human islets of Langerhans with the Gly972→Arg mutation in IRS-1 have a 2-fold increase in the number of apoptotic β-cells as human islets without the IRS-1 mutation [Federici *et al.*, 2001].

Deletion of IRS-1 in mouse islets and in a β-cell tumor line results in reduced insulin secretion upon stimulation with glucose and arginine compared to wild-type controls [Kulkarni *et al.*, 1999b]. In the same IRS-1 null β-cell line, insulin expression is decreased compared to control; however, the level of insulin can be partially restored by re-expression of IRS-1 [Kulkarni *et al.*, 1999b].

Direct stimulation of primary pancreatic β-cells initiates an increase in $[Ca^{2+}]_i$ and insulin secretion via activation of insulin receptors [Aspinwall *et al.*, 1999b]. IRS-1, PI3-K, and protein kinase C are necessary for insulin-stimulated secretion. Insulin-stimulated Ca^{2+} increases are dependent on IRS-1 and PI3-K and occur presumably through an interaction of IRS-1 with SERCA pumps [Aspinwall *et al.*, 2000; Xu *et al.*, 1999], although the Ca^{2+} responses are sensitive to nicotinic acid-adenine dinucleotide phosphate in human pancreatic β-cells [Johnson and Misler, 2002].

The *in vivo* importance of autocrine insulin signaling is found in mice with either tissue-specific or whole animal genetic deletions. β-cell insulin receptor knockout mice have disrupted first phase insulin secretion upon a glucose challenge, similar to that observed in type 2 diabetics [Kulkarni *et al.*, 1999a]. In IRS-1 null mice, increases in plasma insulin levels and β-cell mass are observed compared to control mice [Araki *et al.*, 1994; Kubota *et al.*, 2000]. IRS-2 mice are diabetic due to a 50-80% reduction in β-cell mass [Withers *et al.*, 1998; Kubota *et al.*, 2000]. However, when examining isolated islets from IRS-2 null mice, glucose stimulation results in increased insulin secretion compared to control islets, while islets isolated from IRS-1 knockout mice secrete less insulin in response to glucose compared to control islets [Kubota *et al.*, 2000]. These

results indicate that IRS-2 plays a role in maintaining β-cell growth while IRS-1 is involved in insulin secretion [Sesti *et al.*, 2001].

Defects in insulin receptors, IRS-1, and PI3-K, which help regulate insulin production, Ca^{2+} homeostasis, and insulin secretion in pancreatic β-cells, are also observed in peripheral tissues of type 2 diabetics [Sesti *et al.*, 2001]. Due to the similarities in the insulin signal transduction pathways in β-cells and peripheral tissues, insulin signaling has been postulated as a link between two hallmarks of type 2 diabetes: insulin resistance in peripheral tissues and defective insulin secretion from pancreatic beta cells [Taylor, 1999; Hussain, 1999; Rutter, 1999; Withers and White, 2000].

Based on the aforementioned reports, defects in the insulin signaling pathway would lead to defective insulin secretion; however, other reports have indicated that released insulin has an inhibitory effect on glucose-stimulated insulin secretion [Ammon and Verspohl, 1976; Iversen and Miles, 1971; Liljenquist *et al.*, 1978; Sodoyez *et al.*, 1969, Khan *et al.*, 2001] and that defects in this pathway would lead to increased insulin secretion similar to that observed during insulin resistance [Khan *et al.*, 2001]. These results have been explained in two ways [Leibiger *et al.*, 2002]. The first explanation is the timeframe in which insulin is exposed to β-cells or islets. At short intervals, insulin may induce insulin secretion, while longer exposures could inhibit insulin secretion. The second explanation for the differences in results arises from numerous experimental protocols each research group has used, leading to conflicting reports.

To obtain a better understanding of how defects in the insulin signaling pathway effect insulin release and intracellular Ca^{2+} handling in single β-cells, amperometry and fluorescence measurements were used to quantitate secretory events and $[Ca^{2+}]_i$ from

IRS-1 knock out (KO) and wild type (WT) primary β-cells and islets of Langerhans. Using amperometry with microelectrodes, the number of exocytotic events were quantified and compared from KO and WT cells upon stimulation with glucose, glyceraldehyde, and arginine. Intracellular Ca^{2+} handling in single cells and islets of Langerhans was investigated by Fura-2 fluorescence upon application of the same stimuli as in secretion measurements.

Experimental

Chemicals and Reagents

Bovine insulin, type XI collagenase, and (N-[2-hydroxyethyl]piperazine-N'-[2-ethanesulfonic acid]) (HEPES) were purchased from Sigma (St. Louis, MO) and used without further purification. All chemicals for cell culture were obtained from Life Technologies, Inc. (Carlsbad, CA). Fura-2 acetoxymethylester was from Molecular Probes (Eugene, OR). All other chemicals were from Fisher (Pittsburgh, PA) and of highest purity available.

Cell Culture and Isolation

Homozygous IRS-1 -/- (knockout, KO) and +/+ (wildtype, WT) mice (Araki *et al.*, 1994) were obtained from Dr. Rohit N. Kulkarni and Dr. C.R. Kahn, Harvard Medical School. Islets were isolated by ductal injection of 3-4 mL collagenase type XI, separated from exocrine tissue by a Ficoll gradient, and handpicked under a stereomicroscope. Single cells were procured by shaking islets in a dilute (0.025%) trypsin/EDTA mixture for 6 min in a 37 ºC water bath. For electrochemical experiments, dispersed cells were plated on Nunclon dishes. For intracellular Ca^{2+} measurements, dispersed cells or single islets were plated on Corning no. 0 coverslips. Both cells and islets were incubated in RPMI 1640 containing 10% fetal bovine serum, 100 units/mL

penicillin, 100 μg/mL streptomycin, and kept in a humidified atmosphere at 37 °C. Experiments were performed on cells and islets 2-4 days following isolation. All experiments were performed at 37 °C in a modified Kreb's ringer buffer (KRB), pH 7.4, which consisted of (in mM): 118 NaCl, 5.4 KCl, 2.4 $CaCl_2$, 1.2 $MgSO_4$, 1.2 KH_2PO_4, 3 *d*-glucose, 20 HEPES. Stimulant solutions were composed of 18 mM *d*-glucose, 18 mM glyceraldehyde, and 18 mM arginine in KRB. In experiments noted, 18 mM arginine was applied to cells bathed in KRB supplemented with 11 mM glucose.

Amperometric Measurements

Carbon fiber microelectrodes were constructed as described previously [Kelly and Wightman, 1986]. A 9 μm diameter carbon fiber (P-55S, Amoco Performance Products) was aspirated into a glass pipette and pulled using a microelectrode puller (Narishige, Tokyo, Japan). Exposed carbon fiber was cut flush with the glass pipette using a scalpel under a stereomicroscope, sealed with epoxy, and allowed to cure overnight. Prior to experiments, electrodes were polished at a 45° angle (Sutter Instruments, BV-10) and sonicated in ethanol and water.

Cell media was replaced with media that contained 0.5 mM 5-hydroxytryptamine (5-HT) and incubated at 37 °C, 5% CO_2 overnight. Beta cells accumulate 5-HT into insulin secretory vesicles [Falck and Hellman, 1963; Hutton *et al.*, 1983] and detection of 5-HT has been used as a method to monitor secretory events induced by a stimulus [Zhou and Misler, 1996; Smith *et al.*, 1995; Takahashi *et al.*, 1997]. In addition, 5-HT detection has been shown to be a reliable marker of insulin secretory events [Aspinwall *et al.*, 1999a]. For measurement of secretion, media with 5-HT was removed and cells washed with three aliquots of KRB and held at 37 °C on the stage of an inverted Zeiss Axiovert

100 microscope. A carbon fiber microelectrode was placed ~ 1 μm above a cell and held at 0.65 V *vs.* a sodium-saturated calomel reference electrode. Current from the microelectrode was amplified using an Axon AI-403 amplifier (Axon Instruments, Union City, CA), low pass filtered at 100 Hz, and collected at 500 Hz. A personal computer (Gateway 2000 P5-166) was used to collect data via a data acquisition board (Axon Instruments, DigiData 1200B). To induce exocytosis, a glass pipette containing a stimulant solution was placed approximately 30 μm away from a cell and a pressure of 3 psi was used to expel stimulant from the pipette for 40 s. Single cells amperometric data was recorded for 4 min. A control stimulation of KRB without secretagogue was applied to a cell if secretory events were detected to ensure spikes in current were not due to an artifact of measurement.

Fura-2 Ca^{2+} Measurements

Cells and islets used for Ca^{2+} measurements were incubated for 30 min in 2 μM Fura-2 acetoxymethylester in the cell culture media and maintained at 37 °C, 5% CO_2. After incubation, cells were washed and placed in a 2 mL coverslip holder with KRB and held at 37 °C on the stage of a Zeiss Axiovert 100 microscope. For measurement of Fura-2 fluorescence, a SPEX CMX cation measurement system with DM3000M data acquisition software (Instruments S.A. Group, Edison, NJ) was used. Briefly, light from a 150 W Xe arc lamp was directed to two monochromators at 340 nm and 380 nm and a chopper used to sequentially select excitation light. Incident light was directed into the back of a 40x, 1.3 numerical aperture objective via a 400 nm longpass mirror. Fura-2 emission from a cell was collected with the same objective, passed through the 400 nm longpass mirror, a 510 $\pm$ 10 nm bandpass filter, spatial filter (20 μm for single cells and

200 μm for islets), and finally to a photomultiplier tube. The emission light generated from 340 and 380 nm excitation was collected at 1 Hz and the quantitation of Fura-2 fluorescence was performed as described elsewhere [Grynkiewicz *et al.*, 1985]. Stimulation of single cells with glucose, glyceraldehyde, and arginine was performed as described for electrochemical measurements. To stimulate islets, a perfusion system was used that allowed the exchange of KRB with KRB that contained 10 mM glucose. All perfusion solutions were heated to 37 °C online prior to entering the coverslip holder. Complete washout of the coverslip holder was accomplished in 30 s.

Statistical Analysis

All data are reported as mean $\pm$ standard error of the mean. Statistical differences between means were evaluated using a two-tailed Student's t test. Differences were reported as significant when $p < 0.05$.

Results and Discussion

Glucose-Initiated Ca^{2+} Changes and Secretion

Preliminary experiments were to investigate the role of IRS-1 in Ca^{2+} handling in isolated primary pancreatic β-cells. As seen in Figure 2-1, application of 18 mM glucose increased $[Ca^{2+}]_i$, measured by an increase in Fura-2 fluorescence, in IRS-1 WT and KO β-cells. Onset of the stimulated Ca^{2+} level was designated as the time when the Ca^{2+} concentration increased to three times the standard deviation of the basal level, while latency was described as the time from application of stimulant to the first significant Ca^{2+} level. Duration of Ca^{2+} changes were determined by the time the from the onset of stimulated level to the time when the Ca^{2+} level decreased below significance, or when the Ca^{2+} recording was done, whichever occurred first. In all experiments, stimulant was

applied 30 s after the recording began and the recording stopped 570 s from onset of stimulation.

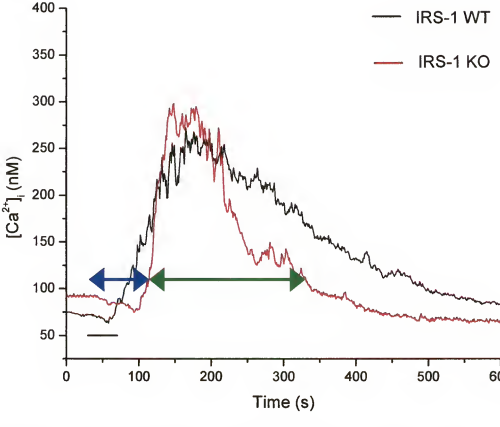

Figure 2-1. Glucose-stimulated Ca^{2+} change in an IRS-1 WT and KO β-cell. Representative Fura-2 trace from application of 18 mM glucose to IRS-1 WT (black trace) and KO (red trace) β-cell. Blue arrow indicates latency to the increase in Ca^{2+} of the KO β-cell, whereas the green arrow signifies the duration of the stimulated Ca^{2+} level. Significant differences ($p < 0.05$) are observed for latency and duration of stimulated levels. The bar underneath traces indicates duration of stimulation with 18 mM glucose.

The latency of the Ca^{2+} increase was significantly increased in IRS-1 KO β-cells compared to WT β-cells (270 $\pm$ 61 s, n = 7 KO β-cells *vs.* 81 $\pm$ 17 s, n = 7 WT β-cells, Figure 2-2). Duration of the stimulated Ca^{2+} signal was also significantly different as WT β-cells maintained stimulated Ca^{2+} levels for 425 $\pm$ 35 s and KO β-cells responded

for 184 ± 15 s (Figure 2-3). Similar to other reports of altered basal Ca^{2+} levels upon overexpression of insulin receptors and IRS-1 [Xu *et al.*, 1999], basal Ca^{2+} concentrations

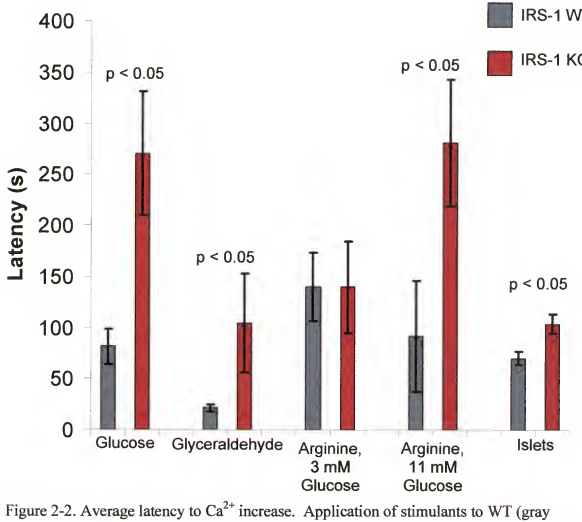

Figure 2-2. Average latency to Ca^{2+} increase. Application of stimulants to WT (gray bars) and KO (red bars) induced significant differences in the latency to the stimulated Ca^{2+} level. Differences in latency may be due to IRS-1 interaction with proteins in the cell, as hypothesized in the text.

were significantly different in β-cells tested for glucose (90 ± 21 nM for IRS-1 WT and 146 ± 19 nM for KO β-cells, Figure 2-4); however, the average basal level in all WT cells was not significantly different from the average basal level in KO β-cells (Figure 2-

4). No statistical difference was observed in the maximum glucose-stimulated Ca^{2+} levels (65 $\pm$ 20 % in IRS-1 WT cells and 52 $\pm$ 21 % in IRS-1 KO cells), expressed as a

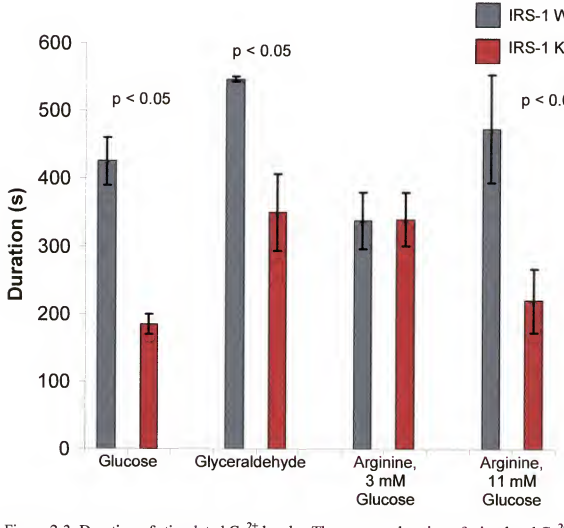

Figure 2-3. Duration of stimulated Ca^{2+} levels. The average duration of stimulated Ca^{2+} levels are shown for IRS-1 WT (gray bars) and IRS-1 KO (red bars) β-cells. The duration of stimulated levels in islets is not shown since perfusion of glucose occurred during the entire recording time.

percent increase over basal to minimize any variation in basal Ca^{2+} concentration (Figure 2-5). These results indicate that IRS-1 may help to regulate the time course of changes in $[Ca^{2+}]_i$, such as latency and maintenance of stimulated Ca^{2+} levels; however, an increase

in stimulated intracellular Ca^{2+} levels via an IRS-1 mechanism was not detected. This conclusion is supported by a report in which peak glucose-stimulated Ca^{2+} increases were not significantly different in β-cells that overexpressed IRS-1 compared to control cells

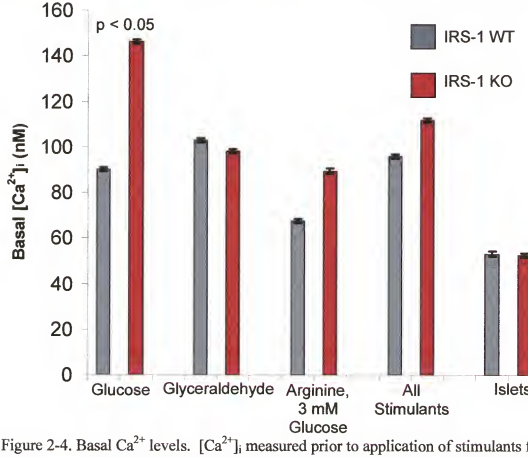

Figure 2-4. Basal Ca^{2+} levels. $[Ca^{2+}]_i$ measured prior to application of stimulants for IRS-1 WT (gray bars) and IRS-1 KO bars. Arginine with 11 mM glucose was not included as the elevated glucose level increased $[Ca^{2+}]_i$. The average of all basal values reported is listed under "All Stimulants" with n = 18 WT β-cells and n = 20 KO β-cells.

[Xu *et al.*, 1999]. Insulin-stimulated Ca^{2+} increases were characterized as having a long and sustained plateau [Aspinwall *et al.*, 2000], similar to the observed increase in duration in IRS-1 WT β-cells compared to KO β-cells.

Due to altered Ca^{2+} handling in KO β-cells, the effect of IRS-1 on glucose-induced exocytosis was determined at the single cell level using amperometry with

microelectrodes. As seen in Figure 2-6, application of 18 mM glucose to IRS-1 WT and KO β-cells resulted in current spikes in the amperometric trace indicative of single exocytotic events. To quantitate the amount of exocytotic events, current spikes were counted for each trace and plotted as the number of exocytotic events per stimulation

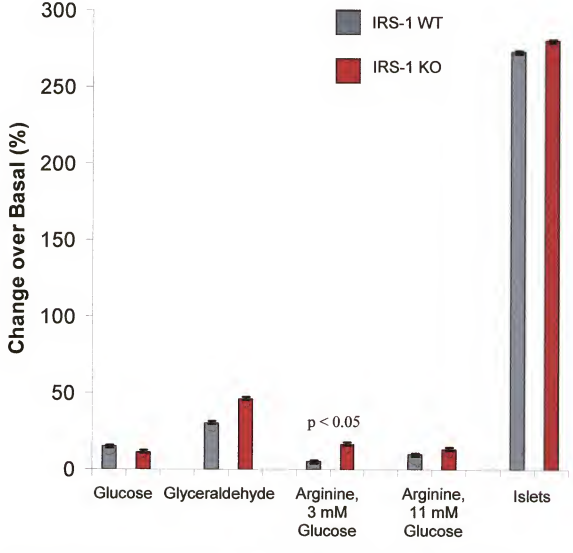

Figure 2-5. Maximum Ca^{2+} increase upon stimulation. The average maximally-stimulated Ca^{2+} increase is reported for IRS-1 WT (gray bars) and IRS-1 KO (red bars) β-cells. Values are reported as percent change over basal to minimize variations in basal concentrations.

(Figure 2-7). There was a statistical difference in the number of secretory events induced by glucose from KO β-cells (7 ± 1, n = 6) compared to WT β-cells (14 ± 1, n = 4 cells).

A reduction in glucose-induced secretion in IRS-1 KO β-cells is in agreement with previous reports using Gly972→Arg IRS-1 tumor cells [Porzio *et al.*, 1999] and null

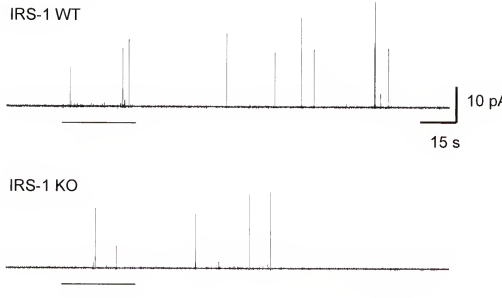

Figure 2-6. Glucose-stimulated secretion. IRS-1 WT (top trace) and IRS-1 KO (bottom trace) β-cells were stimulated with 18 mM glucose for the time indicated by the bar under the traces. Significantly fewer secretory events, seen as spikes in current, were observed in IRS-1 KO β-cells.

tumor cells and islets of Langerhans [Kulkarni *et al.*, 1999b]. Activation of insulin signaling has been shown to increase the transcription of glucokinase through a PI3-K mediated pathway (Leibiger *et al.*, 2001), which may allow more secretion from WT β-cells. However, transcription of glucokinase took 60 min to increase after stimulation with insulin or glucose, well after the time in which the amperometric experiments in this report were performed.

Glucose-Induced Ca^{2+} Changes in Islets of Langerhans

Upon application of glucose to islets of Langerhans, intracellular Ca^{2+} oscillates with a slow and a fast component [Gilon and Henquin, 1995]. Slow oscillations generally have periods greater than 100 s, while fast oscillations have periods less than 20 s and occur superimposed on slow oscillations or on a sustained increase in Ca^{2+}. Increases in intracellular Ca^{2+} are believed to drive insulin secretion [Jonas *et al.*, 1998]

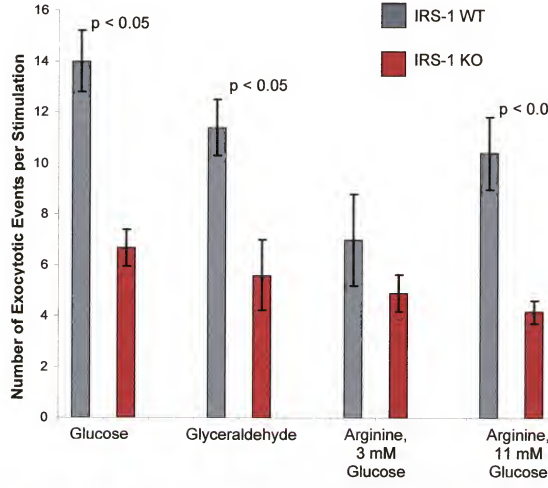

Figure 2-7. Number of exocytotic events induced by various stimuli. Average number of exocytotic events was quantified and compared between IRS-1 WT (gray bars) and IRS-1 KO (red bars) β-cells. Only spikes with S/N > 10 were counted.

and oscillatory insulin secretion from islets of Langerhans correlates with slow oscillations in $[Ca^{2+}]_i$ [Gilon and Henquin, 1995]. Altered insulin oscillations are observed in type 2 diabetics [Pørksen, 2002] and therefore the mechanisms involved in the oscillations of both Ca^{2+} and insulin are important to determine. Based on the effect of IRS-1 in single cells, oscillations of Ca^{2+} were studied using IRS-1 WT and KO islets of Langerhans.

Perfusion of islets with 18 mM glucose evoked increases in Ca^{2+} in both WT and KO islets; however, different patterns of oscillations were observed between the sets of islets. In 5 of 6 WT islets, slow oscillations of Ca^{2+} with fast oscillations superimposed were observed, whereas slow oscillations were observed in 1 of 6 IRS-1 KO islets. The majority of KO islets oscillated irregularly or with only fast oscillations (See Figure 2-8 for examples). Basal and stimulated $[Ca^{2+}]_i$ were statistically similar in IRS-1 WT and KO islets (Figure 2-4 and 2-5, respectively). Similar to single cell measurements, the latency of the Ca^{2+} increases (Figure 2-2) were significantly less in IRS-1 WT (70 ± 6 s) compared to KO islets (104 ± 9 s). The slope of the initial increase in Fura-2 fluorescence upon stimulation with glucose was less in KO islets (1.29 ± 0.22 nM/s versus 2.04 ± 0.48 nM/s *vs.*, for IRS-1 KO and WT islets, respectively), although the difference was not statistically significant. There has been a report of insulin disrupting Ca^{2+} oscillations in islets by opening ATP-sensitive K^+ channels and hyperpolarizing β-cells [Khan *et al.*, 2001]. The opening of ATP-sensitive K^+ channels was only reported at high glucose concentrations making the effect of exogenous insulin difficult to interpret as the high glucose concentration also causes release of insulin from β-cells.

Glyceraldehyde-Induced Ca^{2+} Changes and Secretion

Glyceraldehyde is phosphorylated via triose kinase to glyceraldehyde-3-phosphate upon entering β-cells. As seen in Figure 2-9, glyceraldehyde-3-phosphate is the substrate for glyceraldehyde-3-phosphate dehydrogenase, and can subsequently proceed through glycolysis [Alcazar *et al.*, 1995]. ATP is produced via the abridged glycolysis pathway and the citric acid cycle, which initiates insulin secretion through conventional means. Glyceraldehyde is often used as a stimulant to bypass glucokinase, the rate-limiting step

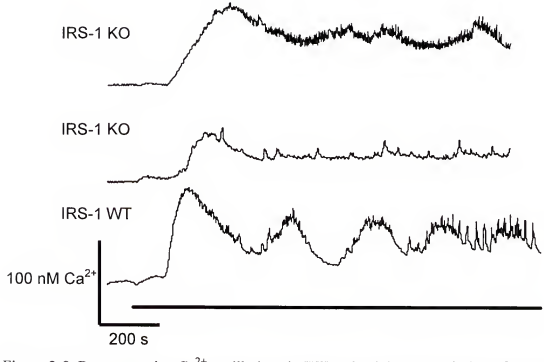

Figure 2-8. Representative Ca^{2+} oscillations in WT and KO islets. Perfusion of 10 mM glucose resulted in oscillations in $[Ca^{2+}]_i$ in islets of Langerhans. IRS-1 KO islets show altered Ca^{2+} oscillations (top two traces) compared to WT islets (bottom trace). Application of glucose is indicated by the line under the WT trace.

in metabolism of glucose [Liang and Matschinsky, 1994]. Consequently, stimulation with glyceraldehyde should increase ATP levels independent of the normal kinetics of metabolism.

Again using Fura-2 to monitor $[Ca^{2+}]_i$ in β-cells, application of 18 mM glyceraldehyde induced an increase in $[Ca^{2+}]_i$ in both IRS-1 WT and KO β-cells (Figure 2-10). As seen in figures 2-4 and 2-5, basal (102 ± 18 nM, n = 6 WT *vs*. 98 ± 19 nM, n =

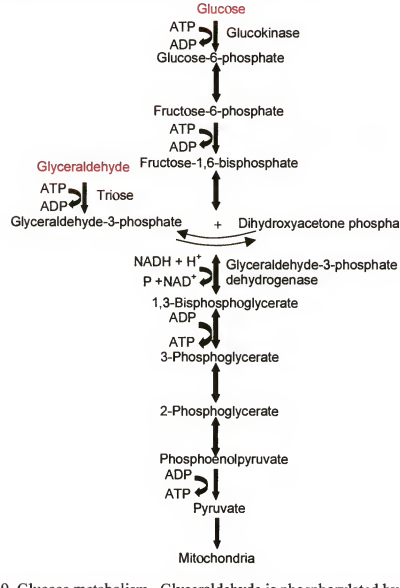

Figure 2-9. Glucose metabolism. Glyceraldehyde is phosphorylated by triose kinase to glyceraldehyde-3-phosphate bypassing glucokinase. Upon glyceraldehyde-3-phosphate entering glycolysis, ATP is produced stimulating insulin secretion via the conventional mechanism.

6 KO) and stimulated Ca^{2+} increases (30 ± 8 % and 58 ± 11 % for WT and KO, respectively) were not significantly different between cell types. However, latency of

Ca^{2+} changes was significantly different. In IRS-1 WT β-cells, latency was 21 ± 3 s while KO β-cells had a latency of 42 ± 6 s (Figure 2-2). Wildtype β-cells showed a significantly increased duration of stimulated Ca^{2+} levels, 547 ± 4 s, compared to KO β-cells, 376 ± 61 s (Figure 2-3).

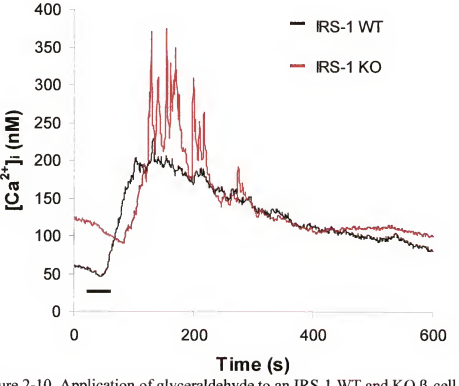

Figure 2-10. Application of glyceraldehyde to an IRS-1 WT and KO β-cell. 18 mM glyceraldehyde was applied for the duration indicated by the bar under the traces and $[Ca^{2+}]_i$ monitored by Fura-2 fluorescence. Statistical differences were observed in the latency to an increase in stimulated Ca^{2+} levels and duration of stimulated Ca^{2+} levels.

Further experiments were performed to determine the effect of glyceraldehyde on inducing secretion from IRS-1 WT and KO β-cells. Application of 18 mM glyceraldehyde to IRS-1 WT β-cells resulted in 10 ± 1 (n = 5 cells) secretory events detected. In comparison, stimulation with glyceraldehyde resulted in 4 ± 1 (n = 6 cells) exocytotic events detected from IRS-1 KO β-cells (Figure 2-7). These secretory differences provide evidence that glucokinase is not affecting the amount of secretion

because glyceraldehyde stimulates secretion independently of glucokinase, therefore, differences in secretory amounts should be distal to this rate-limiting enzyme.

Arginine-Induced Secretion and Ca^{2+} Changes

The mechanism by which arginine initiates insulin secretion remains under investigation, although several hypotheses have been proposed to explain its effect on inducing increases in $[Ca^{2+}]_i$ and secretion from β-cells [Thams and Capito, 1999]. One hypothesis is that depolarization of the cell membrane occurs by the electrogenic transport of arginine into the β-cell. Electrogenic transport is defined as the movement of a net electrical charge across the membrane [Zubay, 1998]. Depolarization of the cell leads to opening of voltage-gated Ca^{2+} channels, initiating secretion [Blachier *et al.*, 1989; Sener *et al.*, 2000]. Another hypothesis is that an increase in intracellular arginine increases the production of nitric oxides, which then potentiate insulin secretion [Schmidt *et al.*, 1992]. Although the mechanism of arginine-induced changes remains controversial, the ability of arginine to increase $[Ca^{2+}]_i$ and cause secretion, independent of glycolysis, is clear [Kulkarni *et al.*, 1999b].

Stimulation with 18 mM arginine in the presence of 3 mM glucose induced statistically different maximum Ca^{2+} increases in IRS-1 KO β-cells (17 ± 7 %, n = 7) compared to IRS-1 WT β-cells (5 ± 1 %, n = 6), Figure 2-5. Latency, duration, and basal Ca^{2+} changes were similar in WT and KO β-cells (Figures 2-2, 2-3, and 2-4, respectively). In the presence of 11 mM glucose, application of 18 mM arginine to IRS-1 WT β-cells resulted in a significantly different latency (92 ± 54 s, n = 4, Figure 2-2) and duration of stimulated Ca^{2+} levels (474 ± 80 s, Figure 2-3) compared to KO β-cells (281

$\pm$ 62 s and 220 $\pm$ 47 s for latency and duration, respectively, n = 4). Maximum-stimulated Ca^{2+} levels (Figure 2-5) were not statistically different in WT and KO β-cells.

There was no significant difference in the number of exocytotic events induced by 18 mM arginine in the presence of 3 mM glucose (5 $\pm$ 1, n = 10 KO cells *vs.* 7 $\pm$ 2, n = 5 WT cells, Figure 2-7). However, in the presence of 11 mM glucose, application of 18 mM arginine to IRS-1 KO β-cells resulted in a significant decrease in the number of secretory events detected compared to WT cells (4 $\pm$ 1, n = 7 KO cells *vs.* 10 $\pm$ 1, n = 5 WT cells) (see Figure 2-11). The similar number of exocytotic events observed in 3 mM

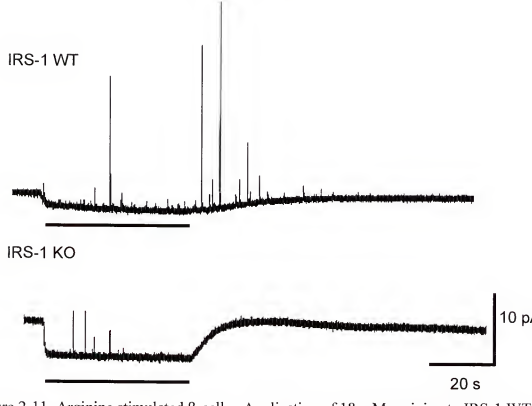

Figure 2-11. Arginine stimulated β-cells. Application of 18 mM arginine to IRS-1 WT (top trace) and KO (bottom trace) β-cells in the presence of 11 mM glucose. Duration of arginine stimulation is indicated by the bar under the traces. A significantly decreased number of exocytotic events were observed in the KO cells compared to WT cells.

glucose is consistent with the hypothesis that arginine is not an effective initiator of insulin secretion, but rather potentiates insulin release through membrane depolarization, an effect observed in mouse islets of Langerhans [Thams and Capito, 1999].

Effect of IRS-1 in Ca^{2+} Handling

In islets of Langerhans and β-cell tumor lines an intact insulin signaling pathway is needed for maintaining β-cell growth [Withers and White, 2000], insulin production [Kulkarni *et al.*, 1999b], and insulin secretion [Porzio *et al.*, 1999; Kulkarni *et al.*, 1999b]. Intracellular Ca^{2+} also appears to be affected by the insulin signaling pathway, although the cause for changes in this secondary messenger is unclear. Basal Ca^{2+} levels were similar in IRS-1 WT and KO β-cells. Application of glucose, glyceraldehyde, and arginine results in similar maximum increases in $[Ca^{2+}]_i$ for IRS-1 KO cells in comparison to the wildtype controls. However, for all stimulants tested, except arginine in the presence of 3 mM glucose, KO β-cells show an increase in latency to Ca^{2+} increases and a shorter duration of stimulated Ca^{2+} levels than WT β-cells.

The mechanism underlying the changes in $[Ca^{2+}]_i$ was not investigated, but other reports have suggested an interaction of IRS-1 with SERCA pumps because insulin-induced Ca^{2+} changes are sensitive to thapsigargin [Xu *et al.*, 1999; Aspinwall *et al.*, 2000]. Evidence for an interaction of IRS-1 and SERCA pumps is found in rat muscle and heart tissue where IRS-1 binds SERCA pumps in an insulin dose-dependent manner [Algenstaedt *et al.*, 1997]. Insulin-stimulated Ca^{2+} increases are also sensitive to nicotinic acid-adenine dinucleotide phosphate, produced via activation of the adenyl cyclase, CD-38 [Johnson and Misler, 2002]. Thus, a novel pathway of Ca^{2+} release in β-cells may be induced upon activation of the insulin signaling pathway.

The reduced latency observed in WT β-cells may be due to a slight basal inhibition of SERCA pumps or other Ca^{2+} dependent proteins by IRS-1. Upon opening of voltage-dependent Ca^{2+} channels in WT cells, the initial Ca^{2+} that enters the cell cannot be taken up by SERCA pumps or Ca^{2+} dependent proteins due to this inhibition. In IRS-1 KO cells, SERCA pumps or Ca^{2+}-dependent proteins are not inhibited and may buffer the initial Ca^{2+} increase delaying an increase in Fura-2 fluorescence. Therefore, the increase to a stimulated Ca^{2+} level is faster in WT β-cells than in KO β-cells. This explanation is supported by the aforementioned IRS-1 inhibition of SERCA pumps in both cardiac and muscle tissues. Also, IRS-1 binds calmodulin, a Ca^{2+}-sensitive protein, in a Ca^{2+}-dependent manner [Li *et al.*, 2000].

The increased duration of stimulated Ca^{2+} levels in IRS-1 WT β-cells could also be explained by IRS-1 inhibition of SERCA pumps. At the end of a glucose challenge, in WT cells, Ca^{2+} may be released from the endoplasmic reticulum via passive diffusion out of SERCA pumps due to IRS-1 inhibition. In IRS-1 KO β-cells, Ca^{2+} can be released immediately from the endoplasmic reticulum (ER) since there is no inhibition of SERCA pumps, thus decreasing the time of stimulated Ca^{2+} levels. One necessary experiment to verify this hypothesis would be the use of an ER-specific Ca^{2+} indicator, such as fluo-5N [Haugland, 1996], which would allow any differences in the flux of Ca^{2+} into and out of the ER to be determined.

Ca^{2+} handling in IRS-1 KO and WT islets of Langerhans

Application of glucose to IRS-1 WT islets results in slow oscillations with fast oscillations superimposed. These patterns of oscillations are typical in islets perfused with glucose [Liu *et al.*, 1998]; however, KO islets show mostly fast oscillations of Ca^{2+}

upon a glucose challenge suggesting a role of IRS-1 in slow oscillations. The slope and latency of the initial increase in Ca^{2+} is decreased in KO islets, possibly due to an increased buffering action by ER or Ca^{2+}-dependent proteins, as mentioned previously.

There have been reports that application of insulin to islets of Langerhans in elevated glucose media results in a loss of Ca^{2+} oscillations via a PI3-K dependent mechanism [Khan *et al.*, 2001], while others report no effect of exogenous insulin on insulin release from islets [Zawalich and Zawalich, 2002]. It was also shown by patch clamp that single cells in islets were hyperpolarized by the insulin application [Khan *et al.*, 2001]. These results are difficult to interpret at the single islet level. Perhaps interislet communication plays a role in the different patterns of oscillations seen in KO islets. It has been suggested that inhibition of IRS-1 increases glucose-stimulated insulin secretion due to reduced glucagon clearance, illustrating the complexities of signaling in islets [Araujo *et al.*, 2002]. Thus, deficiencies of IRS-1 in other cell types of the islet may also contribute to the disrupted oscillations of Ca^{2+} in IRS-1 KO islets.

Reduced Secretion in IRS-1 KO β-Cells

Secretory events are detected from IRS-1 WT and KO β-cells upon application of glucose, glyceraldehyde, and arginine. However, the number of release events detected is significantly less in KO β-cells compared to WT β-cells. This finding is significant since the three pathways of stimulation are distinct and IRS-1 is not thought to be involved in any of the mechanisms. Therefore, the disparity in the number of secretory events in IRS-1 KO and WT β-cells is likely due to a difference after the initial release of insulin, not because of differences in the mechanism by which secretion is initiated. The reduced secretion in KO β-cells may result from a disruption of the insulin signaling pathway.

Other reports provide evidence for this hypothesis, for example, disruption of β-cell insulin receptors *in vivo* [Kulkarni *et al.*, 1999a], IRS-1 in pancreatic islets of Langerhans [Kulkarni *et al.*, 1999b; Kubota *et al.*, 2000], and IRS-1 in β-cell tumor lines [Porzio *et al.*, 1999; Kulkarni *et al.*, 1999b] results in diminished glucose-stimulated insulin secretion in comparison to wildtype controls. In addition, disruption of insulin signaling decreases K^+-induced secretion [Aspinwall *et al.*, 1999b].

As mentioned previously, IRS-1 deletion has been shown to increase glucose-stimulated insulin secretion in mouse islets of Langerhans [Araujo *et al.*, 2002]. Although the positive effect of insulin on insulin secretion was not disputed, a role of IRS-1 deletion in α- and δ-cells in regulating insulin release was reported. Several other effects of IRS-1 deletion on protein transcription and insulin content should also be considered when examining our results. Insulin is known to increase the transcription and translation of insulin, presumably to maintain and replenish any stores depleted [Leibiger *et al.*, 1998; Leibiger *et al.*, 2000]. However, the time reported for the onset of transcription was over 60 min and the time for the amperometric recordings reported here were 4 min. Thus, any insulin produced in the WT cells due to stimulation with glucose, glyceraldehyde, or arginine should not be involved with the secretory events detected.

Conclusions

Stimulation of pancreatic β-cells isolated from IRS-1 WT and KO mice with various secretagogues induces fewer exocytotic events from KO β-cells than with WT β-cells. The difference in the number of exocytotic events may be due to a defect in the positive feedback loop of insulin signaling. This hypothesis is strengthened by the use of multiple stimuli that initiate secretion via different mechanisms. In addition, a difference

in Ca^{2+} handling is observed in IRS-1 KO β-cells, which may be due to IRS-1 interacting with various proteins in the cell. These results lend evidence to the hypothesis that defects in insulin signaling proteins may create a link between insulin resistance in peripheral tissues and defective insulin secretion from pancreatic β-cells.

CHAPTER 3
EFFECT OF THE INSULIN MIMETIC L-783,281 ON INTRACELLULAR CALCIUM CONCENTRATION AND SECRETION FROM PANCREATIC BETA CELLS

Introduction

L-783,281 is a recently isolated fungal metabolite that has insulin mimetic properties [Zhang *et al.*, 1999; Weber *et al.*, 2000]. This compound stimulates insulin receptor tyrosine kinase (IRTK) activity in CHO cells that overexpress human insulin receptors by binding to the β-subunit of the insulin receptor [Zhang *et al.*, 1999]. L-783,281 induced activation of IRTK stimulates downstream signaling proteins including insulin receptor substrate-1 (IRS-1), Akt, and phosphatidylinositol 3-kinase (PI3-K). L-783,281 also induces glucose uptake in a dose dependent manner from rat primary adipocytes and soleus muscle tissue from lean mice. *In vivo* administration of L-783,281 results in correction of hyperglycemia in *db/db* mice and improves glucose tolerance in *ob/ob* mice. Thus, L-783,281 is an insulin mimetic in that it initiates insulin signaling and has antidiabetic effects in rodent models of insulin resistance.

The focus of prior studies with L-783,281 has been on its activation of IRTK and glucose uptake in non-endocrine cells; however, the presence of functional insulin receptors on pancreatic β-cells [Verspohl and Ammon, 1980; Harbeck *et al.*, 1996] suggests that L-783,281 could activate IRTK in β-cells. β-cell IRTK activity is initiated *in vitro* by insulin binding to insulin receptors after its secretion [Rothenberg *et al.*, 1995]. This activity results in phosphorylation of insulin receptor substrates [Velloso *et al.*, 1995] and PHAS-I (an inhibitor of mRNA cap-binding protein, eukaryotic initation

factor-4E) [Xu *et al.*, 1998]. In addition, maximal insulin secretion corresponds with maximal production of phosphatidylinositol 3,4,5-trisphosphate, a major product of PI3-K activity [Alter and Wolf, 1995]. Insulin signaling in the β-cell has physiological responses that are mediated by different insulin receptor substrates. IRS-2 has been implicated in maintaining β-cell growth and development, evidenced by β-cell hypoplasia and a corresponding decrease in insulin secretion in IRS-2 null mice [Withers *et al.*, 1998; Withers *et al.*, 1999; Kubota *et al.*, 2000]. Signaling through IRS-1 in β-cells is also important as it appears to maintain intracellular insulin content and synthesis [Leibiger *et al.*, 1998], regulate Ca^{2+} homeostasis [Xu *et al.*, 2000], and promote insulin secretion [Aspinwall *et al.*, 2000]. Activation of insulin receptor signaling in βTC6-F7 tumor β-cell lines by overexpression of IRS-1 or insulin receptors results in an increase in fractional insulin secretion and an increase in basal intracellular Ca^{2+} concentration ($[Ca^{2+}]_i$) [Xu *et al.*, 1999]. In RIN 1046-38 β-cells overexpressing a Gly972→Arg mutant IRS-1, a decrease in binding of IRS-1 to the regulatory subunit of PI3-K is observed, and glucose- and sulfonylurea-stimulated insulin secretion is diminished [Porzio *et al.*, 1999]. IRS-1 deficient islets and tumor cell lines have decreased insulin content and glucose- and arginine-stimulated insulin secretion, which can be partially restored by re-expression of IRS-1 [Kulkarni *et al.*, 1999b]. Thus, insulin promotes release of intracellular Ca^{2+} and insulin secretion in a pathway involving insulin receptor, IRS-1, and PI3-K. Furthermore, defects in this pathway result in a reduction of insulin secretion [Porzio *et al.*, 1999; Aspinwall *et al.*, 2000; Kulkarni *et al.*, 1999a; Kulkarni *et al.*, 1999b]. The *in vivo* significance of β-cell insulin signaling is demonstrated in β-cell

insulin receptor knockout mice, which exhibit a reduction in glucose-stimulated insulin secretion and impaired glucose tolerance [Kulkarni *et al.*, 1999a].

Although these recent studies have demonstrated positive feedback of insulin on secretion, several earlier studies concluded that insulin inhibits glucose-stimulated insulin secretion [Ammon and Verspohl, 1976; Iversen and Miles, 1971; Liljenquist *et al.*, 1978; Sodoyez *et al.*, 1969]. The majority of these other studies were performed on islets or perfused pancreas with application of exogenous insulin, which makes interpretation as a direct effect on β-cell insulin receptors difficult due to neuronal or hormonal regulation that could interact with exogenous insulin and the presence of large amounts of endogenous insulin under the conditions used. Nevertheless, these discrepancies highlight the possibility that, while newer methods have demonstrated a positive effect of insulin on secretion in β-cells, in an intact system or in the presence of high insulin levels, other regulatory mechanisms may counteract this effect.

Due to the ability of L-783,281 to activate insulin signaling and the apparently important role of insulin in stimulating insulin secretion, we have examined the effect of L-783,281 on insulin secretion and $[Ca^{2+}]_i$ at the single-cell level. The results demonstrate that L-783,281 induces release of Ca^{2+} from thapsigargin-sensitive stores and initiates insulin secretion via a pathway similar to that of insulin at nonstimulatory glucose levels.

Experimental

Chemicals and Reagents

The insulin mimetic L-783,281 and its inactive analog L-767,827 were prepared at Merck Laboratories as described elsewhere [Zhang *et al.*, 1999]. All chemicals for islet

isolation and cell culture were from Life Technologies. All other chemicals were from Sigma Chemical (St. Louis, MO) unless otherwise stated and were of highest purity available. Experiments were performed with cells bathed in a modified Kreb's Ringer buffer (KRB) consisting of (in mM): 118 NaCl, 5.4 KCl, 2.4 $CaCl_2$, 1.2 $MgSO_4$, 1.2 KH_2PO_4, 3.0 *d*-glucose, 20 HEPES. Drugs were dissolved in DMSO and diluted in KRB to give the desired final concentration. A stock solution of LY294002 was dissolved in ethanol before diluting in KRB.

Cell Culture and Isolation

Single β-cells were prepared as previously described [Pralong *et al.*, 1990]. Briefly, male CD1, C57Bl/6 IRS-1 +/+ (WT) or C57Bl/6 IRS-1 -/- (KO) mice [Araki *et al.*, 1994], weighing 20-30 g were sacrificed by cervical dislocation, and islets were isolated by collagenase digestion and hand-picked under a stereomicroscope. Islets were dispersed into single cells using a 0.025% trypsin/EDTA solution for 6 min at 37 °C and plated on 35 mm tissue culture dishes for electrochemical experiments or 25 mm glass coverslips for Ca^{2+} imaging experiments. Cells were maintained in RPMI 1640 culture media supplemented with 10% fetal bovine serum, 100 units/mL penicillin, 100 μg/mL streptomycin, stored at 37 °C in 5% CO_2, and used on days 2-4 following isolation.

Secretion Measurements by Amperometry

Cells were prepared for secretion measurements by incubating in RPMI medium supplemented with 1 mM 5-hydroxytryptamine (5-HT) for 16 hours prior to experiments. This treatment has previously been shown to cause 5-HT to accumulate in secretory vesicles of β-cells [Gylfe, 1978]. During exocytosis, the accumulated 5-HT is co-released with insulin [Aspinwall *et al.*, 1999a] providing a marker of secretion that is

reliably detected by amperometry at carbon-fiber microelectrodes. The validity of this method as a means to measure insulin exocytosis has been verified in several reports [Aspinwall *et al.*, 1999a; Smith *et al.*, 1995; Zhou and Misler, 1996]. To perform secretion measurements, RPMI media containing 5-HT was replaced with KRB and the culture plate mounted on the stage of a Zeiss Axiovert 100 microscope equipped with a microincubator (Medical Systems Corp., Greenvale, NY) to maintain temperature at 37 °C. 5-HT released from the cells was detected with a 9 μm diameter carbon fiber disc electrode prepared as described elsewhere [Kelly and Wightman, 1986]. For amperometric measurements, the electrode was poised at -0.65 V *versus* a sodium-saturated calomel reference electrode using a battery and voltage divider. Amperometric current was collected at 500 Hz and low pass filtered at 100 Hz using a AI 403 current amplifier (Axon Instruments, Foster City, CA), personal computer (Gateway 2000 P5-166) and a data acquisition board (Digidata 1200B, Axon Instruments, Foster City, CA). Amperometric traces were analyzed using software written in-house. For analysis, spikes with signal-to-noise ratio > 10 were counted as significant.

A picospritzer (General Valve Corp., Fairfield, NJ) was used to deliver test solutions to the cells via a glass micropipette positioned ~30 μm from the cell, as described elsewhere [Kennedy *et al.*, 1993]. Independent experiments have confirmed that this method of stimulation delivers drug at the stated concentration to the cell for the duration of stimulation. After stimulation, the drug is quickly diluted to negligible levels by diffusion into the surrounding medium. For all secretion experiments, 10 μM L-783,281 in KRB was applied to isolated cells for 40 s while secretion was measured by amperometry. To compare amount of exocytotic events induced by different

secretagogues, 100 nM insulin or 18 mM glucose were also applied to single β-cells for 40 s. A control solution consisting of drug carrier was applied to the same cell under investigation to ensure amperometric spikes were not due to an artifact of stimulation. To determine LY294002 sensitivity, an individual β-cell was stimulated with 10 μM L-783,281 twice, with 10 min between stimulations, to demonstrate cell activity. After successful stimulations, the cell was incubated with 25 μM LY294002 for 10 min and the same cell stimulated with L-783,281 again to compare the amount of secretory events. Control experiments were performed in which cells were incubated with drug carrier using a similar protocol.

$[Ca^{2+}]_i$ Measurements

β-cells attached to coverslips were incubated with 2 μM fluo-4 acetoxymethyl ester or 2 μM fura-2 acetoxymethyl ester in RPMI media for 30 min at 37 ºC in 5% CO_2 prior to experiments to load dye into the cells [Gee *et al.*, 2000]. Cells were washed 3 times and bathed with KRB. Coverslips containing the cells formed the bottom of a microchamber kept at 37 ºC throughout all experiments via a microincubator (Medical Systems Corp., Greenvale, NY).

Fluo-4 measurements were made using a Nikon RCM8000 confocal microscope that consisted of a Nikon Diaphot 100 inverted microscope and an Ar^+ laser (INNOVA Enterprise 622, Coherent, Santa Clara, CA). The 488 nm line from the Ar^+ laser was focused onto cells by a 40x, 1.15 numerical aperture water immersion objective and scanned across the image plane via galvanometers. Emission was collected through the same objective, passed through a 520 $\pm$ 10 nm bandpass filter and onto a photomultiplier tube. Images were taken at 1 Hz and stored on an optical disk recorder (Panasonic TQ-

FH332). For analysis, images were played back and the ratio (F_1/F_0) of each image (F_1) versus the first image (F_0) of the series was recorded [Aspinwall *et al.*, 2000].

Fura-2 fluorescence was measured using a SPEX CMX cation measurement system and DM3000M data acquisition software (Instruments S.A. Group, Edison, NJ) with a Zeiss Axiovert 100 microscope as previously described [Aspinwall *et al.*, 1999b]. Briefly, fura-2 loaded β-cells were excited at 1 Hz with 340 and 380 nm light focused onto cells by a 40x, 1.3 numerical aperture oil immersion objective. Emission was collected via the same objective, passed through a 400-nm long pass mirror, 510 ± 10 nm bandpass filter, and 20 μm spatial filter, and onto a photomultiplier tube. $[Ca^{2+}]_i$ was quantified as described elsewhere [Grynkiewicz *et al.*, 1985].

For $[Ca^{2+}]_i$ recordings, test solutions were applied to cells using the same protocol as described for secretion measurements. To test the sensitivity of L-783,281-induced Ca^{2+} to drugs, cells were incubated in KRB containing 100 nM wortmannin, 25 μM LY294002, 20 μM nifedipine or 1 μM thapsigargin for 10 min before applying 10 μM L-783,281 for 40 s. Only cells that responded to 200 μM tolbutamide in the presence of wortmannin, LY294002, or thapsigargin were used in the study. The L-783,281 evoked increase in fluo-4 fluorescence recorded in the presence of drugs was compared to that obtained for identical stimulations in the absence of drugs.

Statistical Analysis

All values are reported as mean ± SE. Statistical significance of the difference between means was determined by a two-tailed Student's t-test.

Results and Discussion

Intracellular Ca^{2+} Release

Application of L-783,281 to isolated β-cells in the presence of 3 mM glucose resulted in a concentration dependent increase in $[Ca^{2+}]_i$, whereas no increase for the inactive structural analog, L-767,827, was observed (Figure 3-1). At 10 μM L-783,281, the average maximal increase in fluo-4 fluorescence was 178 ± 10 % (n = 18 cells) with an average latency between stimulation and onset of the increase of 22 ± 17 s. The maximal increase was comparable to that for glucose and tolbutamide stimulations (Figure 3-2). The increase in $[Ca^{2+}]_i$ was long-lived and generally lasted for the entire recording time of 200 s. Further measurements revealed that the $[Ca^{2+}]_i$ stayed within 10% of the maximum stimulated level more than 5 min after the end of stimulation. For comparison, a typical trace obtained with application of 200 μM tolbutamide to a single cell is shown in Figure 3-1. This trace is typical of traces obtained from six different cells.

To determine if the increase in $[Ca^{2+}]_i$ was associated with Ca^{2+} entry through voltage-dependent Ca^{2+} channels, the effect of nifedipine was investigated on the L-783,281-evoked $[Ca^{2+}]_i$ response. As shown in Figure 3-2, pretreatment with 20 μM nifedipine reduced the L-783,281-induced Ca^{2+} increase 33 ± 6 % (n = 6 cells, $p < 0.05$). At this concentration, nifedipine completely abolishes the $[Ca^{2+}]_i$ increases due to K^+ or tolbutamide (data not shown), compounds that evoke an influx of extracellular Ca^{2+} through voltage-dependent Ca^{2+} channels. To determine if the rise in $[Ca^{2+}]_i$ was associated with release from intracellular Ca^{2+} stores, the effect of thapsigargin was examined. Thapsigargin has been shown to deplete intracellular Ca^{2+} stores by inhibiting

sarco/endoplasmic reticulum Ca^{2+}-ATPases [Lytton *et al.*, 1991]. As shown in Figure 3-2, pretreatment with 1 μM thapsigargin for 10 min reduced the L-783,281-induced $[Ca^{2+}]_i$

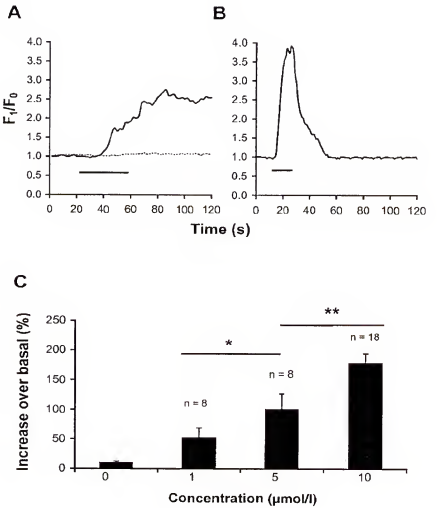

Figure 3-1. L-783,281 increases $[Ca^{2+}]_i$ in pancreatic β-cells at 3 mM glucose. (A) Representative trace of relative fluo-4 fluorescence intensity versus time for stimulation with 10 μM L-783,281 (solid line) and 10 μM of the structural analog, L-767,827 (dashed line), in a single β-cell. Duration of stimulation is indicated by the horizontal bar under trace. Fluo-4 fluorescence was measured by drawing a region of interest around the entire cell and plotted as relative fluorescence intensity (F_1/F_0) as described in the text. (B) Fluo-4 fluorescence from a β-cell stimulated with 200 μM tolbutamide. Note the decrease in fluo-4 fluorescence after stimulation with tolbutamide ended versus that with L-783,281 in A. (C) Average stimulated fluo-4 fluorescence versus concentration of L-783,281 for the number of cells indicated. Data are shown as means ± SE *P < 0.01, **P < 0.001.

change by 82 ± 4 % (n = 6 cells, $p < 0.001$). (Although thapsigargin increases intracellular Ca^{2+} as it depletes the stores, this effect is transient, and measurements were made after $[Ca^{2+}]_i$ had returned to baseline.) Combined, these results suggest that most of the increase in $[Ca^{2+}]_i$ was due to intracellular release from thapsigargin-sensitive stores.

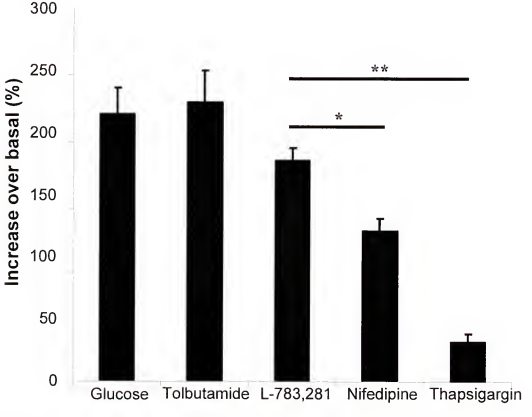

Figure 3-2. Increases in $[Ca^{2+}]_i$ induced by L-783,281. Single pancreatic β-cells were incubated in 3 mM glucose and stimulated for 40 s with 18 mM glucose (n = 7 cells), for 10 s with 200 μM tolbutamide (n = 6 cells), or for 40 s with 10 μM L-783,281 (n = 18 cells), and the peak fluo-4 fluorescence increase over baseline was recorded. To determine the role of intracellular Ca^{2+} stores in the L-783,281-induced $[Ca^{2+}]_i$ change, cells were incubated for 10 min in 20 μM nifedipine (n = 6) or 1 μM thapsigargin (n = 6) and stimulated with 10 μM L-783,281. All values are reported as mean ± SE. Testing of statistical significance for differences in maximal increase over baseline fluorescence was performed versus L-783,281 stimulation in the absence of any drugs. *$P < 0.05$, **$P < 0.001$.

L-783,281-Induced Secretion

Application of L-783,281 to β-cells in the presence of 3 mM glucose resulted in a series of current spikes in the amperometric trace indicative of exocytosis (Figure 3-3A). An average of 12.2 $\pm$ 2.1 exocytotic events per stimulation (n = 14 cells) were detected following application of L-783,281, whereas only 1.2 $\pm$ 0.3 exocytotic events per stimulation (n = 8 cells) were detected with 10 μM L-767,827, the inactive structural analog. For comparison, stimulation with insulin or glucose for an identical period of time resulted in a similar number of spikes detected by amperometry as with L-783,281 (Figure 3-3B). To confirm that this response was due to effects at the insulin receptor, cells were preincubated with 100 nM insulin for 10 min before application of 10 μM L-783,281. Application of 10 μM L-783,281 to these cells caused 0 $\pm$ 0 exocytotic events per stimulation, even though the cells were still viable as application of 40 mM K+ to the same cells resulted in 14.8 $\pm$ 0.5 spikes (n = 4 cells, $p < 0.05$).

Effect of L-783,281 on $[Ca^{2+}]_i$ and Insulin Secretion in β-Cells with IRS-1 Knockout

The potential role of IRS-1 in mediating the insulin secretion and increase in $[Ca^{2+}]_i$ evoked by L-783,281 was investigated by comparing the effect of the drug on β-cells from IRS-1 KO and IRS-1 WT C57Bl/6 mice. As seen in Figure 3-4, stimulation of IRS-1 KO cells with L-783,281 resulted in no significant increases in $[Ca^{2+}]_i$ even though 18 mM glucose was able to evoke substantial increases in $[Ca^{2+}]_i$ in these cells. The average increase induced by L-783,281 was 8 $\pm$ 3 % (n = 5 cells) over basal values, which was not significantly different from the effect of drug carrier alone (data not shown) and significantly less ($p < 0.05$) than the increase of 119 $\pm$ 25 % (n = 5 cells)

observed in the IRS-1 WT β-cells from the same type of mouse. Stimulation of β-cells from IRS-1 KO

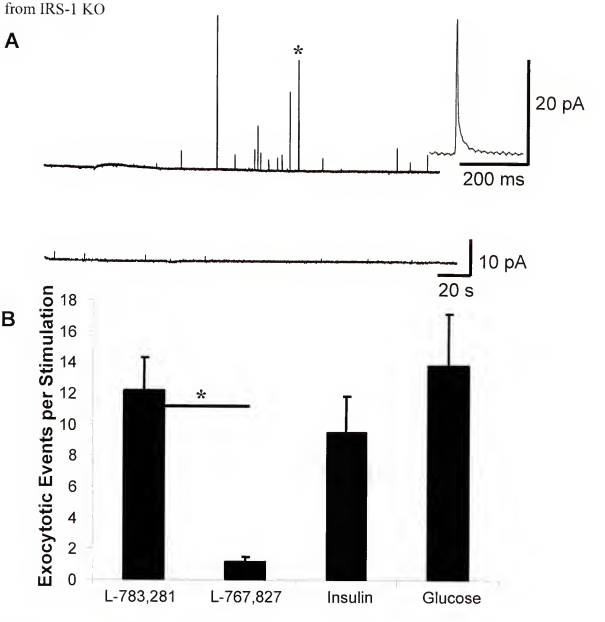

Figure 3-3. L-783,281 induces exocytosis from □-cells incubated with 3 mM glucose. (A) Application of L-783,281 (top) to a single □-cell results in current spikes on amperometric trace indicative of exocytosis. □-Cells were loaded with 5-HT as described in the text, and release events were measured by amperometry using carbon fiber microelectrodes. The inset shows an expanded view of a current spike (indicated by *). Stimulation with 10 □M of the inactive analog, L-767,827 (bottom) lasted for the duration indicated by the horizontal bar under the traces. (B) Number of exocytotic events induced by a 40 s stimulation with 10 □M L-783,281, 10 □M L-767,827, 100 nM insulin, or 18 mM d-glucose. Results are given as means + SE.

mice with L-783,281 resulted in 1.3 ± 0.1 (n = 5 cells) exocytotic events, which was significantly less ($p < 0.05$) than the 11.0 ± 2.0 (n = 5 cells) observed in control cells. The IRS-1 KO cells still responded to stimulation with 18 mM glucose with an average of 6.8 ± 0.1 (n = 8 cells) exocytotic events detected per cell (see Figure 3-4B). These results indicate that the presence of IRS-1 is required for L-783,281 to evoke increases in $[Ca^{2+}]_i$ and insulin secretion in β-cells.

Role of PI3-K in Ca^{2+} Release and Insulin Secretion

Pancreatic β-cells were tested to determine if L-783,281 induced $[Ca^{2+}]_i$ changes were sensitive to the PI3-K inhibitors LY294002 and wortmannin. When cells were pretreated with 25 μM LY294002, application of L-783,281 still increased fluo-4 fluorescence; however, the increase was just 31 ± 3 % (n = 9) of that evoked without LY294002. Similarly, application of L-783,281 in the presence of 100 nM wortmannin caused an increase that was 48 ± 10 % (n = 6) of that observed without wortmannin. Both of these increases were significantly less ($p < 0.05$) than that observed without PI3-K inhibition.

Secretion was also sensitive to LY294002, as the number of detected exocytotic events was reduced to 21 ± 6 % (n = 4 cells, $p < 0.05$) of the L-783,281-induced secretion in the presence of no LY294002 at a given cell (see Figure 3-5). Without application of LY294002, successive applications of L-783,281 at a 10-min interval resulted in no reduction of spike number as the second stimulation yielded 97 ± 5% of the spikes from the first stimulation (n = 8 cells).

Our data support the conclusions that L-783,281 evokes increases in $[Ca^{2+}]_i$ and insulin exocytosis by an IRS-1/PI3-K sensitive mechanism at a non-stimulatory glucose

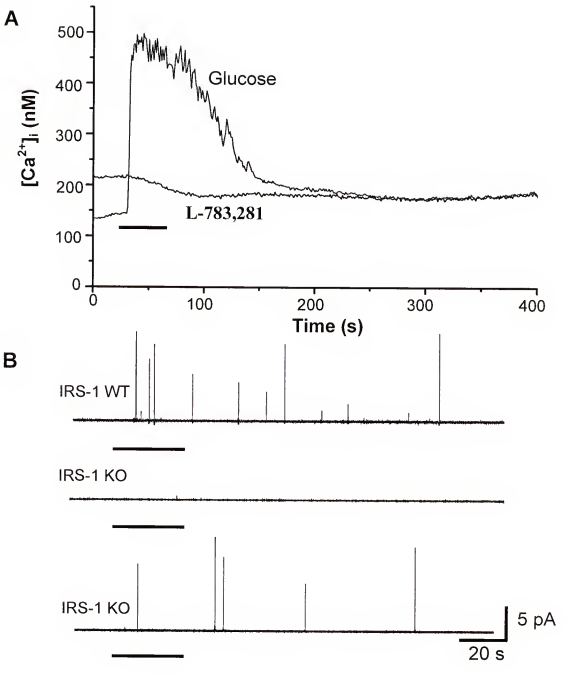

Figure 3-4. Involvement of IRS-1 in L-783,281-stimulated increases in $[Ca^{2+}]_i$ and exocytosis. (A) Representative Ca^{2+} trace of a fura-2 loaded IRS-1 KO β-cell stimulated with 18 mM glucose and the same cell stimulated with 10 μM L-783,281. The horizontal bar under the trace indicates time of stimulation. (B) Amperometric trace of a single IRS-1 WT β-cell stimulated with 10 μM L-783,281 (top), a IRS-1 KO β-cell stimulated with 10 μM L-783,281 (middle), and the same IRS-1 KO β-cell stimulated with 18 mM glucose (bottom).

concentration. Given the known ability of L-783,281 to activate IRTK and its downstream cascade, including IRS-1 and PI3-K in CHO cells, and the similarity of L-783,281 and insulin effects on β-cell $[Ca^{2+}]_i$ and secretion, it is reasonable to conclude that the effects of L-783,281 on β-cells are mediated by insulin receptor activation.

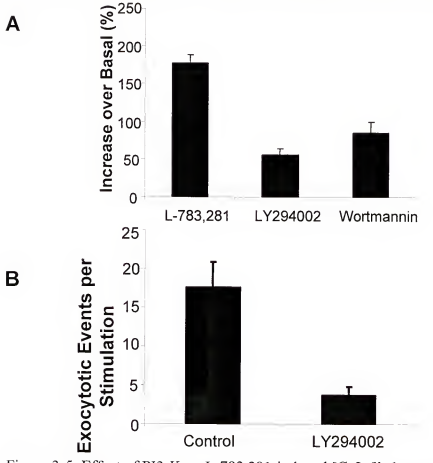

Figure 3-5. Effect of PI3-K on L-783,281-induced [Ca2+]i changes and exocytosis. (A) □-Cells were incubated with 25 □M LY294002 or 100 nM wortmannin for 10 min and stimulated with 10 □M L-783,281, and [Ca2+]i changes were monitored by fluo-4 fluorescence as described in the text and in Figure 3-1. Control indicates the average increase over basal induced by L-783,281 in the absence of drugs. Statistical significance was determined by comparing the mean L-783,281-induced increase in the absence and presence of the indicated drug. (B) The number of exocytotic events induced by 10 □M L-783,281 was recorded and compared with the number of exocytotic events induced by 10 □M L-783,281 in the presence of 25 □M LY294002. Stimulations were performed with cells in 3 mM glucose. $^*P < 0.05$.

Comparison of the Effects of Insulin and L-783,281 on β-Cells

The effects of insulin signaling on β-cell $[Ca^{2+}]_i$ and exocytosis have been reported previously [Xu *et al.*, 2000; Aspinwall *et al.*, 2000; Xu *et al.*, 1999; Aspinwall *et al.*, 1999b]. These data support the idea that insulin binding to the insulin receptor promotes insulin secretion and results in increases in $[Ca^{2+}]_i$ via release of Ca^{2+} from the endoplasmic reticulum by a pathway that involves IRS-1 and PI3-K. Most relevant to the present study is the report of direct application of 100 nM insulin to β-cells which resulted in increases in $[Ca^{2+}]_i$ and exocytosis at β-cells [Aspinwall *et al.*, 2000; Aspinwall *et al.*, 1999b].

Several similarities are observed in the acute effects of direct application of exogenous insulin and L-783,281 on β-cell $[Ca^{2+}]_i$ and secretion. In both cases, the $[Ca^{2+}]_i$ increase is characterized by a latency after application of stimulus, 20 ± 17 s and 12 ± 10 s for L-783,281 and insulin, respectively, followed by a slow increase to a maximum value (~ 30 s) that plateaus and persists for over 120 s. This time course is in contrast to stimulation with depolarizing agents, such as tolbutamide, which have been shown to have a latency of 1-2 s, a peak in $[Ca^{2+}]_i$ at ~5 s and a return to near baseline within a minute after stimulation (Figure 3-1) [Aspinwall *et al.*, 2000]. The pharmacology of the L-783,281-induced $[Ca^{2+}]_i$ increase also resembles that initiated by insulin. Nifedipene has no effect on insulin-induced increases [Aspinwall *et al.*, 2000] and decreases the L-783,281-evoked increase by just 33%. In contrast, thapsigargin has strong effects, resulting in a decrease of 75 and 82% for insulin [Aspinwall *et al.*, 2000] and L-783,281-initiated $[Ca^{2+}]_i$ increases, respectively. PI3-K inhibitors such as wortmannin also significantly inhibit the $[Ca^{2+}]_i$ increases evoked by both insulin and L-

783,281. Insulin and L-783,281 had essentially no effect on β-cell $[Ca^{2+}]_i$ in the IRS-1 knockout model. Likewise, exocytosis evoked by insulin and L-783,281 was strongly inhibited by PI3-K inhibitors and was nonexistent in β-cells from IRS-1 null mice. The similarities between the effects of L-783,281 and insulin on β-cell secretion and $[Ca^{2+}]_i$ support the idea that these compounds exert their effects through a similar mechanism that involves activation of IRS-1/PI3-K.

Another similarity involved in insulin signaling by insulin and L-783,281 is in the effect of regulating insulin gene expression in β-cells. Insulin upregulates its transcription in an autocrine manner [Leibiger *et al.*, 1998]. Similarly, L-783,281 acts to enhance insulin transcription by acting through the insulin receptor/IRS-1 pathway [Xu *et al.*, 2000]. Thus, insulin signaling helps to regulate its bioavailability and secretion.

Mechanism of the Effects of L-783,281

Our data indicate that the majority of the $[Ca^{2+}]_i$ increase that occurs during application of L-783,281 comes from thapsigargin-sensitive stores. Generally, these intracellular stores are considered to be the endoplasmic reticulum and are regulated by IP_3 or ryanodine receptors; however, $[Ca^{2+}]_i$ can also be increased by inhibition of SERCA (sarco/endoplasmic reticulum calcium ATPase) pumps resulting in passive diffusion of Ca^{2+} out of the endoplasmic reticulum. Several lines of evidence point to SERCA inhibition resulting from activation of IRTK or its downstream effectors, including the ability of IRS-1 to interact with SERCA pumps [Algenstaedt *et al.*, 1997], increased basal $[Ca^{2+}]_i$ by IRS-1 inhibition of SERCA pumps thereby inhibiting Ca^{2+} uptake into ER [Xu *et al.*, 1999], and regulation of SERCA gene expression by activation of insulin signaling [Xu *et al.*, 2000]. The present study agrees with these previous

reports in that deletion of IRS-1 inhibits the L-783,281-stimulated $[Ca^{2+}]_i$ increase. The observations of the effects of insulin signaling on $[Ca^{2+}]_i$ are consistent with the hypothesis that activation of the insulin receptor, whether by insulin or L-783,281, releases Ca^{2+} from the endoplasmic reticulum via an interaction involving IRS-1 and SERCA. Whether this Ca^{2+} is responsible for activating exocytosis has yet to be proven.

Implications for In Vivo Effects of L-783,281

Initial studies of L-783,281 demonstrated that this compound enhanced glucose uptake *in vitro* and was antidiabetic inasmuch as it restored normoglycemia in *db/db* and *ob/ob* mice [Zhang *et al.*, 1999]. It is tempting to speculate that part of the reason for an antidiabetic effect of L-783,281 was an increase in insulin secretion due to activation of the pathway observed here; however, it would be premature to reach this conclusion, since the experiments in this report involved only transient application of L-783,281 in the presence of 3 mM glucose. Further experiments are necessary to determine if L-783,281 affects insulin secretion at stimulatory glucose levels, with longer-term stimulation, in whole islets, and *in vivo*. Demonstration of enhanced insulin secretion *in vivo* may be difficult to demonstrate because of multiple effects of the drug, and *in vivo* glucose homeostasis mechanisms may mask effects at the level of β-cells. For example, L-783,281 lowers glucose levels by activating glucose transport and potently increases insulin sensitivity in peripheral tissues [Zhang *et al.*, 1999]; therefore, insulin demand during a glucose challenge is likely less, which could result in a net decrease in insulin secretion even if the drug has a stimulatory effect on insulin secretion by direct action on β-cells.

Conclusions

Type 2 diabetes is characterized by both insulin resistance and impaired insulin secretion, with the possible link between these two symptoms remaining obscure; however, the recent discovery of active insulin receptors on β-cells that promote insulin secretion, insulin synthesis, and β-cell growth has led to the hypothesis that impaired insulin signaling could account for both symptoms [Taylor 1999; Hussain 1999; Rutter 1999; Withers and White, 2000]. We have demonstrated that the insulin mimetic L-783,281, a fungal metabolite previously shown to increase glucose uptake in peripheral tissues, also induces an increase in $[Ca^{2+}]_i$ and insulin secretion from pancreatic β-cells at nonstimulatory glucose concentrations. The effects appear to involve insulin signaling, since they are blocked by knockout of IRS-1 and are sensitive to inhibitors of PI3-K. Other groups have demonstrated that L-783,281 promotes insulin synthesis [Xu *et al.*, 2000]. These results suggest that the actions of insulin mimetics in β-cells should be further investigated as a possible tool in studying insulin signaling in β-cells and for a potential role in diabetes treatments.

CHAPTER 4
MICROFLUIDIC CHIP FOR ONLINE MONITORING OF INSULIN SECRETION FROM AN ISLET OF LANGERHANS

Introduction

Microfluidics has enabled many improvements in chemical analysis of cells including high-throughput, parallel assays, high-speed separations, and microscale sample preparation. While most cellular applications of microfluidics have been directed at analysis of cell contents [Woolley *et al.*, 1996; Schilling *et al.*, 2002; Tang *et al.*, 2002], it is apparent that such automated, miniaturized instrumentation would also be of use for continuous monitoring of chemical events at live cells. This line of research is beginning to emerge with recent reports of using cells as sensors for small molecules [Heo *et al.*, 2003] and monitoring intracellular Ca^{2+} changes upon chemical stimulation [Yang *et al.*, 2002] in microfluidic devices. In this work, we report a microfluidic system that can monitor secretion of a hormone from a cell cluster using a rapid, electrophoresis-based immunoassay. The system is applied to monitoring insulin secretion from single islets of Langerhans.

Islets of Langerhans are microorgans dispersed throughout the pancreas that consist of 2000-5000 endocrine cells each. The majority of islet cells are pancreatic β-cells that release insulin in a tightly controlled manner to regulate blood glucose levels. Assays of insulin secretion from islets are of interest because of their role in diabetes research. Type 1 diabetes, associated with autoimmune destruction of β-cells, and type 2 diabetes, associated with adult onset hyperglycemia, are leading public health problems that

contribute to 19% of the deaths of people over 25 and costs of $132 billion per year [Centers for Disease Control and Prevention, 2002]. Type 2 diabetes is associated with several biological factors including failure of β-cells to secrete sufficient insulin to regulate glucose. With few exceptions, the cause of dysfunctional secretion is unknown. It is known that the primary regulator of insulin secretion is glucose [Henquin, 2000]; however, insulin secretion has complex kinetics that include an initial burst followed by plateau (first and second phase, respectively) and oscillations. The regulation of such dynamics is unclear, but understanding their mechanism is important for understanding the derangements that occur in diabetes. Study of insulin secretion aimed at addressing these questions requires the ability to monitor insulin release over time, preferably at individual islets for kinetics studies. Rapid measurement of insulin secretion may also be of use for evaluating islets for transplant. Islet transplant is a promising treatment for type 1 diabetes; however, such treatments are limited by the inability to easily test islets for viability prior to transplant [Berney *et al.*, 2002].

The most commonly used methods for measuring insulin release are radioimmunoassay and enzyme-linked immunosorbent assay. For temporally resolved measurements islets are perfused and individual fractions assayed. The immunoassays take hours to perform making their application to rapid monitoring or testing of islets impractical. Consider that a single experiment involving monitoring insulin from a single islet at 5 s intervals for 40 min would require 480 assays. Furthermore, the assays would have to be highly optimized to gain the requisite sensitivity for such rapid sampling. As an alternative to these assays, we have developed capillary electrophoresis (CE)-based competitive immunoassays [Schultz and Kennedy, 1993] and demonstrated their

application to monitoring insulin release from islets [Tao *et al.*, 1998]. In this method, a single islet is placed in a small chamber (Teflon tube) and perfused with physiological buffers at low flow rates. Effluent from the islet is mixed online with fluorescein isothiocyanate-labeled insulin (FITC-insulin) and anti-insulin antibody (Ab) and allowed to react prior to injection onto an electrophoresis capillary where the bound (B) and free (F) FITC-insulin are separated. The ratio of the bound to free FITC-insulin (B/F) is used to quantify insulin in the perfusate. Use of a flow-gate interface to control injection and application of 3000 V/cm allowed assays of insulin release to be acquired at 3 s intervals. While this system demonstrates the concept of CE-immunoassay based monitoring, it is limited in scope because the complexity of the instrument, especially the fluidics, precludes simple transfer to clinical or research laboratories. In addition, loading islets into the chamber is difficult, and the enclosed islet chamber precludes access with electrodes or optical techniques to measure other parameters on the islet.

To overcome the limitations of the capillary system, we began to investigate use of a microfabricated chip for performing a similar function. While electrophoresis-based immunoassays were originally performed in capillaries, they have been successfully transferred to chip-based systems [Koutny *et al.*, 1996; Schmalzing *et al.*, 1997; Chiem and Harrison, 1997; Chiem and Harrison, 1998a; Taylor *et al.*, 2001]. Most of this work has involved offline mixing of immunoassay reagents and use of the chip only for separation; however, online mixing and separation have been achieved [Chiem and Harrison, 1998b; Cheng *et al.*, 2001; Qiu and Harrison, 2001]. While these reports illustrate the potential of automated immunoassays on chips, several issues must be addressed in order to extend chip based assays to continuous live cell monitoring. Cells

must be housed in a physiological buffer to maintain viability; however, such buffers often suppress electroosmotic flow (EOF), complicating fluidic control. To continuously monitor release, online mixing must be performed in a fashion that does not interfere with downstream separations or upstream sampling. Finally, the assays must be stable to allow monitoring for the duration of an experiment, typically 30-60 min.

In this work, we report development of a competitive immunoassay for insulin in a microfluidic device with online mixing of reagents suitable for continuous monitoring. The system is successfully applied to detecting changes in insulin secretion from single islets of Langerhans incubated on the chip.

Experimental

Chemicals and Reagents

All cell culture reagents were obtained from Life Technologies, Inc. (Carlsbad, CA). FITC-insulin was purchased from Molecular Probes (Eugene, OR). Monoclonal Ab to human insulin with a dissociation constant of 1 nM was from Biodesign International (Saco, ME). All solutions were made from Milli-Q (Millipore, Bedford, MA) 18 M□ deionized water. Tween-20, insulin, collagenase type XI, 4-(2-hydroxyethyl)piperazine-1-ethanesulfonic acid (HEPES), Ficoll, ethylenediaminetetraacetic acid (EDTA), and bovine serum albumin (BSA) were from Sigma (St. Louis, MO). All other chemicals were from Fisher and were of highest purity available.

Isolation of Islets of Langerhans

Islets of Langerhans were obtained by a previously described method [Pralong *et al.*, 1990]. Briefly, 20-30 g male CD-1 mice were sacrificed by cervical dislocation followed by ductal injection of collagenase type XI. The pancreas was dissected and

incubated in 5 mL collagenase solution at 37 °C for 10 min. Endocrine tissue was separated from exocrine tissue using a Ficoll gradient and islets were picked by hand under a stereomicroscope. The islets were placed in RPMI 1640 cell culture media supplemented with 10% fetal bovine serum, 100 units/mL penicillin, 100 μg/mL streptomycin, and incubated at 37 °C, 5% CO_2. Islets were used 2-6 days following isolation.

Fabrication of Microfluidic Chips

Figure 4-1 illustrates the design of the microfluidic chip used in all experiments. One millimeter thick borofloat photomask blanks (1" x 3") with a 530 nm layer of AZ1518 positive photoresist on a 120 nm chrome layer were purchased from Telic Company (Santa Monica, CA). A collimated UV light source (Optical Associates, Inc., Milpitas, CA) was used to expose a photomask blank through a photomask (Digidat, Pasadena, CA) for 5 s at 26 mW/cm^2. To aid in bonding the chip, excess photoresist 2-3 mm away from channels was removed by a cotton swab saturated with acetone [Roulet *et al.*, 2001]. The exposed photomask blank was placed in AZ915 MIF developer (Clariant Corporation, Summerville, NJ) for 15 s and rinsed with deionized water. The developed blank was then placed in CEP-200 chrome etchant (Microchrome Technologies, Inc., San Jose, CA) until all chrome was removed and rinsed with deionized water. The chip was placed in an etching solution that consisted of 14:20:66 (v:v:v) HNO_3, HF, and H_2O for 10 min [Kern and Deckert, 1978]. The etching rate was approximately 0.3 μm/min which resulted in 20 μm wide by 3 μm deep channels. After etching, 300 μm diameter diamond-tipped drill bits (Tarton Tool Co., Troy, MI) were used to drill fluidic access holes to the channels. The etched chip and a blank piece of glass were placed in a 3:1

(v:v) H_2SO_4:H_2O_2 solution for 20 min, rinsed with water, and placed in a solution of 5:1:1 (v:v:v) H_2O:NH_4OH:H_2O_2 at 60 °C for 20 min. The chip and top plate were rinsed with copious amounts of water and placed into contact with each other. The assembled chip was dried using filtered N_2 and placed between two Macor ceramic plates (Ceramic Products, Inc, Palisades Park, NJ) inside a Neytech Centurion Qex furnace (Pacific Combustion, Los Angeles, CA) [Liu *et al.*, 1999]. A 400 g stainless steel weight was placed on top of the ceramic plates and the temperature was ramped under vacuum at 10 °C/min to 640 °C, held for 8 h, and ramped down to room temperature at 10 °C/min. Microfluidic reservoirs were purchased from Upchurch Scientific (Oak Harbor, WA) and applied to the chip after bonding according to the manufacturer's instructions.

Detection and Injection Scheme

All electrophoresis experiments were performed on the stage of a Zeiss Axiovert 100 microscope equipped with fluorescence optics. The 488 nm line of a 20 mW Ar+ laser (Melles Griot, Carlsbad, CA) was directed onto a 500 nm longpass mirror and through a 40x, 0.6 NA objective (Carl Zeiss, Inc., Thornwood, NY). The emission light was collected with the same objective, passed through the longpass mirror and a 520 ± 10 nm bandpass filter. The light was then spatially filtered with a 1 mm pinhole and detected using a photon counting detector (Thermo Oriel, Stratford, CT). Instrument control and data collection were performed using software written in LabView (National Instruments, Austin, TX).

The voltage scheme used for injection and separation was based on a previously described method (see Figure 4-1A) [Jacobson *et al.*, 1999]. For the entire experiment, sample reservoirs were held at ground, and negative high voltage was applied to the waste reservoir via a high voltage power supply (Spellman High Voltage Electronics,

Hauppauge, NY). During separation, the gate reservoir was held at ground. In this condition, EOF pulled fluid from the Ab, FITC-insulin, and islet reservoirs into the reaction channel. This flow was shunted to the waste channel as fluid from the gate reservoir was split between the waste arm and the separation channel. To make an injection, the voltage on the gate reservoir was floated using a computer controlled high voltage relay (Kilovac, Santa Barbara, CA). Floating this reservoir allowed flow from the reaction channel into the separation channel. Floating the gate reservoir for 1 s allowed ~100 pL of sample to be loaded onto the separation channel (actual injection amount depends upon the buffers being used and resulting flow rates). After 1 s, the gate reservoir was returned to ground and separation occurred for 10 or 15 s after which time another sample plug was injected onto the separation channel.

Offline Mixing Assay

Samples were dissolved in a buffer that consisted of 20 mM NaH_2PO_4, 1 mM EDTA, pH 7.4 with 0.1% (w:v) Tween 20. The separation buffer consisted of 150 mM HEPES, pH 7.4. To obtain a calibration curve, FITC-insulin, Ab, and various amounts of insulin were mixed with sample buffer to a final concentration of 50 nM FITC-insulin, 25 nM Ab, and 0 – 500 nM insulin. Between each concentration of insulin tested, the chip was cleaned for 15 min each with 1 M NaOH and electrophoresis buffers. The voltage used for separation of the offline mixture was -5 kV with an effective separation length of 1 cm. The photon multiplier tube (PMT) integration time was 25 ms with a separation time of 10 s. The average B/F from 15 consecutive electropherograms, beginning at 300 s, was used for each data point of the calibration curve.

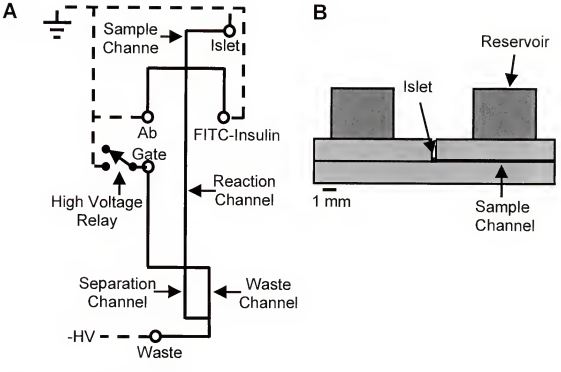

Figure 4-1. Chip layout for a competitive immunoassay and continuous sampling. (A) Microfabricated channels (20 μm wide x 3 μm deep) are indicated by solid lines and electrical connections by dashed lines. Reservoirs (not shown) were glued in place over 300 μm diameter access holes (indicated by circles). The length of the reaction channel is 4 cm, and the total length of the separation channel is 1.5 cm. Detection occurred prior to the 90° turn in the separation channel (1 cm). To load sample onto the separation channel, the high voltage relay was used to switch the voltage on the gate reservoir from ground to float for 1 s and then returned to ground. During separation, flow from the gate reservoir prohibited sample from leaking into the separation channel. (B) Side-on, cutaway view of chip at the sampling reservoir. An islet was housed at the bottom of a 300 μm diameter fluidic access hole. Solution around the islet was sampled by EOF through the sample channel.

Online Mixing of Reagents

The chip was conditioned with 1 M NaOH and electrophoresis buffers for 30 min each prior to experiments. Unless indicated otherwise, a thin-film resistive heater (Minco Products, Inc., Fridley, MN) was taped to the bottom of the chip so that all sample reservoirs and the reaction channel were in contact with the heater. The heater was powered by a 120V AC / 5V DC, 200 mA supply and yielded a temperature of 38 °C as

measured by a thermocouple in the reservoirs. All samples and reagents were dissolved in 20 mM NaH_2PO_4, 1 mM EDTA, pH 7.4 buffer that contained 0.1% (w:v) Tween 20 and 10 μM BSA, termed PETA buffer. Electrophoresis buffer (placed in the gate and waste reservoir of Figure 4-1A) consisted of 150 mM HEPES, pH 7.4. To obtain a calibration curve, 150 nM FITC-insulin was placed in the FITC-insulin reservoir, 75 nM Ab was placed in the Ab reservoir, and 0-1500 nM insulin was placed in the islet reservoir. After loading an equal volume of solutions in the chip, a plastic cap with a hole for electrode access was placed over each reservoir. Separation voltage was -4 kV with an effective separation length of 1 cm. The integration time of the PMT was 10 ms and separation time was 15 s.

Online Islet Monitoring

Conditions for online islet monitoring were the same as online mixing, except for the following. After conditioning all sample reservoirs with PETA buffer for 30 min, RPMI 1640 with 3 mM glucose was placed in the islet reservoir and conditioning continued for an additional 30 min. During conditioning with RPMI 1640, the chip was heated using the resistive heater to ensure the temperature was constant prior to experiments. Calibration curves were obtained by diluting various amounts of insulin in RPMI 1640 with 3 mM glucose in the islet reservoir, 75 nM Ab in PETA buffer in the Ab reservoir, and 150 nM FITC-insulin in PETA buffer in the FITC-insulin reservoir. All reservoirs contained 70 μL of solution.

After calibration, a single islet was placed in the islet reservoir using a pipette, caps were placed on reservoirs, electrodes inserted, and injections started. After 2-4 min,

islets were stimulated by the addition of 1.2 μL of 1 M glucose in water to give a final concentration of 20 mM glucose in the islet reservoir.

The response time of the system was measured by grounding all sample reservoirs and mixing online 75 nM Ab in PETA buffer in the Ab reservoir, 150 nM FITC-insulin in PETA buffer in the FITC-insulin reservoir, and RPMI 1640 in the islet reservoir. A separate reservoir contained 1 μM insulin in RPMI 1640 and was connected to the islet reservoir via a 5 cm channel (not shown in Figure 4-1). Positive high voltage (+3 kV) was applied to the reservoir containing insulin, pumping insulin into the reaction channel and lowering the B/F detected in the separation channel. Once a low, stable B/F was attained, the reservoir containing insulin was floated and the time for the B/F to increase was measured. The delay time was the time required to reach 10% of the maximal increase. The response time was the time required to change from 10% to 90% of the maximal increase.

Data Analysis

All values are reported as average ± one standard deviation. To quantify insulin concentration, a weighted nonlinear least squares curve was fit to the B/F ratios from peak heights versus insulin concentration using a four parameter logistic model [Christopoulos and Diamandis, 1996] with the aid of Microsoft Excel solver [Harris, 1998]. Detection limits were calculated by using the calibration curve to determine the concentration of insulin that would decrease the B/F ratio of a blank solution by an amount greater than three times the standard deviation of the B/F ratio of a blank solution [Schultz and Kennedy, 1993; Taylor *et al.*, 2001].

Results and Discussion

Offline Mixing Assay

Preliminary experiments were performed with offline mixing to test the separation and quantification of insulin and provide a baseline for comparison to online assays. Although only a single sample reservoir is needed for an offline assay, all three sample reservoirs shown in Figure 4-1 were filled with sample to avoid dilution. Electropherograms, acquired at 10 s intervals, stabilized with respect to peak heights 2 min after addition of samples to the reservoirs and yielded good resolution of the bound and free peaks (Figure 4-2A). B/F varied with insulin concentration as expected for a competitive assay (Figure 4-2B) and had relative standard deviations (RSDs) of 2-6% (n = 15 electropherograms collected in series) depending on insulin concentration. These results are comparable to those achieved previously on the capillary system [Tao *et al.*, 1998]. Detection limits were 1 nM, which is about 3-fold higher than that achieved on the capillary system [Tao *et al.*, 1998]. The difference is at least partially due to use of higher reagent concentrations. It was found that with the microfluidic system Tween 20 was required to achieve stable electropherograms and good detection limits even though this additive was not required for the capillary system. As Tween 20 is a nonionic surfactant used to prevent adsorption, these results suggest that adsorption of reagents and sample is a more significant problem in the microchip than in the capillary format. This effect may be attributed to the higher surface area to volume ratio of the chip and differences in surface chemistry between glass chips and fused silica capillaries.

Online Mixing of Reagents

Online mixing of the reagents was evaluated by placing FITC-insulin, Ab, and insulin into their respective reservoirs. The buffers used in the offline assay were not

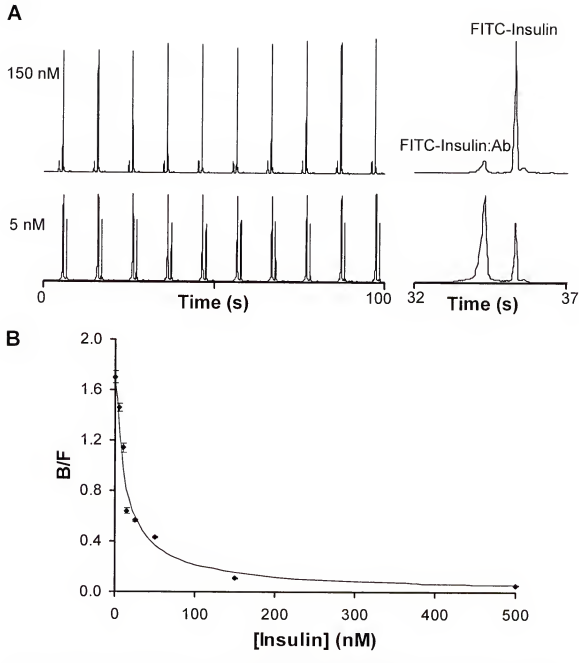

Figure 4-2. Electropherograms and calibration curve obtained from offline mixing of reagents. (A) Equal volumes of a solution containing 50 nM FITC-insulin, 25 nM Ab, and 5 nM insulin (bottom) or 150 nM insulin (top) were placed in all three sample reservoirs and injections made once every 10 s with a separation voltage of -5 kV. At right is an expanded view of electropherograms taken from 30-40 s. (B) Calibration curve for 0-500 nM insulin mixed with 50 nM FITC-insulin, and 25 nM Ab. The trendline is a best fit curve from a least squares regression of a four parameter logistic model. Points are the average from 15 consecutive electropherograms and error bars are 1 standard deviation.

satisfactory in the online mode as the B/F did not stabilize but instead continued to increase with time. Addition of 10 μM BSA to sample buffer, an attempt to block sample adsorption, was only partially able to prevent the increase of B/F with time. The continued increase in B/F was attributed to evaporation of solutions in the reservoirs. Evaporation could increase B/F by concentrating the analytes, thus favoring complex formation, and by causing an increase in salt concentration thereby slowing EOF and increasing reaction time. Placing plastic caps over the reservoirs, along with adding BSA to the sample buffer, stabilized B/F ratio and allowed calibration of the chip (see Figure 4-3).

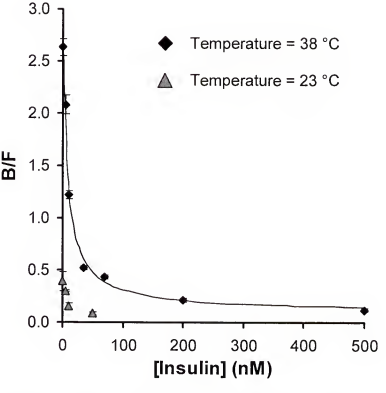

Figure 4-3. Calibration of immunoassay with online mixing of reagents through a 4 cm reaction channel. Reservoirs contained 150 nM FITC-insulin, 75 nM Ab, and 0-1500 nM insulin in 20 mM NaH_2PO_4, 1 mM EDTA buffer, pH 7.4 with 0.1% (v:v) Tween 20, and 10 μM BSA. Points are the average of 15 electropherograms with 1 standard deviation as the error bars. Curves show the effect of heating the reaction channel and reservoirs.

Although stable electropherograms and calibration could be obtained under these conditions, it was found that B/F ratio and dynamic range were much smaller than in the offline case. This was attributed to a limited reaction time (35 s) in the online mixing mode. To circumvent this problem, the sample reservoirs and reaction channel on the chip were heated to 38 °C to enhance reaction kinetics [Tao *et al.*, 1998] and the voltage was lowered to -4 kV to allow a longer mixing time (50 s). With these modifications, the B/F were improved to levels comparable to the offline mixing assay (compare Figures 4-3 and 4-2B). The reaction apparently reaches a steady state under these conditions as stopping the flow for 5 min prior to injection did not increase B/F. Detection limits were the same as for the offline assay and RSDs were comparable at 3-8% (RSD measured from 15 electropherograms collected in series for each concentration of insulin).

The conditions used for Figure 4-3 would be suitable for an automated assay wherein samples are added to the sample reservoir and automatically analyzed; however, the buffers were not suitable for incubating islets on the chip for automated sampling. Initial experiments using physiological solutions such as Kreb's Ringer buffer (a standard buffer used in islet experiments that contains in mM: 118 NaCl, 5.4 KCl, 2.4 $CaCl_2$, 1.2 $MgSO_4$, 1.2 KH_2PO_4, 3 *d*-glucose, and 20 HEPES) in the islet reservoir revealed that EOF from the sample chamber was so low (approximately 1 pL/s) that assays could not be performed. The low EOF was attributed to the high concentration of salts, especially divalent cations, interacting with the glass surface. After exploring several physiological solutions and chip pretreatments, it was found that sufficient flow through the sample channel (approximately 20 pL/s) could be achieved using cell culture media, RMPI 1640, in the islet reservoir and pretreating the microchips with PETA buffer. (RMPI 1640 cell

culture media contains 20 amino acids, electrolytes, and multiple vitamins such as thiamine, riboflavin, vitamin B12, and folic acid). These results reveal that reliance on EOF, which is strongly dependent on surface and solution chemistry, to sample and mix reagents is a limitation of the chip design described here. Use of hydrodynamic pumping may be necessary to make this system more versatile.

Using online mixing with RMPI 1640 as the solvent for insulin, calibration curves had a similar overall shape to those obtained under other conditions; however, the B/F was considerably higher (see Figure 4-4A). Detection limit was slightly higher, 3 nM, due to reduced sensitivity (i.e., shallower slope of the calibration curve). The increased detection limit and increased B/F may be due to a lower mobility of RPMI 1640 as compared to PETA buffer, effectively increasing the ratio of Ab and FITC-insulin mixed with sample in the reaction channel. Electropherograms under these conditions were stable with no drift in B/F for over 100 consecutive assays and RSDs of 2-6% (see Figure 4-4B). After approximately 30 min of use, the RSD typically increased; however, this was apparently due to alteration in reservoir contents as refreshing the solutions restored stable performance. Due to the low RSD values, the disparity in several of the points to the best fit line are likely due to errors in making the solutions, not due to errors in the measurement.

Since the chip was to be used for monitoring, the response time to a step change in insulin in the reaction channel was evaluated (protocol given in Experimental section). The time for reagents to travel the reaction channel with RPMI was 50 s. The response time, the time for electropherograms to stabilize following a step change in insulin concentration, was 30 s (two electropherograms). Therefore, increasing the rate at which

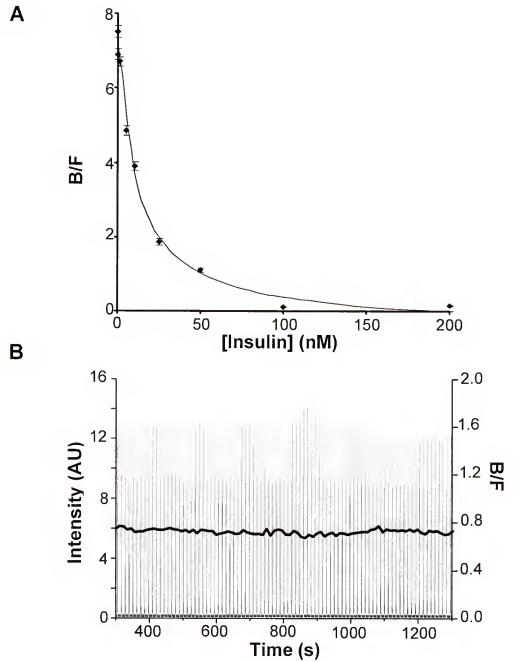

Figure 4-4. Results from online sampling and mixing using RPMI 1640 cell culture media as the solvent for insulin. (A) Calibration curve obtained using 75 nM Ab in PETA buffer, 150 nM FITC-insulin in PETA buffer, and 0-600 nM insulin in RPMI 1640 were mixed online with heating to 38 °C. Data points are the average of 15 consecutive electropherograms with error bars of 1 standard deviation. (B) Series of 110 electropherograms with online mixing of 150 nM FITC-insulin, 75 nM Ab, and 150 nM insulin acquired 200-1300 s after the start of injections. The black line through the peaks shows the B/F ratio plotted against the right axis. RSDs for online mixing ranged from 2-6% over the course of 30 min.

the reaction channel is sampled (e.g., 1 s injections with a 5 s separation time) should allow for more accurate determination of response time.

An important feature of this chip and the voltage scheme is that it allows continuous sampling and online mixing i.e., flow is not stopped even as injection and separation occur. Continuous sampling of the islet reservoir during separation would not be possible using a double tee [Effenhauser *et al.*, 1994] or pinched injection [Jacobson *et al.*, 1994] as the reagents are typically "pushed back" to ensure that analyte does not leak into the separation channel. Pushing reagents back during separation will likely mix the analyte back into the sample reservoir and possibly mix concentration pulses moving through the reaction channel. A double tee injection scheme for continuous sampling has been accomplished using a shunt channel [Chiem and Harrison, 1998b]; however, with this design and all other double tee or pinched injection schemes, time is needed to refill the injection area with reagents prior to separation, possibly lowering the temporal resolution. The design used here avoids these problems enabling high temporal resolution.

Online Sampling from Islets of Langerhans

To test the ability of the chip to monitor insulin secretion from live cells, a single islet was placed in the fluidic access hole of the islet reservoir (Figure 4-5A) using a pipette after the chip had been calibrated. Islets were transferred in RPMI 1640 containing 3 mM glucose. Placing the islet in the reservoir did not appear to effect the separation of bound and free FITC-insulin (Figure 4-5B). Increasing the glucose concentration to 20 mM while monitoring insulin with the immunoassay resulted in a substantial increase in the detected insulin concentration as shown Figure 4-6 (traces representative of 4 islets). The peak level reached was 148 ± 55 nM ($n = 4$ islets). As the

solution in the islet reservoir is static, except for what is sampled, insulin secreted by the islet continues to build up in the chamber meaning that the chip acts as an integrating detector. Kinetic information can be obtaining by taking the derivative of the trace as shown in Figure 4-7. This analysis reveals an initial burst lasting 404 $\pm$ 190 s (first

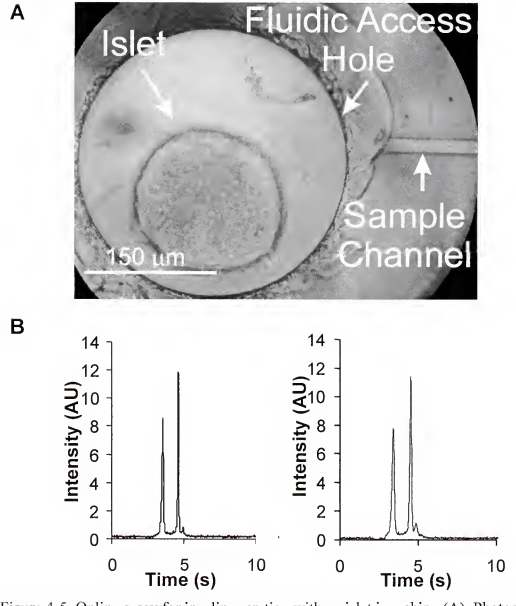

Figure 4-5. Online assay for insulin secretion with an islet in a chip. (A) Photograph of an islet in a 300 μm diameter fluidic access hole and the channel for sampling the solution by EOF. (B) Comparison of electropherograms for online mixing of a standard solution consisting of 150 nM FITC-insulin in PETA buffer, 75 nM Ab in PETA buffer, and 75 nM insulin in RPMI 1640 (left) and the same Ab and FITC-insulin solutions with an islet in the sample chamber (right).

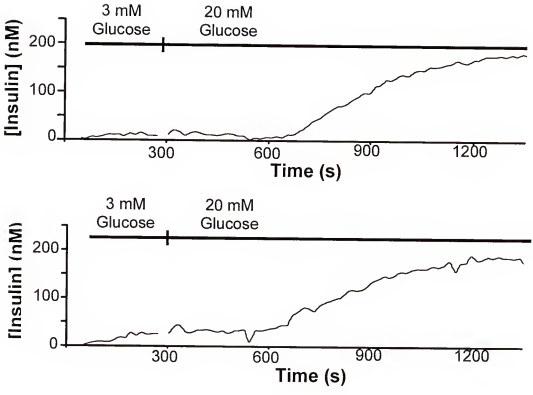

Figure 4-6. Insulin release measured from a single islet of Langerhans on a microfluidic chip. For plots of insulin concentration versus time, the insulin concentration was determined from B/F of individual electropherograms and online calibration. Representative traces of insulin release measured upon application of 20 mM glucose (n = 4 islets). Break in traces occur when islets were stimulated.

phase) followed by decrease to a low plateau of insulin release (second phase) [Henquin *et al.*, 2002; Gerich, 2002].

As configured, this system is not a perfect integrating detector because released insulin does not equilibrate through out the chamber before it is sampled and analyzed. In addition, while the islet is confined to 300 μm hole drilled in the chip (~ 70 nL volume), this hole is in fluid contact with the larger sample reservoir (see Figure 4-1B) where insulin may diffuse away and be substantially diluted. For more quantitative

kinetic studies, it would be necessary to perfuse the islet chamber and assay the effluent. Such modifications are currently under investigation.

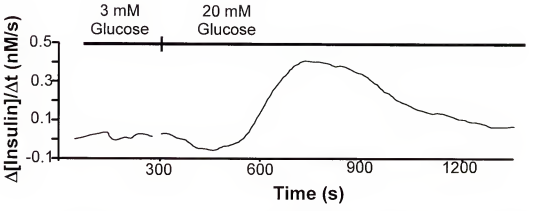

Figure 4-7. Kinetic determination of insulin secretion. First derivative of the top trace in Figure 4-6. Upon stimulation with 20 mM glucose (indicated by bar above trace), rate of insulin concentration increased quickly followed by a slower, long lasting release rate.

Conclusion

This work demonstrates the potential of microfabricated fluidic systems for monitoring the chemical environment of live cells. The fluidic and voltage scheme combined with suitable buffers and glass pretreatments allowed continuous sampling, online reaction, and electrophoresis-based immunoassay. The islets responded to glucose stimulation and showed no morphological changes over the course of the experiment indicating that chip and buffers used provided a suitable physiological environment. With simple operation, easy loading of tissue samples, a detector based on a commercial microscope, and microfabricated fluidics this system has the potential to be adopted for research and clinical applications such as studies of insulin secretion or testing islets for viability before transplant. While this work emphasized islets, it is anticipated that the method could readily be extended to other live cell or tissue preparations. Improvements

being developed include continuous perfusion of the cell chamber and simultaneous measurements of other biochemical changes in the islet.

CHAPTER 5
PERFUSION OF ISLETS

To monitor insulin secretion from islets quantitatively, all or a constant percentage of the released insulin needs to be measured. Because of this requirement, a perfusion system should be developed for the microfluidic chip. An ideal perfusion system would entail continuous removal of solution around the islet, with this solution then sampled for insulin by the microchip immunoassay. Perfusion would also allow for the islet to remain viable for a longer period of time by replenishing the islet solution and would allow for facile addition of stimulants or drugs. Several perfusion systems were attempted with the current microfluidic design; however, none were successful.

Top Down Perfusion

In the top down perfusion method, an air pressure system was used to drive heated solution to the islet reservoir via a 16" length of 0.02" inner diameter (i.d.) tubing. A vacuum line at the top of the reservoir removed liquid so solutions did not overflow (Figure 5-1). 75 nM Ab, 150 nM FITC-insulin, and RPMI 1640 were placed in the Ab, FITC-insulin, and islet reservoir, respectively, and RPMI 1640 perfused into the islet reservoir at 0.8 mL/min. These conditions produced a high B/F detected in the separation channel, expected in the absence of insulin. The perfusion solution was switched to RPMI 1640 containing 1 μM insulin using a 6-port electronically-actuated valve. Time for the B/F to decrease to a minimum was 1500 s (Figure 5-2A). To test if this time was dependent on the rate of perfusion, the flow was increased to 1.6 mL/min and did not

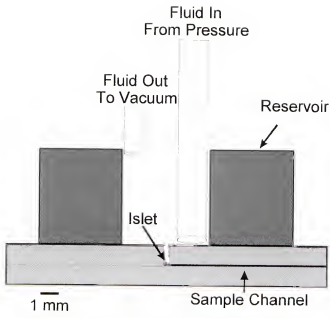

Figure 5-1. Schematic for top-down perfusion. Pressure was used to drive fluid from 0.02" i.d. tubing into the islet reservoir at various flow rates. To prevent solution overflow, a vacuum line at the top of the reservoir was used to remove solution. Due to the small size of the fluidic access hole, the perfusion line could not deliver solution directly to the islet.

significantly effect the time to a decrease in B/F (Figure 5-2B). A molecule with a diffusion coefficient of 2 x 10^{-6} cm^2/s would need 2500 s to diffuse 1.1 mm, the depth of the fluidic access hole. Therefore, the time needed to decrease the B/F appeared to be due to a combination of the perfusion system and diffusion of insulin down the fluidic access hole.

To test this perfusion method, the chip was calibrated and an islet placed in the islet reservoir according to the same procedure given in Chapter 4. Initially, an islet was perfused at 1.6 mL/min with RPMI 1640 containing 3 mM glucose. After obtaining basal release values, the valve was switched to perfuse 11 mM glucose in RPMI 1640. For the first islet tested (Figure 5-3A), the insulin concentration increased in 60 s upon application of 11 mM glucose. However, the concentration detected was below the limit of detection after 250 s. After 1200 s of perfusion, a second increase in insulin

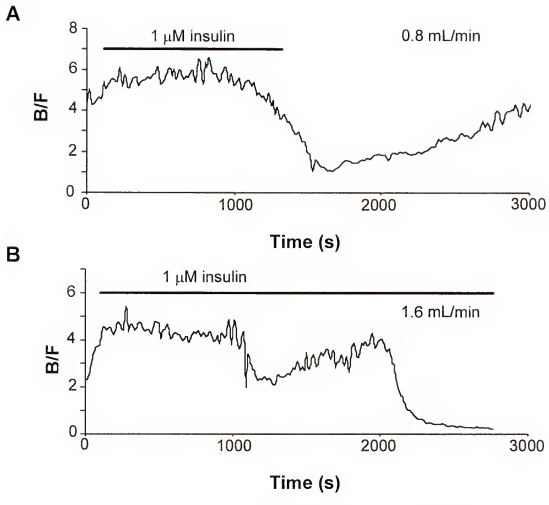

Figure 5-2. B/F changes induced by top-down perfusion. (A) A high B/F was detected when 150 nM FITC-insulin and 75 nM Ab were mixed online with RPMI 1640 perfused into the islet reservoir at 0.8 mL/min. When the perfusion solution was switched to 1 μM insulin (indicated by the horizontal bar above trace), B/F decreased to a minimum in 1500 s. (B) Increasing the perfusion flow rate to 1.6 mL/min did not reduce the time for the B/F to decrease compared to perfusion at 0.8 mL/min. This result indicates that the perfusion system was not limiting the time needed for the B/F to decrease.

concentration was detected with a peak value of 40 nM, but dropped below the limit of detection in 60 s. With a different islet, the concentration of insulin detected increased in 300 s after glucose was perfused and peak insulin concentration was 5400 nM (Figure 5-3B). After stimulated values were obtained, the perfusion solution was switched to 3 mM glucose; however, the insulin concentration detected was still high for 600 s.

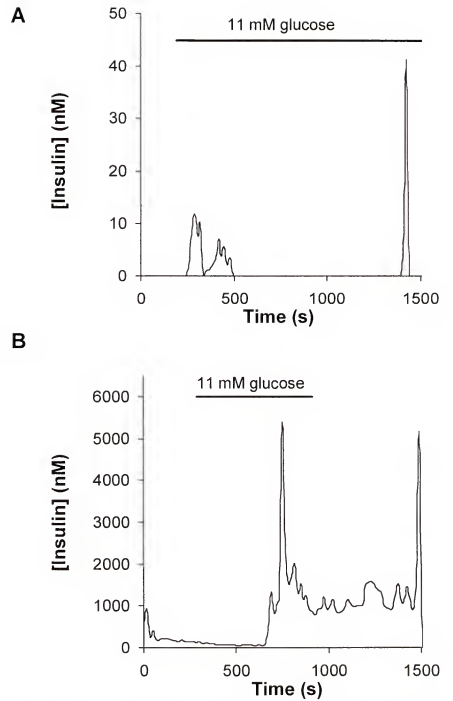

Figure 5-3. Stimulated release from islets perfused with the top-down method. (A) Perfusion of an islet with 11 mM glucose (duration of perfusion indicated by bar above trace) at 1.6 mL/min increased the detected insulin concentration in 250 s, but was below the limit of detection for 1200 s. (B) Application of 11 mM glucose to a different islet increased the insulin concentration detected; however, values never returned to pre-stimulatory levels after perfusion was stopped. Note the difference in insulin concentrations detected between A and B.

Because the volume of the fluidic access hole is unknown due to the method of drilling, it is difficult to calculate the amount of insulin released from the islets to compare to literature values. The difference in apparent perfusion times, for example, 1500 s to decrease the B/F when perfusing an insulin standard compared to stimulated release occurring after 300 s of glucose perfusion, are difficult to explain. There is a difference in diffusion coefficient of insulin and glucose (diffusion coefficient of glucose is 6.7×10^{-6} cm^2/s [Weast, 1975]); however, the difference in times cannot be accounted for by difference in diffusion coefficients. Also, there is a two order of magnitude difference in insulin release for the two islets tested. Due to these conflicting results, no other top-down perfusion experiments were attempted.

Pressure From Perfusion Channel

The next perfusion system tested involved a perfusion reservoir that intersected the grounded islet reservoir via a 5 cm channel (Figure 5-4). 75 nM Ab, 150 nM FITC-insulin, and RPMI 1640 were mixed online according to the standard protocol. Upon detecting a stable B/F, 1.5 psi of gas pressure was applied to a syringe containing 1 μM insulin in RPMI 1640 with tubing (30 cm, 0.02" i.d.) connecting the syringe to the perfusion reservoir. With this system, the peaks had poor S/N, the B/F increased upon addition of insulin, and the peaks were broad (Figure 5-5). These results could be explained by flow from the perfusion channel splitting into the reaction channel, effectively diluting the reagents, reducing reaction time, and reducing increasing the amount of reagents injected, respectively.

Intuitively, it would appear the perfusion flow would exit the fluidic access hole of the islet reservoir (0.11 cm height, 71000 μm^2 cross sectional area) rather than down the

chip (7 cm length, 51 μm^2 cross sectional area). The amount of flow into the chip can be estimated by the following. Assuming that the resistance of each channel is directly proportional to the length of the channel and inversely proportional to the cross-sectional area, most (>99.99%) of the pressure applied to the syringe was dropped along the perfusion channel prior to entering the fluidic access hole of the reservoir. The flow rate through the chip can be calculated according to [Giddings, 1991]:

$$< v >= \frac{\Delta P d^2}{12 L \eta}$$

where <*v*> is the average velocity, ΔP is the applied pressure, d is the depth of the channel, L is the length of the channel, and η is the viscosity of the solution. If L is taken as 7 cm, the calculated flow rate due to the flow split was 8 fL/s. The flow rate out of the islet reservoir was 10 pL/s due to electroosmotic flow (EOF), thus, with this rough calculation, the perfusion system increased the flow rate of the sample channel by 0.1%. This flow rate is a low estimate as the calculation does not take into account the additional resistance of flow to the islet reservoir due to gravity. Nor does the calculation account for splitting the flow to the other sample reservoirs (FITC-insulin or Ab reservoir, both with L = 3 cm) instead of through the entire chip (L = 7 cm).

Lower flow rates of the perfusion system were attempted; however, pressures lower than 1.5 psi were unstable. Different configurations of this setup were also attempted, such as lowering the volume in the islet reservoir (with and without the evaporation cap) to reduce the flow resistance in the fluidic access hole further. However, with the increased temperature that was needed for online mixing, the solution in the islet reservoir evaporated and electrical contact was lost. Thus, this type of perfusion system was not used to perfuse islets.

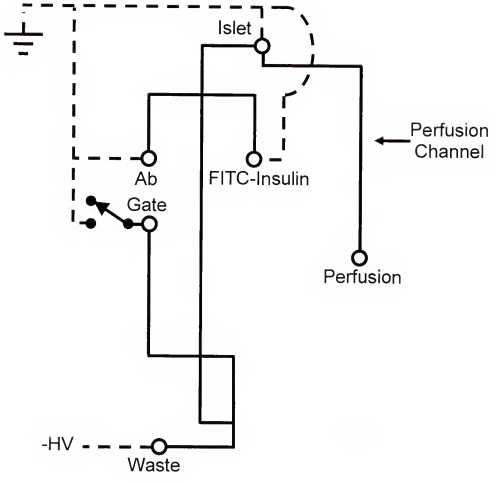

Figure 5-4. Chip layout with perfusion reservoir. Fluidic channels are shown as solid lines and electrical connections are dashed lines. The perfusion reservoir was connected to the islet reservoir via a 5 cm channel (20 μm wide, 3 μm deep). To generate flow from the perfusion reservoir, a pressure system was coupled to the perfusion reservoir or EOF was generated by applying +HV to the perfusion reservoir.

Perfusion Via Electroosmotic Flow

The previous perfusion examples demonstrate the difficulties associated with coupling macroscopic systems to microfluidic chips. In an attempt to integrate the perfusion system into the chip, 75 nM Ab was placed in the Ab reservoir, 150 nM FITC- insulin placed in the FITC-insulin reservoir, and RPMI 1640 placed in the islet reservoir with

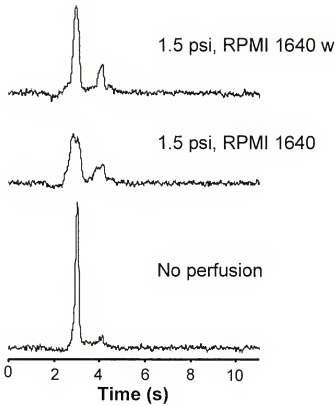

Figure 5-5. Effect of pressure-induced flow from the perfusion reservoir on B and F peak shapes and ratios. Prior to perfusion (bottom electropherogram), B and F FITC-insulin peaks are sharp. Application of 1.5 psi to a syringe filled with RPMI 1640 connected to the perfusion reservoir decreased and broadened B and F FITC-insulin peaks (middle electropherogram) possibly due to splitting of perfusion flow through the chip. Switching the perfusion solution to 1 μM insulin increased the B/F ratio (top electropherogram).

all reservoirs grounded (Figure 5-4). Online mixing was performed and a high B/F detected. RPMI 1640 with 1 μM insulin was placed in the perfusion reservoir and +3 kV applied. EOF transported insulin to the islet reservoir where it was sampled into the reaction channel. B/F decreased to a low stable level and removal of voltage to the perfusion reservoir increased the B/F detected (Figure 5-6).

This perfusion system was used to stimulate two islets. Both islets were stimulated by applying +3 kV to the perfusion reservoir that contained 10 or 20 mM

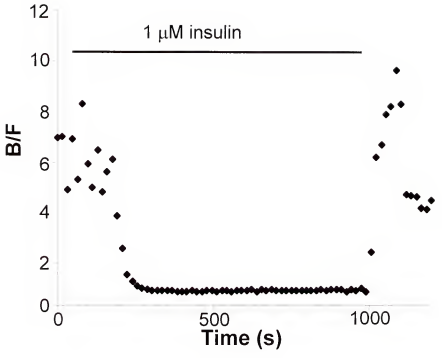

Figure 5-6. Electrokinetic perfusion of insulin to islet reservoir. Online mixing of 150 nM FITC-insulin, 75 nM Ab, and RPMI 1640 with all sample reservoirs grounded produced high B/F ratios. Application of +3 kV to the perfusion reservoir (indicated by bar above trace) that contained 1 μM insulin in RPMI 1640 lowered the B/F detected in the separation channel. Removing the voltage from the perfusion reservoir caused the B/F to increase to pre-stimulatory levels.

glucose in RPMI 1640. Secretory profiles from the two islets showed a slow increase in insulin concentration, indicating either the islets were not responsive, or the islets were not stimulated (Figure 5-7). After experiments were performed, several cells in the first islet appeared ruptured, whereas the second islet showed no difference in morphology after the experiment. It may be possible that application of +HV to the perfusion reservoir

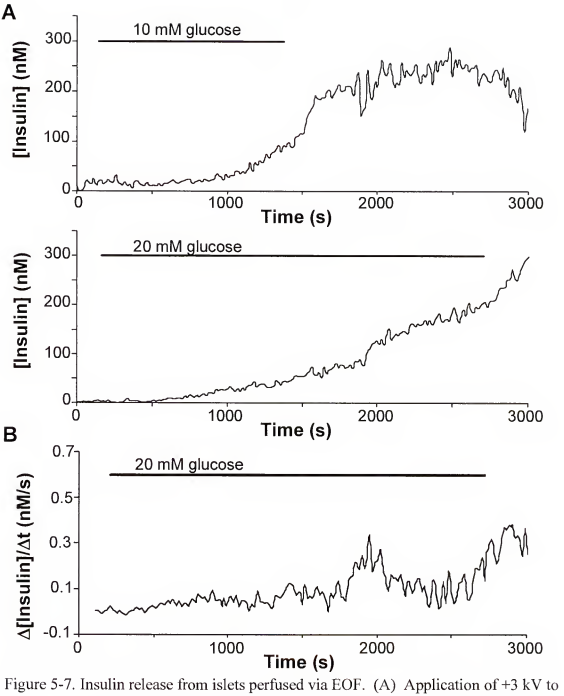

Figure 5-7. Insulin release from islets perfused via EOF. (A) Application of +3 kV to the perfusion reservoir (duration indicated by horizontal bar over traces) containing 10 (top trace) or 20 (bottom trace) mM glucose in RPMI 1640 caused a slow increase in insulin release. Several cells in the islet from the top trace appeared to have ruptured during stimulation, possibly accounting for the increased insulin concentration detected after perfusion was stopped. (B) First derivative of secretion from the bottom trace in A. An increase in the rate of secretion was observed 1600 s after initiation of voltage to the perfusion reservoir. The length of time needed for an increase in secretion rate may be due to diffusion of glucose throughout the fluidic access hole as the glucose is sampled into the reaction channel.

caused insulin or glucose to be sampled down the reaction channel without complete washout of the solution in the fluidic access hole of the islet reservoir. As shown in Figure 5-7B, an increase in the rate of insulin secretion occurred after 1600 s of perfusion, possibly due to lateral diffusion of glucose throughout the fluidic access hole as the glucose was sampled to the reaction channel.

Conclusion

The current problem with coupling perfusion to the microfluidic chip is the interface of the macro perfusion components to the microchip. Although no method was found that was amenable to perfusion, Chapter 6 provides a brief outline of one possible solution.

CHAPTER 6
SUMMARY AND FUTURE STUDIES

Insulin Signaling Pathway

Application of glucose, glyceraldehyde, and arginine to insulin receptor substrate-1 (IRS-1) knockout (KO) isolated β-cells results in reduced secretion compared to wildtype (WT) cells. This result is consistent with other reports using IRS-1 KO β-cell tumor lines and islets in that defects in the insulin signaling pathway result in reduced secretion induced by a variety of secretagogues [Kulkarni *et al.*, 1999b; Porzio *et al.*, 1999; Kubota *et al.*, 2000]. IRS-1 also appears to help maintain temporal response of Ca^{2+} changes upon stimulation with glucose, glyceraldehyde, and arginine, as KO β-cells have statistically significant differences in latency and duration of Ca^{2+} increases compared to WT β-cells.

L-783,281, shown to initiate glucose uptake in peripheral tissues by activation of the insulin receptor tyrosine kinase [Zhang *et al.*, 1999], also induces intracellular Ca^{2+} changes and secretion from single pancreatic β-cells. The mechanism behind the effect of the insulin mimetic appears to involve several of the proteins involved in the pathway of insulin-stimulated insulin secretion, including IRS-1 and phosphatidylinositol 3-kinase.

The results of both the IRS-1 KO and L-783,281 studies provide more evidence to the hypothesis of the insulin signaling pathway being a link between defective insulin

secretion from β-cells and insulin resistance in peripheral tissues. To further these studies, the effects of other proteins involved in insulin signaling should be investigated.

IRS-2 KO islets secrete more insulin upon a glucose stimulation compared to WT islets [Kubota *et al.*, 2000]. An increase in insulin secretion is observed at the onset of type 2 diabetes, although it is not known if increased insulin secretion leads to insulin resistance, or if insulin resistance leads to the increase in insulin secretion. Therefore, a defect in IRS-2, as well as IRS-1, could link both hallmarks of diabetes. However, again due to the difficulties associated with interpreting results from islets of Langerhans, secretion from isolated IRS-2 KO β-cells should be investigated.

The effect of IRS-2 deletion on changes in intracellular Ca^{2+} concentration ($[Ca^{2+}]_i$) would also be important to determine. In IRS-1 KO islets, disrupted $[Ca^{2+}]_i$ oscillations are observed upon glucose perfusion (see Chapter 2), implicating disrupted insulin secretion as changes in $[Ca^{2+}]_i$ are believed to drive insulin secretion [Jonas *et al.*, 1998]. However, the role of IRS-2 in maintaining Ca^{2+} oscillations has not been investigated. Also, in an attempt to confirm the hypothesis of an interaction of IRS-1 with SERCA pumps and Ca^{2+}-sensitive proteins set forth in Chapter 2, differences in latency and duration of stimulated Ca^{2+} changes from IRS-2 KO β-cells should be compared to IRS-2 WT β-cells. The use of Fluo-5N as described in Chapter 2 as a marker of endoplasmic reticulum Ca^{2+} would also provide data for the aforementioned hypothesis.

Microfluidic Chips

The design for the microfluidic chip enabled fast, quantitative values of insulin secretion using offline or online mixing of reagents combined with offline sampling. There are several applications for the measurement of release with these types of formats,

including testing viability of islets prior to transplantation. In addition to these measurements, the ability to place an islet on the chip allows for the determination of secretion kinetics. However, to quantitatively measure complex release patterns (such as oscillations) with high temporal resolution, modifications of the chip design are necessary. New designs for decreasing the response time and the ability to perfuse islets within the chip are described in the following sections.

Response Time

As mentioned in Chapter 4, the response time of the system was 30 s, or the time required to make two separations. However, this value may be overestimated as faster sampling of the reaction channel would lead to a determination of the actual response time of the system. The response time should be determined by band broadening in the reaction channel and the time for separation. Assuming no dead volume in the system, the predicted value for the response time is 5 s, or the time needed for separation of bound (B) and free (F) FITC-insulin. Therefore, to reduce response time, axial diffusion of reagents in the reaction channel should be limited, and fast sampling and separation of reagents is needed

Reducing mixing time

To reduce axial diffusion, the time reagents spend in the reaction channel should be determined by the time needed to mix completely and for the reaction to proceed to equilibrium. As mentioned in Chapter 4, 50 s allows complete mixing and reaction of insulin, FITC-insulin, and Ab. Assuming a diffusion coefficient of 1.98×10^{-6} cm^2/s for insulin [Huang *et al.*, 1995], complete mixing occurs in 10 s (the time for insulin to diffuse across the reaction channel ten times). Thus, the reaction is complete in less than 40 s. If reaction kinetics is optimized or if the time needed for complete mixing is

decreased, the time spent in the reaction channel could be reduced, resulting in less band broadening.

To increase the mixing in microfluidic chips, several methods have been developed. One example used in glass chips was to split the reagent channel into several smaller channels and then recombining, thus mimicking a multiple flow path system [He *et al.*, 2001]. With this type of system, complete mixing of fluorescein and water was observed after reagents had traveled 200 μm, while laminar diffusion across a channel led to mixing in 3 mm. Of course, with this type of mixing scheme there will be band broadening due to eddy diffusion, although the benefits of mixing quickly may overcome this disadvantage. One possible method to reduce axial diffusion and mix quickly is to insert a non-miscible liquid [Song *et al.*, 2003] or air [Edwards *et al.*, 1999] into the reaction channel at constant intervals. Reagents between these boundaries will mix due to convective flow, while limiting axial diffusion.

Fast sampling and separations

The next step in decreasing the response time is to optimize the rate at which sample is injected onto the separation channel. In the current experimental setup, an injection is made every 15 s although separation of B and F FITC-insulin is accomplished in 5 s. The simplest way to decrease response time would be to make one injection every 5 s. One problem with this method is the flow rate in the reaction channel is approximately 55% higher during an injection than during a separation due to an increase in voltage across the channel. Therefore, the sampling rate cannot be so high that the mixing or reaction time of reagents is decreased. The designs to increase mixing proposed in the previous section may allow for faster sampling without hindering the

mixing or reaction time. If the sampling rate is increased, to improve response time further, faster separation of B and F needs to be accomplished.

To decrease the separation time, a higher separation voltage can be applied; however, because one power supply controls both the separation and reaction voltage, reagents would spend less time in the reaction channel. Multiple power supplies could be used to separate the flow rates of the reaction channel and separation channel, but ideally, the components of the system would be kept to a minimum. One possible method for increasing the velocity of the reagents in the separation channel is to increase the electric field, although this would slightly perturb the electric field of the reaction channel.

The electric field can be increased by decreasing the length or decreasing the width of the separation channel. Decreasing the length of the separation channel should be trivial with a slight modification of the current design and should not effect the separation of B and F FITC-insulin as resolution in CE is independent of the length of the separation channel [Giddings, 1991]. To illustrate this point, a microfabricated device has been used with a 200 μm channel for separation of a binary mixture in 0.8 ms using an electric field of 53 kV/cm [Jacobson *et al.*, 1998].

The width of the separation channel can be decreased by two methods. First, the procedure for making chips can be optimized to reduce broadening of channels during fabrication. For example, in Chapter 4, a photomask blank was exposed to UV light for 5 s at 26 mW/cm^2; however, a 1 s exposure at this irradiance is sufficient to make the photoresist soluble in developer solution. Thus, any time after 1 s leads to line broadening of the exposed region. Also, each subsequent step in photolithography (developing photoresist, etching chrome, and etching glass) should be optimized because

isotropic removal of material leads to further broadening. Second, a photomask with a smaller linewidth for the separation channel can be obtained. Unfortunately, the linewidth currently used for the mask (5 μm) is the limit of most cost-effective commercial lithography equipment and can only be decreased by using electron beam or x-ray lithography, both increasing the cost of the photomask.

One consideration of changing the resistance of the separation channel is the effect on the injection scheme. For the gating flow to properly shunt reagents away from the separation channel during separation, one of two conditions must be met [Jacobson *et al.*, 1999]: 1) the electric field of the reaction channel must be equal to or less than the electric field of the waste channel opposite the separation channel, or 2) the electric field of the gate channel must be equal to or greater than the electric field of the separation channel. Therefore, a calculation of relative electric fields should be performed prior to changing the width or length of the separation channel to ensure the injection scheme will be effective. The program B2 SPICE A/D v4 Lite is available as freeware on the web from Beige Bag Software, Inc. and can be used to calculate relative electric fields by measuring the voltage dropped across channels.

Future Perfusion Studies

Besides the methods of perfusion mentioned in Chapter 5, other methods are available that may make perfusion of an islet in a chip possible. One way to meet the requirement of sampling all release from an islet with the current microfluidic design is to couple the perfusion system directly to the islet reservoir. When flow is started, all solution containing the released insulin would be driven down the reaction channel to mix with Ab and FITC-insulin. Injection of this mixture onto the separation channel

could be performed with the current injection scheme. To perfuse directly to the islet reservoir, the flow rate from the perfusion system would need to be low to prevent dilution of released insulin and to ensure the flow does not split to the Ab and FITC-insulin reservoirs. The difficulty of this method would be ensuring the perfusion flow rate is equal to or lower than the flow rate from the Ab and FITC-insulin reservoirs (10 pL/s) while still able to completely flush out the solution in the fluidic access hole of the Islet (70 nL) in a relatively fast time. Simultaneous measurement of intracellular messengers would also be difficult with this system due to the background fluorescence of the coupling devices used in the perfusion system.

Another possible method is to place an islet in a flow-through channel. For example, in two reports, pressure was used to drive solution through a large flow channel (3 mm wide x 40 μm deep) where the majority of flow exited a reservoir at the output of the large channel and a small percentage of flow was split to a perpendicular channel (80 μm wide x 40 μm deep) [Chen *et al.*, 2002; Lin *et al.*, 2001b]. This perpendicular channel was shunted to a waste channel via an electroosmotic flow-gate and injections onto a separation channel could be performed.

Building on this idea, if an islet was placed inside a flow channel and perfused with a physiological solution, the effluent containing insulin could be sampled, mixed with FITC-insulin and Ab, and injected onto a separation channel for determination of B/F (Figure 5-8). Several features of this possible design are described below.

To hold the islet, a 250 μm deep channel (3 mm in length, 1 mm wide) is etched into a photomask blank (shown as "Islet Channel" in Figure 5-8). After etching the Islet Channel, a different mask with the remaining channel design is used to expose the same

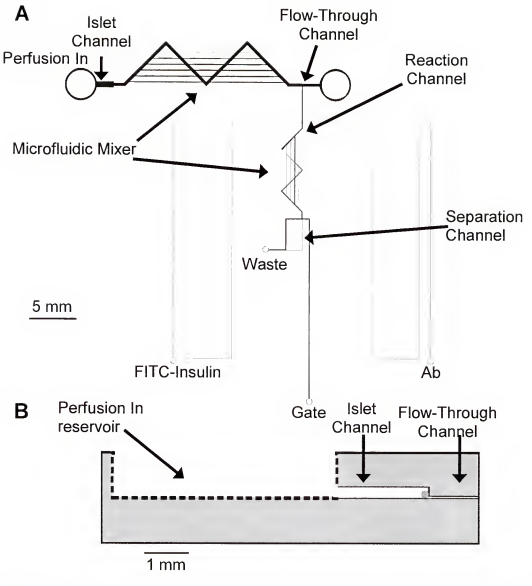

Figure 5-8. New microfluidic design for perfusion of islets. (A) An islet situated in the Islet Channel is perfused by applying pressure to the "Perfusion In" reservoir. The effluent containing insulin passes through a mixing region to ensure a homogeneous solution. After passing through the mixing region, the majority of flow exits the chip, while a small percentage is split down the reaction channel where insulin mixes with Ab and FITC-insulin. After passing through another mixing region, injection onto the separation channel occurs by the same injection scheme currently used. The channels leading to the FITC-Insulin, Ab, Gate, and separation channel are more resistive to flow compared to the reaction and waste channels to ensure flow is not split toward these channels. Also, the separation channel is small allowing a large electric field for fast separations. (B) Cut away view of an islet in the Islet Channel. The small depth of the Flow-Through Channel holds the islet in place.

photomask blank and the resulting channels etched 10 μm deep. The "Flow-Through Channel" intersecting the Islet Channel is 500 μm wide to ease in aligning the second mask to the etched Islet Channel. After drilling fluidic access holes and bonding to a top plate, the Islet Channel is big enough to hold an islet, and the small depth of the remaining channels will hold the islet in place.

Upon application of pressure to the perfusion reservoir, effluent containing insulin travels through a microfluidic mixer to homogenize the insulin concentration and is split down a perpendicular channel. The insulin is mixed with Ab and FITC-insulin in the reaction channel (20 mm in length, 100 μm wide) where a second microfluidic mixer is used to ensure fast mixing of reagents. The channels from the Ab and FITC-insulin reservoirs are resistant to flow (150 mm long, 25 μm wide) so the pressure system does not split effluent to these reservoirs.

The injection scheme for the new design is similar to the current injection scheme. To make an injection, a high voltage relay is used to switch the voltage on the gate reservoir from ground to float for a set period of time and returned to ground. The separation channel is smaller than the waste channel (5 μm vs. 100 μm) so effluent flow will not leak into the separation channel. Also, a smaller separation channel will allow higher voltages to be applied for separation. The electric field is lower in the reaction channel compared to the waste channel (due to the longer length of the reaction channel), satisfying one of the design criteria for this injection scheme (Jacobson *et al.*, 1999]. Placing the islet inside the flow-through channel would inhibit access to the islet, making the measurement of intracellular messengers with electrodes difficult; however, optical detection of intracellular sensors (such as Fura-2 for intracellular Ca^{2+} changes) should

still be possible. The use of a flow-through channel should allow for quantitative determination of insulin secretion and be amenable to continuous, fast sampling.

APPENDIX A
FABRICATION OF MICROFLUIDIC CHIPS

Material Specifications

Glass is a popular substrate for microfluidic (μF) chips, although plastics are becoming more common due to the ease in fabrication of plastic μF chips. Several types of glass are used in μF devices, such as soda lime, quartz, and borosilicate. Soda lime glass is easy to work with as it etches quickly, bonds at relatively low temperatures, and is inexpensive; however, the etching quality is suspect and autofluorescence of the glass can be problematic. Therefore, this type of glass is typically used in preliminary studies. The most optically useful substrate is quartz as it is transparent from ultraviolet through infrared. Unfortunately, quartz is difficult to work with as the etching rate is slow and the annealing temperature is approximately 1000 °C, too high for some furnaces. Additionally, the cost of quartz substrates can be almost 2-3-fold higher than soda lime glass; however, quartz is one of the few substrates suitable for low noise optical detection with UV-excitable dyes. The most common glass substrate used in the production of μF chips is borosilicate glass because of its optical characteristics (transparent from approximately 350 nm through 700 nm) and its physical properties (annealing temperature of 640 °C, resistant to most chemicals).

Borosilicate glass incorporates a variety of subtypes, with all borosilicate glasses containing a minimum of 5% B_2O_3 [Corning Glass website, 2003]. Most borosilicate glasses used for μF chips are produced by the float method, which is a technique used to

produce optically flat glass. In the float method, molten borosilicate glass is floated on molten tin and the glass is drawn from the tin producing an extremely flat substrate. Flat glass is necessary for the manufacture of μF chips as uneven glass is difficult to bond to other pieces of glass.

Fabrication of μF chips using borosilicate glass produced by the float method (borofloat glass) involves photolithography, wet chemical etching, and bonding. Each of these steps will be explained in detail in the following sections.

Photolithography

The intended channel design is drawn in AutoCAD 2000 (San Rafael, CA) and submitted to Digidat (Pasadena, CA) for the production of a right reading, anti-reflective chrome down, 4" x 4" x 0.90" soda lime or white crown photomask. Photomasks should be handled with care as any scratches in the chrome can ruin the design.

The glass used to produce μF chips are intended for the production of photomasks, and are known as photomask blanks. Schott borofloat photomask blanks are acquired from Telic Company (Santa Monica, CA) with a 520 nm layer of AZ1518 positive photoresist on a 120 nm layer of chrome. Although other companies claim to sell Schott borofloat glass, the material specifications do not always correspond to the specifications given by Schott. Acquisition of Schott borofloat glass is essential since the fabrication procedure has been optimized for this type of glass. Physical characteristics of Schott borofloat glass are: 560 °C annealing temperature, 32.5 x 10^{-7} K^{-1} thermal expansion, 2.23 g/cm^3 density, and 1.472 refractive index. Therefore, if photomask blanks are purchased from a different company, the physical characteristics of the new glass should be compared to the above to ensure the procedure outlined below is relevant.

UV Exposure

The following steps are performed in a class 10000 cleanroom unless stated otherwise. Filtered N_2 is used to remove surface particles from the photomask and a photomask blank. The UV exposure unit currently used in the lab (Optical Associates, Inc., Milpitas, CA) is intended for contact exposure, meaning the photomask and photomask blank must touch during exposure to ensure even linewidths in the photoresist. The photomasks presently used in the lab are fabricated such that the chrome surface (brownish-gold in color) should be in contact with the photomask blank. To secure the photomask to the photomask blank, two methods are used. The first method entails a cassette that the photomask blank is placed in and the mask is laid over the top. This method is the most reproducible in chip-to-chip production. The second method uses two pieces of scotch tape (one at either end of the blank) to secure the mask to the blank. The only precaution in the UV exposure step is to ensure that the mask is centered on the blank. Centering the mask prevents overhanging reservoirs in the finished μF chip. The photomask/photomask blank assembly is placed under the UV exposure unit, which has been turned on for at least 5 min to warm up the lamp, and the chip is exposed for a minimum of 1 s at 26 mW/cm^2. After exposure, the mask is immediately placed in its protective holder to protect from solutions in the remaining steps.

Development and Chrome Etching

To aid in bonding, excess photoresist is removed from the photomask blank. Removal of excess photoresist allows the glass non-adjacent to the channels to be etched in a future step leaving only a small area of the glass to bond. Using a cotton swab saturated with acetone, photoresist 2-3 mm away from all channels is removed. The chip must be held at a certain angle in the light to reveal the channels, although a cursory

movement of the hand enables visualization. Enough photoresist must remain at the end of each channel so that fluidic access holes can be drilled. Removing excess photoresist prior at this point is a precautionary measure so that if a UV-exposed region is accidentally removed, little time has been invested in the fabrication process.

After removing excess photoresist, the exposed blank is placed in ~15 mL of AZ915MIF (Clariant Corporation, Summerville, NJ) developer. The solution is swirled over the top of the blank for 15-20 s then rinsed with deionized water. After development, the photomask blank is placed in 25 mL CEP-200 chrome etchant (Microchrome Technologies, Inc., San Jose, CA). The solution is swirled over the top of the chip until no chrome remains, typically 1-2 min. Chrome etchant is a hazardous material and is only shipped by truck. Shipping takes approximately a month for delivery; therefore, it is best to order the chrome etch solution well in advance.

Wet Etching of Glass

The next step in the fabrication procedure is to etch the photomask blank. Etching solution contains a mixture of 14:20:66 (v:v:v) HNO_3:HF:H_2O. Extreme caution needs to be taken when working with HF as the acid is a highly dangerous substance. Plastic dishes should be used for all steps and butyl gloves and eye goggles should be worn. In a clean plastic dish, 17 mL HNO_3 is added to a stirring solution of 79 mL H_2O; afterwards, 24 mL of 40% HF is added. The solution is allowed to stir for ~1 min to ensure homogeneity of the solution. During this time, the developed photomask blank is rinsed with water to remove any particles and then placed in the etching solution for an appropriate amount of time. The etching rate has previously been found to be 0.3 μm/min, although the etching rate should be periodically tested with a profilometer.

After the etched blank is removed with plastic forceps and placed in a 1 L beaker of water, etching solution is discarded into the proper waste receptacle. The etched glass is removed from the 1 L beaker of water, rinsed extensively with deionized water, dried, and brought outside the cleanroom to drill fluidic access holes.

Drilling of Fluidic Access Holes

Using a drill press and an appropriate sized diamond-tipped drill bit (Tarton Tool Co., Troy, MI), fluidic access holes at the end of each channel are drilled. It is best to drill with the etched channels toward the drill bit as the glass will "pop" out the backside when drilling. Care must be taken so that the glass is not broken during drilling or the bit does not come into contact with more than one channel. After drilling, the etched chip is aggressively rinsed with water to remove all glass fragments. A good method to aggressively rinse the etched chip is to pinch a hose attached to a water spigot, increasing the velocity of the water. To further facilitate removal of glass particles, the etched glass is placed (channels down) in a clean beaker and sonicated for 10-15 min in Milli-Q (Millipore, Bedford, MA) water.

Cleaning of Drilled Chips

There are multiple steps in the cleaning procedure and it is vital that the glass be cleaned properly prior to bonding to have a functional chip. Because of this reliance on cleaning, individual steps in the following procedure are numbered. (1) In the cleanroom, acetone and chrome etchant are used to remove the remaining photoresist and chrome from the etched blank and another piece of photomask blank (used for the top plate). It is imperative to use matching types of glasses for the etched chip and top plate because different thermal expansions will cause the glass to shatter during the bonding process. In addition to having the same type of glass, all chrome must be removed from both the

etched blank and top plate as a small amount of chrome left on either piece of glass will ruin bonding; therefore, both pieces of glass are left in a stirring chrome etch solution for ~ 10 min. (2) While etching the chrome, 150 mL deionized water is poured into a clean, 250 mL beaker and placed on a hotplate in the hood. The temperature of the hot plate is set to 60 °C. (3) To this beaker, 30 mL NH_4OH is added and the hot plate with the beaker are moved to the back of the hood to allow the temperature to reach 60 °C. (4) Another clean, 250 mL beaker is placed in the hood and filled with 180 mL H_2SO_4. The next step is very exothermic and should be performed with great care. (5) The sulfuric acid is returned to its cabinet and 60 mL of 30% H_2O_2 is added to the beaker with H_2SO_4. This mixture is called piranha solution. (6) The piranha solution is stirred with a metal spatula and the etched blank and top plate are rinsed of chrome etch solution and placed in piranha for 20 min. Piranha solution is used to aggressively clean the glass of any organic material; therefore, all organic solvents should be removed from the hood as they are highly reactive with piranha. (7) During the cleaning with piranha, 30 mL of 30% H_2O_2 is added to the beaker on the hot plate, resulting in a mixture known as RCA solution. (8) After 20 min in piranha, the chip and top plate are removed and rinsed for 2-3 min under the deionized water spigot tracing the channels with the water stream. (9) After rinsing, the chip and top plate are placed in the RCA solution for 20-40 min. The chip and top plate must be completely covered with RCA solution during the cleaning process. If the solution evaporates, more water is added.

After cleaning with RCA, the chip and top plate are removed with forceps and each piece is briefly rinsed with deionized water. After this initial rinsing, both pieces of glass are held in one hand and vigorously rinsed with deionized water from the spigot for 4-5

min. It is best to trace the etched regions with the water stream, ensuring that no debris is left in the channels. This rinsing step is crucial to obtaining clean chips prior to bonding. Immediately after cleaning, the plates are brought into contact while still wet. Filtered N_2 or a crew wipe is used to dry the outside of the chip. The chip is squeezed from the middle towards the outside to removed trapped air bubbles. If this process is followed, the assembled chip should be fairly stable with capillary action holding the two pieces of glass together.

Bonding Chips

The assembled chip is placed inside a Neytech Centurion Qex furnace (Pacific Combustion, Los Angeles, CA) between two pieces of ¼" thick Macor ceramic plates. A 400 g stainless steel weight is placed on top of the Macor plates and the temperature is ramped, under vacuum (~20 mm Hg) at 10 °C/min to 640 °C, held for 6-8 hours, and ramped down to room temperature at 10°C/min. After bonding, a microscope is used to examine all channels in the chip. If any particulates are in the channels, it is best to discard the chip and make another. Since the electric fields and therefore flow rates are dependent on the resistances of the channels, a small particle can have a large impact on the performance of the μF chip. If there are no particulates in the channels and the chip has unbonded regions that intersect a channel, a second bonding cycle is performed by placing the chip in the furnace (with the opposite side facing up as compared to the first bonding) for another 6-8 hours using the same temperature ramp as before. When bonding is complete, chips are stored in capped 50 mL plastic centrifuge tubes to ensure no dust or particulates come into contact with the chip. No solutions should be introduced to the chip until reservoirs have been applied. Microfluidic reservoirs are

bought from Upchurch Scientific (Oak Harbor, WA) and applied according to the manufacturer's instructions.

APPENDIX B
EVERYDAY USE AND PROBLEMS OF MICROFLUIDIC CHIPS

Experiments with Microfluidic Chips

After securing reservoirs to a microfluidic chip, the reservoirs are flushed for 15 s with water. After flushing, a 5 mL syringe connected to a 0.2 μm nylon syringe filter is used to fill all reservoirs with 1 M NaOH. Electrodes are placed in all reservoirs and the current limit is set to 10 μA. High voltage (-4 or -5 kV) is applied to the waste reservoir with all other reservoirs grounded. Once all bubbles and water are out of the waste and separation channels, the current will increase to 10 μA and the voltage will decrease to a stable level. Once a stable voltage is attained, injections are started using a 5 s injection time with a 5 s separation time. During an injection, the voltage will increase and the current will decrease until all water and air bubbles are out of the reaction and sample channels. After these channels are filled with NaOH, the current during injections will increase to 10 μA and the voltage will decrease to a stable level. Once a stable voltage is acquired for both injection and separation (the voltage will be lower during separation than during an injection), the current limit is increased to 50 or 100 μA and injections continued for ~ 1 hour. After this first conditioning with NaOH, each subsequent day experiments are performed, the chip is conditioned with NaOH according to the same procedure, but for 15-30 min.

After conditioning with base, NaOH is removed from the reservoirs by shaking the chip upside down and by flushing out with water from the Milli-Q dispenser by pinching

the hose according to the same procedure as described in Appendix A. After flushing each reservoir for 30 s, buffers are placed in the appropriate reservoirs again using syringes connected to 0.2 μm nylon filters. Electrodes are inserted into reservoirs and current limit is lowered to 10 μA. The voltage and injection scheme that will be used in experiments is applied and the current will decrease (with a concomitant increase in voltage) as the NaOH is flushed from the chip. Once stable voltage and current are attained, solutions are removed by shaking the chip and the resistive heater is taped to the back. The heater is turned on, reservoirs are again filled with buffers, and conditioning proceeds for 20 min. After 20 min, the buffers are removed with a pipette and experiments are performed. It is important to use a pipette to add and remove solutions so the heater will not be placed in a different position on the chip. Different placements of the heater lead to different temperatures of the chip, causing irreproducible migration and reaction times.

After experiments are finished for the day, water from the Milli-Q water supply is used to flush all reservoirs and the chip is cleaned with 1 M NaOH for 15 min. After cleaning with NaOH, the chip is placed in a beaker or 50 mL centrifuge tube completely immersed in Milli-Q water. No bubbles should be left in the reservoirs when the chip is stored overnight.

Clogging

Clogging is a significant issue with the microfluidic chips, especially when using small channel dimensions. Experience will allow the user to determine which clogs are removable, although no method has been found to reproducibly remove clogs from chips. By far, the best method is to reduce the possibility of clog formation. There are two

major sources of clogging: during fabrication and during experimentation. If the procedure in Appendix A is followed, few clogs should be observed after fabrication. If several chips in a row are clogged after the fabrication procedure, the cleanroom and all beakers used for fabrication should be thoroughly cleaned. Additionally, it is best to slow down and ensure that care is taken with all steps.

Most clogs occur during experimentation, and the best way to reduce the chance for clogging is to filter all solutions as they are introduced to the chip. Buffers are filtered once made and new buffers should be made every 2 days (not from stock solutions). For all solutions, a syringe and syringe filter is used for filling reservoirs during conditioning stages. However, this filling method cannot be used for experiments as it is necessary to have equal volume of solutions in all reservoirs to reduce pressure-induced flow. Thus, all buffers to be used for experiments are first placed into vials using a syringe and syringe filter. The most significant source of clogging is found when poly(propylene) tubes are used as the vials; therefore, clean glass vials are used. When performing an experiment, equal volumes of solution from these vials are placed in the chip using a pipette.

When working with protein solutions, nylon syringe filters cannot be used as proteins bind to the filter. Several types of filters are designed for proteins, such as polyvinylidene fluoride (PVDF) and Al_2O_3 filters, although these filters have not been tested with the chip system. Clogging can be reduced if a small volume of protein stock solution is added to a glass vial containing filtered buffer solution.

Initial filling of the chip with NaOH can also result in a clog if a bubble is in a channel and the current limit is increased to 50 or 100 μA. These clogs may be produced

due to Joule heating of the solution around the bubble. There is little to be done once a clog like this has formed, as no solvent has been found to dissolve these types of clogs. The best way to reduce the chance of these clogs is ensuring no bubbles are present (seen as spikes or instability in the current) in the channels when the current limit is increased. To reduce bubble formation during initial filling of the chip, methanol or ethanol can be added to the 1 M NaOH (1-5% by volume) and this solution used to fill the chip. This method should only be used if bubbles are a continuous problem.

Running the chip for extended periods of time with protein solutions can also induce the formation of clogs, possibly due to protein precipitation, especially when using the heater. Concentrated HNO_3 or 1 M NaOH can be used to remove these clogs, but care must be taken that the copper alligator clips do not come into contact with the acid as the clips will dissolve. When buffers with a higher pH are placed in the chip, the copper precipitates resulting in another clog. One way to reduce the likelihood of this type of clog is to frequently (every 3-4 h) condition the chip with NaOH.

Upon introduction of fluids to the chip, the chip should not be heated above 100 °C. Heating the chip with buffers in the channels, occassionally even Milli-Q water, results in clogs. Thus, it is important to use new epoxy rings for the reservoirs, because if the reservoirs leak (seen only after introduction of solutions), there is sufficient method to reseal the reservoirs. The only recourse to a leaking reservoir is to seal the leak with an epoxy that does not require heat to cure.

The most successful method to remove clogs and bubbles is to use a syringe coupled to the chip. With this method, many clogs have been removed, although the method does not work 100% of the time. A gastight syringe (Hamilton Company, Reno,

NV) with a luer tip (Upchurch Scientific, Oak Harbor, WA, Part number 81020) is connected to a piece of PEEK tubing (1/16" o.d., 0.02" i.d.) via a luer-1/16" tubing adaptor (Upchurch Scientific, Part number P-658). The output of the tubing is connected to a 1/4-28 nut with a vacutight fitting (Upchurch Scientific, Part number P-938X) and screwed into the reservoir closest to the clog. Placing the chip on the stage of a microscope, the clog is brought into view and pressure applied by hand causing the clog to move. If the clog does not move, the 1/4-28 nut can be screwed into a different reservoir and pressure applied again. If the syringe method cannot get the clog out, it is best to use a new chip. It is imperative to have a clean chip, as no experiment has ever worked with a clog in any channel.

LIST OF REFERENCES

Alcazar, O.; Gine, E.; Qiu-Yue, Z.; Tamarit-Rodriguez, J. *Biochem. J.* **1995**, *310*, 215-220.

Algenstaedt, P.; Antonetti, D. A.; Yaffe, M. B.; Kahn, C. R. *J. Biol. Chem.* **1997**, *272*, 23696-23702.

Alter, C. A.; Wolf, B. A. *Biochem. Biophys. Res. Commun.* **1995**, *208*, 190-197.

Ammon, H. P. T.; Verspohl, E. *Endocrinology* **1976**, *99*, 1469-1476.

Araki, E.; Lipes, M. A.; Patti, M-E.; Bruning, J. C.; Haag, B., III; Johnson, R. S.; Kahn, C. R. *Nature* **1994**, *372*, 186-190.

Araujo, E. P.; Amaral, M. E. C.; Souza, C. T.; Bordin, S.; Ferreira, F.; Saad, M. J. A.; Boschero, A. C.; Magalhaes, E. C.; Velloso, L. A. *FEBS Letters* **2002**, *531*, 437-442.

Aspinwall, C. A.; Brooks, S. A.; Kennedy, R. T.; Lakey, J. R. T. *J. Biol. Chem.* **1997**, *272*, 31308-31314.

Aspinwall, C. A.; Huang, L.; Lakey, J. R. T.; Kennedy, R. T. *Anal. Chem.* **1999a**, *71*, 5551-5556.

Aspinwall C. A.; Lakey, J. R. T.; Kennedy, R. T. *J. Biol. Chem.* **1999b**, *274*, 6360-6365.

Aspinwall, C. A.; Qian, W-J.; Roper, M. G.; Kulkarni, R. N.; Kahn, C. R.; Kennedy, R. T. *J. Biol. Chem.* **2000**, *275*, 22331-22338.

Avruch, J. *Mol. Cell. Biochem.* **1998**, *182*, 31-48.

Bao, J. J. *J. Chromatogr. B* **1997**, *699*, 463-480.

Berney, T.; Bubler, L.; Cauldfield, A.; Oberbolzer, O.; Toso, C.; Alejandro, R.; Cooper, D. K. C.; Ricordi, C.; Morel P. *Swiss Med. Wkly.* **2002**, *132*, 671-688.

Blachier, F.; Mourtada, A.; Sener, A.; Malaisse, W. J. *Endocrinology* **1989**, *124*, 134-141.

Centers for Disease Control and Prevention. National Diabetes Factsheet: General Information and National Estimates on Diabetes in the United States, 2000. Atlanta, GA: US Department of Health and Human Services, Centers for Disease Control and Prevention, 2002.

Chen, S-H.; Lin, Y-H.; Wang, L-Y.; Lin, C-C.; Lee, G-B. *Anal. Chem.* **2002**, *74*, 5146-5153.

Cheng, S. B.; Skinner, C. D.; Taylor, J.; Attiya, S.; Lee, W. E.; Picelli, G.; Harrison, D. J. *Anal. Chem.* **2001**, *73*, 1472-1479.

Chiem, N.; Harrison, D. J. *Anal. Chem.* **1997**, *69*, 373-378.

Chiem, N. H.; Harrison, D. J. *Electrophoresis* **1998a**, *19*, 3040-3044.

Chiem, N. H.; Harrison, D. J. *Clin. Chem.* **1998b**, *44*, 591-598.

Christodoulides, N.; Tran, M.; Floriano, P. N.; Rodriguez, M.; Goodey, A.; Ali, M.; Neikirk, D.; McDevitt, J. T. *Anal. Chem.* **2002**, *74*, 3030-3036.

Christopoulos, T. K.; Diamandis, E. P. In *Immunoassay*; Diamandis, E. P., Christopoulos, T. K., Eds.; Academic Press, Inc.: San Diego, CA, 1996, pp 25-50.

Corning Glass website, Accessed June 12, 2003 http://www.cmog.org/page.cfm?page=279

Edwards, J. L.; Bauman, R.; Spence, D. M. *Anal. Chim. Acta* **1999**, *401*, 209-214.

Effenhauser, C. S.; Paulus, A.; Manz, A.; Widmer, H. M. *Anal. Chem.* **1994**, *66*, 2949-2953.

Eteshola, E.; Leckband, D. *Sensor. Actuat. B* **2001**, *72*, 129-133.

Falck, B.; Hellman, B. *Experientia* **1963**, *19*, 139-140.

Federici, M.; Hribal, M. L.; Ranalli, M.; Marselli, L.; Porzio, O.; Lauro, D.; Borboni, P.; Lauro, R.; Marchetti, P.; Melino, G.; Sesti, G. *FASEB J.* **2001**, *15*, 22-24.

Foster, M. C.; Leapman, R. D.; Li, M. X.; Atwater, I. *Biophys. J.* **1993**, *64*, 525-532.

Gee, K. R.; Brown, K. A.; Chen, W. N.; Bishop-Stewart, J.; Gray, D.; Johnson, I. *Cell Calcium* **2000**, *27*, 97-106.

Gerich, J. E. *Diabetes* **2002**, *51*, S117-S121.

Giddings, J. C. *Unified Separation Science*; A Wiley Interscience Publication: New York, NY, 1991.

Gilon, P.; Henquin, J-C. *Endocrinology* **1995**, *136*, 5725-5730.

Good, J. A. L.; Ziegler, W. H.; Parekh, D. B.; Alessi, D. R.; Cohen, P.; Parker, P. J. *Science* **1998**, *281*, 2042-2045.

Gorski, W.; Aspinwall, C. A.; Lakey, J. R. T.; Kennedy, R. T. *J. Electroanal. Chem.* **1997**, *425*, 191-199.

Grynkiewicz, G.; Poenie, M.; Tsien, R. Y. *J. Biol. Chem.* **1985**, *60*, 3440-3450.

Gupta, B. B. P. *Curr. Sci.* **1997**, *73*, 993-1003.

Gylfe, E. *J. Endocrinol.* **1978**, *78*, 239-248.

Haisma, J.; Spierings, G. A. C. M. *Mat. Sci. Eng. R* **2002**, *37*, 1-60.

Harbeck, M. C.; Louie, D. C.; Howland, J.; Wolf, B. A.; Rothenberg, P. L. *Diabetes* **1996**, *45*, 711-717.

Harris, D. C. *J. Chem. Ed.* **1998**, *75*, 119-121.

Harrison, D. J.; Fluri, K.; Seiler, K.; Fan, Z. H.; Effenhauser, C. S.; Manz, A. *Science* **1993**, *261*, 895-897.

Haugland, R. P. *Handbook of Fluorescent Probes and Research Chemicals*, 6th ed.; Molecular Probes: Eugene, OR, 1996.

He, B.; Burke, B. J.; Zhang, X.; Zhang, R.; Regnier, F. E. *Anal. Chem.* **2001**, *73*, 1942-1947.

Henquin, J-C. *Diabetes* **2000**, *49*, 1751-1760.

Henquin, J-C.; Ishiyama, N.; Nenquin, M.; Ravier, M. A.; Jonas, J-C. *Diabetes* **2002**, *51*, S60-S67.

Heo, J.; Thomas, K. J.; Seong, G. H.; Crooks, R. M. *Anal. Chem.* **2003**, *75*, 22-26.

Holman, G. D.; Kasuga, M. *Diabetologia* **1997**, *40*, 991-1003.

Huang, L.; Shen, H.; Atkinson, M. A.; Kennedy, R. T. *Proc. Nat. Acad. Sci. U.S.A.* **1995**, *92*, 9608-9612.

Huang, Z.; Sanders, J. C.; Dunsmor, C.; Ahmadzadeh, H.; Landers, J. P. *Electrophoresis* **2001**, *22*, 3924-3929.

Hussain, M. A. *Eur. J. Endocrin.* **1999**, *141*, 95-97.

Hutton, J. C.; Peshavaria, M.; Tooke, N. E. *Biochem. J.* **1983**, *210*, 803-810.

Iversen, J.; Miles, D. W. *Diabetes* **1971**, *20*, 1-5.

Jacobson, S. C.; Culbertson, C. T.; Daler, J. E.; Ramsey, J. M. *Anal. Chem.* **1998**, *70*, 3476-3480.

Jacobson, S. C.; Ermakov, S. V.; Ramsey, J. M. *Anal. Chem.* **1999**, *71*, 3273-3276.

Jacobson, S. C.; Hergenröder, R.; Koutny, L. B.; Warmack, R. J.; Ramsey, J. M. *Anal. Chem.* **1994**, *66*, 1107-1113.

Johnson, J. D.; Misler, S. *Proc. Natl. Acad. Sci. U.S.A.* **2002**, *99*, 14566-14571.

Jonas, J-C.; Gilon, P.; Henquin, J-C. *Diabetes* **1998**, *47*, 1266-1273.

Kahn, C. R. *Diabetes* **1994**, *43*, 1066-1084.

Kelly, R. S.; Wightman, R. M. *Anal. Chim. Acta* **1986**, *187*, 79-87.

Kennedy, R. T.; Huang, L.; Atkinson, M. A.; Dush, P. *Anal. Chem.* **1993**, *65*, 1882-1887.

Kenny, S. J.; Anbert, R. E.; Geiss, L. S. In *Diabetes in America*, 2nd ed.; NIH Publication No. 95-1468, 1995.

Kern, W.; Deckert, C. A. In *Thin Film Processes*; Vossen, J. L., Kern, W., Eds.; Academic Press, Inc.: San Diego, CA, 1978, pp 401-496.

Khan, F. A.; Goforth, P. B.; Zhang, M.; Satin, L. S. *Diabetes* **2001**, *50*, 2192-2198.

Koutny, L. B.; Schmalzing, D.; Taylor, T. A., Fuchs, M. *Anal. Chem.* **1996**, *68*, 18-22.

Krook, A.; Bjornholm, M.; Galuska, D.; Jiang, X. J.; Fahlman, R.; Myers, M. G., Jr.; Wallberg-Henriksson, H.; Zierath, J. R. *Diabetes* **2000**, *49*, 284-292.

Krook, A.; O'Rahilly, S. *Baillieres Clin. Endocrinol. Metab.* **1996**, *10*, 97-122.

Kubota, N.; Tobe, K.; Terauchi, Y.; Eto, K.; Yamauchi, T.; Suzuki, R.; Tsubamoto, Y.; Komeda, K.; Nakano, R.; Miki, H.; Satoh, S.; Sekihara, H.; Sciacchitano, S.; Lesniak, M.; Aizawa, S.; Nagai, R.; Kimura, S.; Akanuma, Y.; Taylor, S. I.; Kadowaki, T. *Diabetes* **2000**, *49*, 1880-1889.

Kulkarni, R. N.; Bruning, J. C.; Winnay, J. N.; Postic, C.; Magnuson, M. A.; Kahn, C. R. *Cell* **1999a**, *96*, 329-339.

Kulkarni, R. N.; Winnay, J. N.; Daniels, M.; Bruning, J. C.; Flier, S. N.; Hanahan, D.; Kahn, C. R. *J. Clin. Invest.* **1999b**, *104*, R69-R75.

Lagally, E. T.; Medintz, I.; Mathies, R. A. *Anal. Chem.* **2001**, *73*, 565-570.

Leibiger, I. B.; Leibiger, B.; Moede, T.; Berggren, P. O. *Mol. Cell* **1998**, *1*, 933-938.

Leibiger, B.; Wahlander, K.; Berggren, P. O.; Leibiger, I. B. *J. Biol. Chem.* **2000**, *275*, 30153-30156.

Leibiger, B.; Leibiger, I. B.; Moede, T.; Kemper, S.; Kulkarni, R. N.; Kahn, C. R.; de Vargas, L. M.; Berggren, P. O. *Mol. Cell* **2001**, *7*, 559-570.

Leibiger, I. B.; Leibiger, B.; Berggren, P. O. *FEBS Letters* **2002**, *532*, 1-6.

Li, Z.; Joyal, J. L.; Sacks, D. B. *Biochemistry* **2000**, *39*, 5089-5096.

Liang, Y.; Matschinsky, F. *Ann. Rev. Nutr.* **1994**, *14*, 59-81.

Liljenquist, J. E.; Horwitz, D. L.; Jennings, A. S.; Chiasson, J-L.; Keller, U.; Rubenstein, A. H. *Diabetes* **1978**, *27*, 563-570.

Lin, J. M.; Sternesjo, J.; Sandler, S.; Bergsten, P. *Endocrinology* **1999**, *140*, 3999-4004.

Lin, J. M.; Ortsater, H.; Fakhrai-Rad, H.; Galli, J.; Luthman, H.; Bergsten, P. *Diabetes* **2001a**, *50*, 2737-2743.

Lin, Y-H.; Lee, G-B.; Li, C-W.; Huang, G-R.; Chen, S-H. *J. Chromatogr. A* **2001b**, *937*, 115-125.

Liu, S.; Shi, Y.; Ja, W. W.; Mathies, R. A. *Anal. Chem.* **1999**, *71*, 566-573.

Liu, Y. J.; Tengholm, A.; Grapengiesser, E.; Hellman, B.; Gylfe, E. *J. Physiol.* **1998**, *508*, 471-481.

Lytton, J.; Westlin, M.; Hanley, M. R. *J. Biol. Chem.* **1991**, *266*, 17067-17071.

Mathews C. K.; Van Holde, K. E. *Biochemistry*, 2nd ed; The Benjamin/Cummings Publishing Company, Inc: Menlo Park, CA, 1996.

Metz, S. A. *Diabetes* **1988**, *37*, 3-7.

Okada, T.; Kawano, Y.; Sakakibara, T.; Hazeki, O.; Ui, M. *J. Biol. Chem.* **1994**, *269*, 3568-3573.

Orci, D.; Vassalli, J. D.; Perrelet, A. *Sci. Am.* **1988**, *259*, 85-94.

Patel, Y. C.; Amherdt, M.; Orci, L. *Science* **1982**, *217*, 1155.

Persaud, S. J.; Asare-Anane, H.; Jones, P. M. *FEBS Letters* **2002**, *510*, 225-228.

Pessin, J. E.; Thurmond, D. C.; Elmendorf, J. S.; Coker, K. J.; Okada, S. *J. Biol. Chem.* **1999**, *274*, 2593-2596.

Poitout, V.; Olson, L. K.; Robertson, R. P. *Diabetes Metab.* **1996**, *22*, 7-14.

Pørksen, N. *Diabetologia* **2002**, *45*, 3-20.

Porte, Jr., D.; Kahn, S. E. *Diabetes* **2001**, *50*, S160-S163.

Porzio, O.; Federici, M.; Hribal, M. L.; Lauro, D.; Accili, D.; Lauro, R.; Borboni, P.; Sesti, G. *J. Clin. Invest.* **1999**, *104*, 357-364.

Powis, G.; Bonjouklian, R.; Berggren, M. M.; Gallegos, A.; Abraham, R.; Ashendel, C.; Zalkow, L.; Matter, W. F.; Dodge, J.; Grindey, G.; Vlahos, C. J. *Cancer Res.* **1994**, *54*, 2419-2423.

Pralong, W-F.; Bartley, C.; Wollheim, C. B. *EMBO J.* **1990**, *9*, 53-59.

Qiu, C. X.; Harrison, D. J. *Electrophoresis* **2001**, *22*, 3949-3958.

Ravier, M. A.; Gilon, P.; Henquin, J-C. *Diabetes* **1999**, *48*, 2374-2382.

Rondinone, C. M.; Wang, L-M.; Lonnroth, P.; Wesslau, C.; Pierce, J. H.; Smith, U. *Proc. Nat. Acad. Sci. U.S.A.* **1997**, *94*, 4171-4175.

Rothenberg, P. L.; Willison, L. D.; Simon, J.; Wolf, B. A. *Diabetes* **1995**, *44*, 802-809.

Roulet, J-C.; Volkel, R.; Herzig, H. P.; Verpoorte, E.; de Rooij, N. F.; Dandliker, R. *J. Microelectromech. Syst.* **2001**, *10*, 482-491.

Rutter, G. A. *Curr. Biol.* **1999**, *9*, R443-R445.

Saltiel, A. R. *Am. J. Physiol.* **1996**, *270*, E375-E385.

Schilling, E. A.; Kamholz, A. E.; Yager, P. *Anal. Chem.* **2002**, *74*, 1798-1804.

Schmalzing, D.; Koutny, L. B.; Taylor, T. A.; Fuchs, M. *J. Chromatogr. B* **1997**, *697*, 175-180.

Schmidt, H. H.; Warner, T. D.; Ishii, K.; Sheng, H.; Murad, F. *Science* **1992**, *258*, 1376-1378.

Schultz, N. M.; Kennedy, R. T. *Anal. Chem.* **1993**, *65*, 3161-3165.

Schultz, N. M.; Huang, L.; Kennedy, R. T. *Anal. Chem.* **1995**, *67*, 924-929.

Sener, A.; Best, L. C.; Yates, A. P.; Kadiata, M. M.; Olivares, E.; Louchami, K.; Jijakli, H.; Ladriere, L.; Malaisse, W. J. *Endocrine* **2000**, *13*, 329-340.

Sesti, G.; Federici, M.; Hribal, M. L.; Lauro, D.; Sbraccia, P.; Lauro, R. *FASEB J.* **2001**, *15*, 2099-2111.

da Silva Xavier, G.; Varadi, A.; Ainscow, E. K.; Rutter, G. A. *J. Biol. Chem.* **2000**, *275*, 36269-36277.

Smith, P. A.; Duchen, M. R.; Ashcroft, F. M. *Pflugers Arch. Eur. J. Phys.* **1995**, *430*, 808-818.

Sodoyez, J. C.; Sodoyez-Goffaux, F.; Foá, P. P. *Proc. Soc. Exp. Biol. Med.* **1969**, *130*, 568-571.

Song, H.; Tice, J. D.; Ismagilov, R. F. *Angew. Chem. Int. Ed.* **2003**, *42*, 767-772.

Takahashi, N.; Kadowaki, T.; Yazaki, Y.; Miyashita, Y.; Kasai, H. *J. Cell Biol.* **1997**, *138*, 55-64.

Tang, T.; Badal, M. Y.; Ocvirk, G.; Lee, W. E.; Bader, D. E.; Bekkaoui, F.; Harrison, D. J. *Anal. Chem.* **2002**, *74*, 725-733.

Tao, L.; Kennedy, R. T. *Anal. Chem.* **1996**, *68*, 3899-3906.

Tao, L.; Aspinwall, C. A.; Kennedy, R. T. *Electrophoresis* **1998**, *19*, 403-408.

Taylor, S. I. *Cell* **1999**, *97*, 9-12.

Taylor, J.; Picelli, G.; Harrison, D. J. *Electrophoresis* **2001**, *22*, 3699-3708.

Thams, P.; Capito, K. *Eur. J. Endocrinol.* **1999**, *140*, 87-93.

Unger, M. A.; Chou, H. P.; Thorsen, T.; Scherer, A.; Quake, S. R. *Science* **2000**, *288*, 113-116.

Velloso, L. A.; Carneiro, E. M.; Crepaldi, S. C.; Boschero, A. C.; Saad, M. J. A. *FEBS Letters* **1995**, *377*, 353-357.

Verspohl, E. J.; Ammon, H. P. T. *J. Clin. Invest.* **1980**, *65*, 1230-1237.

Weast, R. C. *CRC Handbook of Chemistry and Physics*; CRC Press: Boca Raton, FL, 1975.

Weber, M. A.; Lidor, A.; Arora, S.; Salituro, G. M.; Zhang, B. B. Sidawy, A. N. *J. Vasc. Surg.* **2000**, *32*, 1118-1125.

Westerlund, J.; Wolf, B. A.; Bergsten, P. *Diabetes* **2002**, *51*, S50-S52.

White, M. F. *Mol. Cell. Biochem.* **1998**, *182*, 3-11.

White, M. F.; Maron, R.; Kahn, C. R. *Nature* **1985**, *318*, 183-186.

Wightman, R. M.; Jankowski, J. A., Kennedy R. T.; Kawagoe, K. T.; Schroeder, T. J.; Leszczyszyn D. J.; Near, J. A.; Diliberto, E. J., Viveros, O. H. *Proc. Nat. Acad. Sci. U.S.A.* **1991**, *88*, 10754-10758.

Withers, D. J.; White, M. *Endocrinology* **2000**, *141*, 1917-1921.

Withers, D. J.; Gutierrez, J. S.; Towery, H.; Burks, D. J.; Ren, J. M.; Previs, S.; Zhang, Y.; Bernal, D.; Pons, S.; Shulman, G. I.; Bonner-Weir, S.; White, M. F. *Nature* **1998**, *391*, 900-904.

Withers, D. J.; Burks, D. J.; Towery, H. H.; Altamuro, S. L.; Flint, C. L. White, M. F. *Nat. Genet.* **1999**, *23*, 32-40.

Woolley, A. T.; Hadley, D.; Landre, P.; de Mello, A. J.; Mathies, R. A.; Northrup, M. A. *Anal. Chem.* **1996**, *68*, 4081-4086.

Xu, G.; Marshall, C. A.; Lin, T-A.; Kwon, G.; Munivenkatappa, R. B.; Hill, J. R.; Lawrence, J. C., Jr.; McDaniel, M. L. *J. Biol. Chem.* **1998**, *273*, 4485-4491.

Xu, G. G.; Gao, Z. Y.; Borge, P. D.; Wolf, B. A. *J. Biol. Chem.* **1999**, *274*, 18067-18074.

Xu, G. G.; Gao, Z-Y.; Borge, P. D., Jr.; Jegier, P. A.; Young, R. A.; Wolf, B. A. *Biochemistry* **2000**, *39*, 14912-14919.

Yalow, R. S. *Science* **1978**, *200*, 1236-1240.

Yang, M. S.; Li, C. W.; Yang, J. *Anal. Chem.* **2002**, *74*, 3991-4001.

Yang, T.; Jung, S-Y.; Mao, H.; Cremer, P. S. *Anal. Chem.* **2001**, *73*, 165-169.

Zawalich, W. S.; Zawalich, K. C. *J. Biol. Chem.* **2002**, *277*, 26233-26237.

Zhang, B.; Salituro, G.; Szalkowski, D.; Li, Z.; Zhang, Y.; Royo, I.; Vilella, D.; Diez, M. T.; Pelaez, F.; Ruby, C.; Kendall, R. L.; Mao, X.; Griffin, P.; Calaycay, J.; Zierath, J. R.; Heck, J. V.; Smith, R. G.; Moller, D. E. *Science* **1999**, *284*, 974-977.

Zhou, Z.; Misler, S. *J. Biol. Chem.* **1996**, *271*, 270-277.

Zubay, G. *Biochemistry*, 4th ed.; William C. Brown Publishers: Dubuque, IA, 1998.

BIOGRAPHICAL SKETCH

Michael Gabriel Roper was born in Austin, TX, and grew up in Victoria, TX. In 1994, Michael started college at The Victoria College and from 1995-1998 attended The University of Texas at Austin. From 1997-1998, Roper worked in the lab of Professor Allan J. Bard in the search for new co-reactants in the electrogenerated chemiluminescence of $Ru(bpy)_3^{2+}$. In 1998, Michael began his graduate studies at the University of Florida working under the supervision of Professor Robert T. Kennedy.

I certify that I have read this study and that in my opinion it conforms to acceptable standards of scholarly presentation and is fully adequate, in scope and quality, as a dissertation for the degree of Doctor of Philosophy.

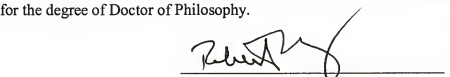

Robert T. Kennedy, Chairman
Professor of Chemistry

I certify that I have read this study and that in my opinion it conforms to acceptable standards of scholarly presentation and is fully adequate, in scope and quality, as a dissertation for the degree of Doctor of Philosophy.

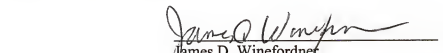

James D. Winefordner
Graduate Research Professor of Chemistry

I certify that I have read this study and that in my opinion it conforms to acceptable standards of scholarly presentation and is fully adequate, in scope and quality, as a dissertation for the degree of Doctor of Philosophy.

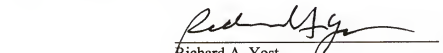

Richard A. Yost
Professor of Chemistry

I certify that I have read this study and that in my opinion it conforms to acceptable standards of scholarly presentation and is fully adequate, in scope and quality, as a dissertation for the degree of Doctor of Philosophy.

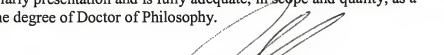

Jon D. Stewart
Associate Professor of Chemistry

I certify that I have read this study and that in my opinion it conforms to acceptable standards of scholarly presentation and is fully adequate, in scope and quality, as a dissertation for the degree of Doctor of Philosophy.

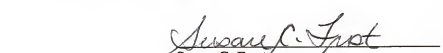

Susan C. Frost
Professor of Biochemistry and Molecular Biology

This dissertation was submitted to the Graduate Faculty of the Department of Chemistry in the College of Liberal Arts and Sciences and to the Graduate School and was accepted as partial fulfillment of the requirements for the degree of Doctor of Philosophy.

August 2003

_____

Dean, Graduate School